

**BEHAVIOUR OF SMALL-DIAMETER BURIED STEEL PIPES SUBJECTED TO
AXIAL GROUND MOVEMENT**

by

© Darren Andersen

A Thesis Submitted to the

School of Graduate Studies

In partial fulfillment of the requirements for the degree of

Master of Engineering

Faculty of Engineering and Applied Science

Memorial University of Newfoundland

May 2024

St. John's

Newfoundland and Labrador

Canada

ABSTRACT

Small-diameter steel pipes are often used to distribute gas to residential homes. These pipelines sometimes run through landslide-prone areas, highlighting a need to understand their response to ground movements. To investigate the axial behaviour of pipe subjected to ground movements, previous studies were conducted in the laboratory by pulling a pipe through a static soil mass. However, in real landslides, a soil mass moves while the pipe is restrained in stable ground. In this regard, a test facility was designed at Memorial University of Newfoundland where a soil mass can move against a pipe restrained on one end, simulating the condition expected during ground displacement. This thesis presents results for steel pipes of 26.7-, 60.3-, and 114.3 mm diameters subjected to axial ground movements using the test facility. The stop-start cycles during testing investigated the effects of intermittent ground movements on the axial soil force on pipes. Pipe axial force, axial strain, and tank displacement were recorded during the tests. Results showed the dimensionless axial peak forces were higher during soil pulling than those from pipe pulling available in literature. No reduction of axial force was found during the intervals of subsequent pulling. However, peak axial forces reduced with unloading-reloading cycles that developed at relatively reduced soil box displacement. Measurements from the fibre-optic sensor attached along the pipe length showed negligible axial strain, and thus elongation, indicating that the pipe behaves as a rigid body. Finally, the applicability of existing design guidelines was evaluated by performing beam-on-spring analysis to simulate full-scale laboratory experiments. The study revealed that earth pressure coefficients recommended in the design guidelines are incapable of accurately predicting the maximum axial soil resistance measured during the full-scale tests. K-values for the tests were then back-calculated using the design equation and applied to the beam-on-spring analysis to simulate the test results.

ACKNOWLEDGEMENTS

The author would like to acknowledge the assistance and dedication of the entire research team through the past 2 years; Auchib Reza, Saifa Prioty, Sudipta Chakraborty, Sudipto Priyom, and Thirojan Jayabalasingham. As well, thanks to the staff and faculty from Memorial University such as Professor Ashutosh Dhar, Bipul Hawlader, Billy Bidgood and the entire technical services staff as well as laboratory staff Jamal Tinkov and Shawn Oregan. Without their guidance and expertise, this thesis and research would not have been possible. Furthermore, the author would like his family and friends, whose support and patience were invaluable throughout the degree. Finally, the author would like to gratefully acknowledge the financial support and/or in-kind support provided by the Alliance Grants program of the National Science and Engineering Research Council of Canada, FortisBC Energy Inc., SaskEnergy Canada Inc., and WSP Canada Inc. for conducting this research.

Table of Contents

ABSTRACT.....	II
ACKNOWLEDGEMENTS.....	III
LIST OF FIGURES.....	VI
LIST OF TABLES.....	IX
LIST OF SYMBOLS.....	X
CHAPTER 1: INTRODUCTION.....	1-1
1.1 BACKGROUND.....	1-1
1.2 MOTIVATION.....	1-3
1.3 OBJECTIVES.....	1-6
1.4 FRAMEWORK OF THESIS.....	1-7
1.5 KEY CONTRIBUTIONS.....	1-9
CHAPTER 2: LITERATURE REVIEW.....	2-1
2.1 GENERAL.....	2-1
2.2 CURRENT DESIGN GUIDELINES.....	2-1
2.3 EXPERIMENTAL STUDIES.....	2-3
2.4 NUMERICAL MODELING.....	2-9
2.5 SUMMARY.....	2-13
2.6 REFERENCES.....	2-14
CHAPTER 3: LABORATORY INVESTIGATION OF BURIED SMALL-DIAMETER STEEL PIPES SUBJECTED TO AXIAL GROUND MOVEMENT.....	3-1
3.1 ABSTRACT.....	3-1
3.2 INTRODUCTION.....	3-2
3.3 TESTING METHODS.....	3-8
3.3.1 <i>Apparatus</i>	3-8
3.3.2 <i>Backfill Material</i>	3-9
3.3.3 <i>Pipe Instrumentation</i>	3-10
3.3.4 <i>Test Programme</i>	3-11
3.4 TEST RESULTS.....	3-13
3.4.1 <i>Load–Displacement Responses</i>	3-13
3.4.2 <i>Comparison of Axial Forces</i>	3-15
3.4.3 <i>Force–Time and Relaxation Response</i>	3-17
3.4.4 <i>Successive Pulling Tests</i>	3-20
3.4.5 <i>Strain Distributions</i>	3-22
3.5 CONCLUSIONS.....	3-27
3.6 ACKNOWLEDGEMENTS.....	3-29
3.7 REFERENCES.....	3-30

CHAPTER 4: BEAM-ON-SPRING MODELLING OF BURIED STEEL PIPES IN SAND SUBJECTED TO AXIAL LOADS.....	4-1
4.1 ABSTRACT.....	4-1
4.2 INTRODUCTION.....	4-2
4.3 FULL-SCALE TESTING.....	4-7
4.4 FINITE-ELEMENT MODEL.....	4-9
4.4.1 <i>Modelling Techniques</i>	4-9
4.4.2 <i>PSI Elements</i>	4-11
4.4.3 <i>Nonlinear Springs</i>	4-13
4.5 MODEL RESULTS.....	4-14
4.5.1 <i>Load–Displacement Responses</i>	4-14
4.5.2 <i>K-Value Comparisons</i>	4-18
4.6 <i>PIPE AXIAL STRAIN</i>	4-18
4.7 <i>CONCLUSIONS</i>	4-20
4.8 <i>ACKNOWLEDGEMENTS</i>	4-22
4.9 <i>REFERENCES</i>	4-22
CHAPTER 5: CONCLUSIONS AND RECOMMENDATIONS FOR FUTURE RESEARCH.....	5-1
5.1 <i>CONCLUSIONS</i>	5-1
5.2 <i>MAJOR FINDINGS FROM THE FULL-SCALE TESTING PROGRAMME</i>	5-1
5.3 <i>MAJOR FINDINGS FROM THE BEAM-ON-SPRING ANALYSIS</i>	5-3
5.4 <i>RECOMMENDATIONS</i>	5-4
5.5 <i>REFERENCES (GENERAL)</i>	5-5
APPENDIX A: CHALLENGES AND ISSUES DURING FULL-SCALE TESTING.....	A-1

List of Figures

Figure 1-1: Pipe loading during ground movement event. (Karimian 2006)

Figure 1-2: Damage from the Northridge Earthquake in San Fernando Valley, California, Los Angeles Times (accessed 2023-12-19).

Figure 3-1: Testing facility frame configuration: (a) without soil tank; (b) with soil tank.

Figure 3-2: (a) Tank ram-end view with LVDT and tank-ram connection; (b) Connection between the load cell and pipe.

Figure 3-3: Fibre-optic strain sensing equipment.

Figure 3-4: Fibre-optic strain sensor application; (a) Strain sensor path mapped and temporarily adhered using Kapton dot; (b) Application of cyanoacrylate adhesive between Kapton dots; (c) Silicone caulking applied to pipe after adhesive curing; (d) Sheathing tape covering pipe to protect caulking and reduce friction increase.

Figure 3-5: Axial soil resistance with tank displacement for Pulling Phase 1.

Figure 3-6: Normalized axial soil resistance with tank displacement for Pulling Phase 1.

Figure 3-7: Normalized peak axial resistance with pipe diameter (including both the soil box displacement and pipe pullout tests).

Figure 3-8: Pipe axial force variation, with time, during each phase for: (a) Test ST-01; (b) Test ST-06.

Figure 3-9: Axial soil resistance with tank displacement: (a) Test ST-01 ($D=26.7$ mm); (b) Tests ST-03-04 ($D=60.3$ mm) and ST-05-06 ($D=114.3$ mm).

Figure 3-10: Peak soil resistances in different pulling phases with tank displacement.

Figure 3-11: Strain distribution along the length of the pipe at the beginning of the test and displacement corresponding to the peak load for each pulling and pushing phase: (a) $D=26.7$ mm pipe (ST-02); (b) $D=60.3$ mm pipe (ST-04); (c) $D=114.3$ mm pipe (ST-06).

Figure 3-12: Strain distribution along the length of the pipe during ST-04 for various displacements: (a) Test start, Pull1 peak and mid Relax1; (b) Test start, Pull2 peak and mid-Relax2.

Figure 4-1: Full-scale testing layout: (a) Pipe fixed-end connection to load cell and back-stop, (b) Pipe free-end with ram connection to tank, (c) Data acquisition system for pipe load and tank position, (d) Axial strain recording setup including controller, signal interrogator, standoff cable, remote module, sensor and port cleaner (Andersen et al. 2024)

Figure 4-2: Mesh convergence analysis for PSI elements

Figure 4-3: Pipe–soil interaction (PSI) model

Figure 4-4: Current design guidelines: (a) Axial loading; (b) Vertical loading (ALA 2005).

Figure 4-5: Idealized representation of soil using discrete springs connected to a buried pipe (ALA 2005).

Figure 4-6: Comparison of force–displacement plots with the measurements: (a) $D=26.7$ -mm, (b) $D=60.3$ -mm, (c) $D=114.3$ -mm

Figure 4-7: Force–displacement plots comparing results from PSI elements to traditional nonlinear spring elements.

Figure 4-8: Force–displacement results for analyses P16, P18, P20 and P22 using: (a) $K=K_0$, and (b) K =Back-calculated K -fit value in Eq. (4-1).

Figure 4-9: Variation of K with pipe diameter

Figure 4-10: Strain distributions along the length of the pipes

Figure A-1: Results from the first test on 60.3 mm diameter pipe deemed unsuccessful: (a) Force–displacement plot showing load-cell capacity and power outage timing, (b) Axial strain distribution along the pipe at varying soil displacements

Figure A-2: Results from an initial trial of ST-03 (60.3 mm pipe) showing saw-tooth behaviour: (a) Force vs time, (b) Force–displacement plot showing erroneous tank behaviour during Pull 2

Figure A-3: Results from an unsuccessful trial of ST-19 (26.7 mm diameter) (Force–displacement plot showing erroneous tank movement during Pull 1).

List of Tables

Table 2-1: Pipe coating factors for common coatings (ALA 2005)

Table 3-1: Backfill soil parameters

Table 3-2: Test programme

Table 3-3: Soil displacement at corresponding peak load for first pull

Table 3-4: Testing parameter comparisons

Table 4-1: Backfill soil parameters (Saha et al. 2019)

Table 4-2: Model matrix

Table 4-3: Testing parameter comparisons (Andersen et al. 2024)

Table 4-4: Model parameter comparisons

Table 4-5: *K-fit* Values Calculated using Equations 5

List of Symbols

The following symbols are used in this thesis:

A	pipe cross-sectional area
D	pipe outer diameter
E	modulus of elasticity of pipe material
F	interface friction reduction factor
H	burial depth measured from ground surface to pipe centre
K	equivalent lateral earth pressure coefficient
K_0	coefficient of lateral earth pressure at rest
K^*	modified earth pressure coefficient
L	buried pipe length
P_u	maximum axial soil resistance of pipe
T_u	axial soil resistance of pipe
γ	unit weight of soil
δ	pipe–soil interface friction angle
ε	axial strain
ν	Poisson's ratio of soil

CHAPTER 1: Introduction

1.1 Background

Pipelines are an integral part of modern infrastructure in Canada and worldwide. They carry water, oil, gas and solids across vast distances above and below ground and can be made of cast iron, steel or plastic. According to Reed et al. (2012), CEPA operates over 100,000 km of pipelines within Canada and the US. The Canadian Energy Pipeline Association (CEPA) is a consortium of companies operating transmission pipelines in Canada. A transmission pipeline is one that carries product in a large diameter pipe, at a high operating pressures and runs between provincial, or state, boundaries. A distribution line carries products at lower operating pressures in a smaller-diameter pipe to the end user (AGA 2019). Small-diameter steel pipes, usually 150 mm diameter and below, are often used as distribution lines carrying the product to its end-user in urban and rural settings. Given their importance in transportation infrastructure, they must run across all terrains to deliver their products.

Permanent ground deformations are a type of hazard that can affect buried pipelines. They may occur due to natural disasters, human activities and underlying geotechnical issues. Examples of the latter include, surface faulting, landslides, liquefaction-induced spreading and settlement (Ni et al. 2018). When landslides or other ground-movement events occur, unstable soil moves around a buried pipe, causing stresses and strains to develop. The response of the buried pipe will differ depending on the direction of ground movement in relation to the pipe. If ground movement occurs parallel to the pipe, it will experience primarily axial force, while movement perpendicular to the pipe will produce bending in the pipe. If the ground movement is at some angle between this, both bending and axial forces can occur, and is deemed oblique

movement. Fig. 1-1 shows an illustration of the aforementioned movement where one pipe experiences ground movement in the axial direction and another experiences ground movement in the lateral direction.

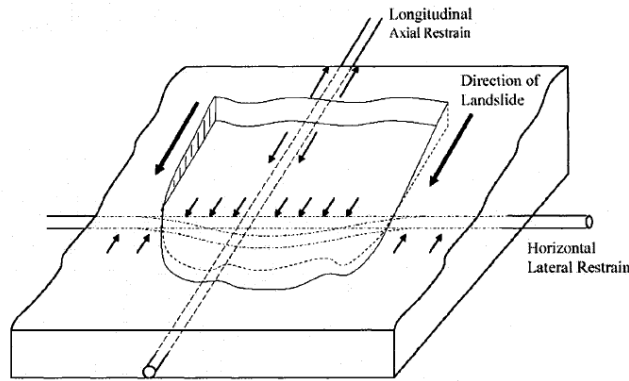


Fig. 1-1. Pipe loading during ground-movement event (Karimian 2006)

Small-diameter steel pipes are used in Western Canada by various oil and gas companies to transport their product. Western Canada also contains many landslide-prone areas that these pipelines must traverse to reach their destination, such as the Fraser-Thompson or Howe Sound-Lillooet corridors in South-Western British Columbia. These areas were studied by Hungr et al. (1999) to develop a risk assessment using Magnitude-Cumulative Frequency (MCF) data from over 3,500 logged landslides. Another area of concern in British Columbia is the town of Quesnel, which is situated on a large landslide, whose movement has been monitored for the past 20 years (Wood Monitoring Report, 2020). Many countries worldwide experienced pipeline damage due to landslides, such as India (Gupta and Satyam 2022), Iran (Vasseghi et al. 2020), Japan (Hara et al. 2020), Peru (Lee et al. 2008), and Turkey (Cevik and Topal 2003) among many others. Damage to a pipeline may result in the shutoff of that service while crews investigate or perform repairs. In a worst case, the product may leak causing environmental

concerns as well. For example, as a result of the Northridge Earthquake in Southern California in 1994, a large block-slide ground movement occurred rupturing a high-pressure natural gas transmission line, a natural gas distribution line and two water lines (Bain et al. 2023). The former, caused an explosion, while the latter flooded the road causing erosional damage. See Fig. 1-2 for a photo of the aftermath. The widespread nature of pipeline damage due to ground movement highlights the importance of studying their response.



Fig. 1-2. Damage from the Northridge Earthquake in San Fernando Valley, California, Los Angeles Times (accessed 2023-12-19)

1.2 Motivation

Many previous studies investigate the pipe's behaviour when subjected to ground-movement events. However, research in this area is typically performed by moving a buried pipe through a

static soil mass. The relative motion between pipe and soil is believed to produce similar results regardless of which body is translating and which is fixed.

Numerous studies move a soil mass with respect to a fixed pipeline, though almost all investigate differing loading scenarios, including lateral (Alafari et al. 2021; Ansari et al. 2021) , and various fault movements (Liu et al. 2022; Ni et al. 2017; Saiyar et al. 2015). Only one study found at the time of writing performs soil movement around an axially fixed pipe, Rostami et al. (2022). However, their test involved a 1/10th scale copper pipe of 15 mm diameter (to simulate a 60 mm steel pipe) under loose soil conditions. In addition, their goal was to determine the axial resistance in order to accurately calculate axial spring stiffness for use in full-scale strike-slip fault testing. They did not investigate the effect of soil-pull compared to pipe-pull. To date, no studies exist that determine whether the movement of a soil mass axially around a stationary, fixed pipe produces equivalent results to that of a pipe pulled axially through a stable soil mass.

There are no studies, pipe-pull or otherwise, that investigate the behaviour of small-diameter steel pipes loaded axially. The smallest diameter pipe found was 175 mm tested by Bilgin and Stewart (2009), while Murugathasan et al. (2021) tested a similar sized pipe of 178 mm diameter. All other studies that performed axial testing on buried steel pipes did so using diameters greater than 150 mm, highlighting a gap in understanding for the response of smaller-diameter distribution pipes. Thus, the current study focuses on small-diameter steel pipes, with the smallest of 26.7 mm and largest being 114.3 mm in diameter. Pipes of these sizes are commonly used in gas distribution systems in Canada.

A further gap in knowledge exists in the form of pipe behaviour during intermittent ground movement, whereby a soil-mass does not move fully down its failure slope, but instead moves in increments. An example of this concept is presented by Wood Environment & Infrastructure Solutions (2021) in their document titled Monitoring Report 2020. In it, they describe the process and outcome of ground-movement data collection from Quesnel, BC; as Quesnel sits partially on a landslide that has moved intermittently for over 20 years. GPS hubs and slope inclinometers were used to capture the data which shows that ground movement often occurred in small, closely spaced events and in larger single events further spaced. Between each movement event, the pipe and soil can relax, which may redistribute stresses and strains developed in both. Undoubtedly, once several movement events have occurred, the bond between soil and pipe will be weakened affecting the stress and strains that can transfer from soil to pipe. These conditions are of importance and are explored further in the research detailed herein.

Typically, the preferred method of researching pipe behaviour during axial ground movement events has been to perform a pipe-pull test. During these tests, a pipe is buried in a stationary soil mass, and then pulled out, recording the pipe's displacement and axial force developed during pulling, among other parameters. The guidelines (ALA 2005; PRCI 2009) offer a straight-forward equation capable of calculating the maximum resistance (pullout force) against pipe movement in the axial direction that the soil is able to provide per unit length of pipe, as below.

$$T_u = \pi D H \bar{\gamma} \frac{1+K}{2} \tan \delta \quad (1-1)$$

Where T_u is the maximum axial resistance per unit length, D is the pipe outer diameter, H is the burial depth, $\bar{\gamma}$ is soil density, K is the lateral earth pressure coefficient (ratio of the horizontal to the vertical soil pressure) and δ is the interface friction coefficient. It should be noted that K is taken as high as 2.0 in PRCI (2009), as discussed later, while K equal to the earth pressure coefficient at-rest (K_0) is used in ALA (2005). Equations are also given to calculate the force in the lateral and vertical directions as well; however these are not the focus of the current study. Multiple studies have been published whereby the maximum axial resistance recorded from full-scale testing of steel pipes did not compare well with results calculated from ALA (2005) or PRCI (2009) guidelines. Murugathasan et al. (2021), Sheil et al. (2018), Bilgin and Stewart (2008) and Wijewickreme et al. (2009) performed full-scale tests in the dense sand condition. All of them showed that ALA (2005) poorly predicted the maximum axial soil resistance. Wijewickreme et al. (2009) measured normal stresses around the pipe during pullout, showing that they were not equal to the geostatic condition and increased around the pipe during pullout. To account for this difference, a higher value of K was back-calculated and then suggested for use in the axial soil resistance equation. PRCI (2009) subsequently adopted this change, allowing for better peak force predictions in some cases. However, this K -value may be dependent on various factors, such as backfill compaction, pipe diameter, and burial depth. It is the intent to investigate how these factors affect the axial resistance (i.e., back-calculated K -value) when moving a soil-mass over a pipe versus pulling a pipe through a stationary soil-mass

1.3 Objectives

The main objective of this thesis is to develop an understanding of small-diameter steel pipes subjected to axial ground movement, specifically by loading the pipe by moving a soil-mass

around a fixed pipe. Additionally, to determine whether any modification to existing guidelines is required based on the unique soil-moving setup. Below are more detailed objectives of the research:

- 1) Design and develop of a novel testing facility for investigating the axial resistance between soil and buried pipe segments by applying relative displacement using moving tank.
- 2) Determine whether the movement of a soil mass over a buried pipe fixed in place will produce the same results as one pulled through a stationary soil mass.
- 3) Investigate the development of strains along the pipe length during axial soil movement.
- 4) Investigate the effect of intermittent soil movement on a buried steel pipe.
- 5) Review and evaluate the applicability of existing design guidelines by simulating the test results using Winkler beam-on-spring analysis.

1.4 Framework of Thesis

This thesis is organized in manuscript format. The outcome of the study is presented in five chapters and one appendix.

Chapter 1: Introduction

This first chapter introduces the background related to the topic and the motivations of the thesis. It also lays out the research objectives and the major contributions from that research, which have been included in the thesis.

Chapter 2: Literature Review

This chapter presents the findings of the extensive review of current literature on buried pipe behaviour subjected to axial ground movement. Research investigating alternate methods of

movement was also studied to identify the scope of current knowledge. Furthermore, the existing knowledge relating to finite element analysis of these conditions was reviewed.

Chapter 3: Laboratory Investigation of Buried Small-Diameter Steel Pipes Subjected to Axial Ground Movement

Chapter 3 discusses the setup of a novel testing facility to perform full-scale soil-pull testing, whereby a soil tank is pulled along rails over a stationary steel pipe fixed at one end and free at the other. The application of distributed fibre optic sensors used to measure the complete strain distribution along the length of the pipe is discussed. Then, the behaviour of the pipes during consecutive soil movements and relaxation periods are explored. A version of this chapter will be submitted as a technical paper in a journal. Parts of this study have been published as a conference paper in the 76th Canadian Geotechnical Journal, GeoSaskatoon 2023, SK, Canada.

Chapter 4: Beam-on-Spring Modelling of Buried Steel Pipes in Sand Subjected to Axial Loads

This chapter evaluates the applicability of existing design guidelines by performing beam-on-spring analysis for small-diameter steel pipes experiencing relative axial ground movements. The beam-on-spring analysis technique with modified spring-force is presented, to evaluate full-scale testing results. A preliminary relationship between the spring parameter and the pipe's diameter was then proposed. Finally, the effect of the modified spring force is presented for a sufficiently long pipeline subjected to axial ground movements.

Chapter 5: Conclusions and Recommendations

The final chapter includes summarized conclusions developed from the findings presented in the previous chapters and recommendations for further testing.

Appendix A: Challenges and Issues During Full-Scale Testing

This appendix outlines various challenges experienced during the testing programme, and details the unsuccessful tests. Results obtained from these tests are also presented.

1.5 Key Contributions

Conference paper

Andersen, D., Dhar, A. 2023. Investigation of small-diameter steel pipes subjected to axial ground movement, 76th Canadian Geotechnical Conference, Geo Saskatoon2023, Saskatoon, SK, Canada, October 1st4th.

Journal paper

Andersen, D. Reza, A. and Dhar, A. 2024. Laboratory Investigation of Buried Small-Diameter Steel Pipes Subjected to Axial Ground Movement, (to be submitted).

Co-authorship Statement

All research work presented at the conference and to be submitted in journals were carried out by the author of this thesis, Darren Andersen, under the supervision of Dr. Ashutosh Dhar. The first draft of the manuscript is also prepared by Darren Andersen and subsequently revised based on the co-author's feedback and the peer-review process. As a co-author, Dr. Ashutosh Dhar provided support in developing the idea, provided guidance on the aspects to detail further, and reviewed the manuscript. Dr. Reza contributed to the organization of manuscripts, assisted in numerical modelling, and reviewed the documents.

CHAPTER 2: Literature Review

2.1 General

Pipelines are an important part of modern infrastructure, transporting water, oil, and gas across land and sea to their intended destinations. Large-diameter steel pipes are utilized in the pipeline network as transmission lines, running from processing facilities to distribution centres in a given area. From here, small-diameter pipes are used in the pipeline network as distribution lines, ultimately running to the end-user. As pipelines traverse large distances to the end-user, they may travel through ground-movement-prone areas and must be designed to withstand this movement, or else their function to the end-user is moot. To ensure safe design of the pipeline network and to improve understanding of the interaction between the pipes and the soil during ground movements, a detailed investigation of these pipelines subjected to relative movement is an essential step. Numerous research has been conducted in the past few decades to determine how buried pipes respond to ground movement. This chapter discusses the existing pipe design guidelines and the previous experimental and numerical research related to axial pipe–soil interaction. A literature review specific to the work is also presented in Chapters 3 and 4.

2.2 Current Design Guidelines

Current design guidelines, such as ALA (2005) and PRCI (2009), recommend the use of nonlinear springs to represent the soil surrounding a buried pipe, defined using elastic-perfectly-plastic behaviour, with the pipe modelled as a beam element. Each movement direction, axial, lateral and vertical, will have independent springs that define the force–displacement behaviour in that direction. An independent behaviour means that movement in one direction, axial for

instance, will not affect the response in another direction. The maximum soil resistance in the axial direction (per meter of pipe length) is calculated using Eq. 2-1, as below:

$$T_u = \pi DH \bar{\gamma} \frac{1+K_0}{2} \tan \delta \quad (2-1)$$

Where T_u is the maximum axial resistance per unit length of pipe, D is the outside diameter of the pipe, H is the burial depth, $\bar{\gamma}$ is the unit weight of soil, K_0 is the lateral earth-pressure coefficient at-rest, and δ is the pipe–soil interface friction angle calculated using the internal friction angle of soil (ϕ) multiplied by a material coating factor (f). The material coating factor is given in ALA (2005) per various common pipe coatings as shown in Table 2-1.

Table 2-1. Pipe coating factors for common coatings (ALA 2005)

Pipe Coating	<i>f</i>
Concrete	1.0
Coal Tar	0.9
Rough Steel	0.8
Smooth Steel	0.7
Fusion Bonded Epoxy	0.6
Polyethylene	0.6

Eq. (2-1) calculates the maximum axial resistance of soil based on the average of the normal stress around the pipe, which is the mean of the vertical overburden pressure (γH) and at-rest horizontal earth pressure ($K_0 \gamma H$) at the pipe springline. However, PRCI (2009) adopted the K -value (up to 2.0) instead of K_0 in the Equation (2-1) based on recommendations made by

Wijewickreme et al. (2009). Despite the guideline procedure update, many studies have found that this equation may not accurately predict the maximum axial soil resistance in dense sand, while accurately predicting the results in loose sand. The studies previously alluded to will be discussed in the following section.

2.3 Experimental Studies

Many experimental studies have investigated the pipe–soil interaction surrounding buried steel pipes subjected to relative ground movement (Murugathasan et al. 2021; Ali-Khazaali and Vanapalli 2019; Sheil et al. 2018; Wijewickreme et al. 2009). Murugathasan et al. (2021) performed five full-scale pipe-pull tests on a 2.7 m long 178 mm diameter ductile iron pipe buried in loose and medium-dense sand at a testing facility developed by Memorial University of Newfoundland. A 4 m long, 2 m wide, and 1.5 m deep steel tank was filled 587 mm with locally manufactured sand before the pipe was inserted and buried to a depth of 690 mm to 825 mm. The soil was compacted to a dry density between 15.70 and 17.76 kN/m³ across all tests, corresponding to a relative density of 75-80%. Once prepared, the pipe was pulled for 100 mm at a constant rate using a hydraulic ram. Pipe pulling force, leading-end displacement and vertical/horizontal soil pressures near the pipe were recorded during testing. Pulling rates of 0.5 mm/s, 1.0 mm/s and 1.0 mm/min were used across various tests. Results showed that the relative density of soil significantly impacts pipe pullout force, and that higher burial depth corresponds to higher pullout forces for soils with similar compaction levels. In addition, the ALA design guideline has been reported to reasonably predict the axial pullout resistance measured during tests for pipes buried in loose sand, whereas underpredict in dense sand.

Ali-Khazaali and Vanapalli (2019) performed full-scale pipe-pull testing on a prototype steel pipe in unsaturated cohesionless soil to determine how matric suction affects the axial pullout force. The pipe was a 1.35 m long steel pipe with an outer diameter of 114.3 mm and was knurled using a lathe, with cuts made 1 mm apart, 0.25 mm deep at 115° angles from one another. The knurling depth was chosen based on the median particle size of the soil ($d_{50} = 0.25$ mm) to obtain a uniform pipe roughness to control any possible testing variables. Other important variables, such as peak internal friction angle and critical state friction angle, were determined by performing Direct Shear Tests (DSTs) using a knurled bottom plate similar to the pipe. To perform the pipe-pull testing, a 1.5 m long, 1.2 m wide and 1.1 m deep steel tank with a transparent acrylic window was used to observe water levels during saturation and desaturation. The tank included a drainage system of three perforated pipes to control the soil saturation during testing. The soil was a poorly graded quartz silica sand compacted at optimum moisture (14.3%) to 69% relative density at 250 mm above the pipe. The pipe was pulled using a hollow-core screw-jack with load measured with an S-load cell and movement with a Linear Variable Differential Transducer. Their results showed that matric suction significantly impacted the pullout force, with unsaturated soil producing over two times the force compared with saturated.

Sheil et al. (2018) performed cyclic loading on a steel pipe 2.1 m long with a 350 mm outside diameter. To do this, a 1.31 m long, 0.95 m wide and 1.83 m high testing box was constructed at the University of Oxford with a screw-jack mounted to reaction frames at one end. Three differing methods were used to apply the overburden loading to the pipe: first, strictly soil filling the tank up to the maximum depth of 1.18 m (1.355 m from the pipe springline). Second, a flexible wooden platform was placed on the soil surface of a 1.1 m cover (1.275 m from pipe

springline), with a pressurized bag sitting on top. Lastly, a rigid 0.7 m thick wooden block was placed on top of 0.35 m soil cover (0.525 m from pipe springline) with a pressurized bag exerting additional pressure above this. Each overburden scenario mimicked a different field condition of a narrow trench, a wide trench and an in-between case. A rigid hollow-square sectional supporting spoke was placed inside to prevent the pipe from collapsing or ovalizing due to the overburden pressure. Six Stroud-type load sensors were placed inside the pipe, at intervals around its circumference, to record the force variation, while a load cell connected to the screw-jack recorded the axial resistance during testing. Two soil types were used across eight tests, with four differing moisture contents and three compaction methods (raining, hand tamping and full compaction with a plate-tamper). Results from their tests showed that initial normal stresses on the crown of the pipe were larger than those calculated from the overburden, indicating a rigid inclusion effect. Conversely, the initial pressures on the side of the pipe were lower than lateral earth pressure calculations. Axially displacing the pipe was shown to cause a redistribution of normal stresses around the pipe, particularly increasing pressures on the side wall. Additionally, the settlement of the pipe was significant for the first cycles, which diminished after four or five displacement cycles.

Wijewickreme et al. (2009) performed axial pullout testing on a 457 mm diameter steel pipe, with a 12.7 mm wall thickness, buried in a testing cell 5.0 x 2.5 x 2.5 m ($L \times W \times H$) using sandy soil. Four tests were performed overall; three with soil in a dense state and one with soil in a loose state. Prior to testing, five pressure transducers were installed at intervals around the circumference of the pipe with the goal of capturing the normal stress variations during pipe pullout. The transducer locations were positioned at the pipe's invert, haunch, springline,

shoulder, and crown positions. Pipe pullout force and displacement were also measured during each test. Results obtained using loose sand matched those predicted by ALA (2005), however, dense sand results were more than two times greater. From the pressure transducer data, they found that normal stresses on the pipe increased during pulling, when buried in dense sand, due to constrained soil dilation during shearing. To account for the increased average normal stress during pipe movement, they proposed a higher K -value termed the equivalent lateral earth pressure coefficient for use in design Eq. (2.1) instead of K_0 with a value $K = 2.0$.

Full-scale axial pullout tests were also available for flexible pipes, such as medium-density polyethylene (MDPE) pipe (Reza and Dhar 2021; Reza et al. 2023) and polyvinyl chloride (PVC) pipe (Matymish et al. 2023). Reza and Dhar (2021) performed axial pull-out testing on MDPE pipes buried in loose to medium dense sand. The pipes tested were 60.3 mm in diameter, with a wall thickness of 5.48 mm and a buried length of 4.0 m. The testing facility included a steel testing cell of dimensions 4.0 x 2.0 x 1.5 m ($L \times W \times H$) with a hydraulic ram at one end capable of pulling the pipe and a linear variable displacement transducer (LVDT) monitoring the pipe free end. Pipes were buried in dry, well-graded sand of average density 14.5 kN/m³. During testing, pullout load, pipe leading and free end displacements, as well as strain at discrete locations, were measured. The pipe was pulled at constant rates of 0.5, 1.0 and 2.0 mm/min depending on the test, with tests of each rate being duplicated. Results of the programme showed clearly that an increased pulling rate affected the peak maximum pullout force. Three-dimensional FE analysis of the tests was performed to explore the mechanics of soil interaction. The results showed that interface friction angles of $0.75\phi'$, $0.86\phi'$, and $0.9\phi'$ can successfully simulate the test conditions for pulling rates of 0.5, 1, and 2 mm/min, respectively.

Matymish et al. (2023) tested 100 mm diameter PVC pipes with and without fusion weld joints, recording the axial strain induced during axial pulling. Pipes were buried in sand compacted all around using a vibrating plate tamper, except for the pipe cover which was hand tamped. The testing chamber consisted of a wooden enclosure 5.47 x 1.83 x 1.8 m ($L \times W \times H$) built in a larger concrete enclosure. Pipes were pulled using a 500 kN hydraulic ram attached to the wall of the concrete enclosure. A distributed fibre-optic strain sensor was attached to pipes to record the axial strain data. Three tests were conducted using the facility to assess the development of axial resistance and the impact of non-continuous pulling and fusion weld joints. The first test pulled an unfused pipe at 0.1 mm/min in intervals of 0.25 mm, holding the pipe steady for 4 minutes at each interval before proceeding. After 10.5 mm of displacement in this way, the pipe was pulled at a higher rate of 0.5 mm/min for the remaining 7.5 mm of displacement. The second and third tests were performed by pulling an unfused and a fused pipe, respectively, at a rate of 0.1 mm/min for the first 1.5 mm and 0.5 mm/min thereafter. Results revealed that the load-displacement response was not influenced by non-continuous pulling or changes to the pulling rate. Measurement of strains showed that the distribution of strains along the length of the pipe was nonlinear before the full mobilization of soil friction along the pipe–soil interface. At full mobilization, the distribution becomes linear. The residual axial strain (i.e., “locked-in” strain) distributions along the length of the pipe, after force removal, have also been measured using fibre-optic sensors. It was found that after removal of the axial pulling force, the elongated pipe rebounds until it reaches equilibrium and 30% of the axial strain remained in the pipe.

All studies mentioned above have pulled a pipe through a soil static mass to investigate the axial soil resistance. However, research has been performed where a soil mass is moved instead of the pipe itself. This method was used to study the behaviour of pipes crossing strike-slip faults using split box in the laboratory (Liu et al. 2022; Saiyar et al. 2015). At the time of writing, only one study has been published that moved soil mass along a fixed pipe to investigate axial pipe–soil shear resistance (Rostami et al. 2022). Rostami et al. (2022) investigated the influence of far-field effects in buried pipelines crossing reverse faults using a 1/10th scaled model setup. Reverse faulting was simulated using a split-box apparatus under 1g conditions. As soil displaces in the fault region, it causes bending locally (close to the fault), which leads to tension in the pipe far from the fault. In order to define the axial soil-spring force at far-field locations, they performed a pure axial pullout test in loose sand by moving the sand box. For the test, a model pipe made of copper with a 15 mm diameter was used to simulate a 60 mm diameter steel pipe. A soil box of 1.2 m long and roughly 0.4 m deep was bolted on top of a shake table. The pipe was fixed to a load cell at one end, with the other end free, and extending outside the box at the free end. To perform the test, the soil box was pulled along the pipe’s free end at a constant speed of 15 mm/min for a total displacement of 50 mm. The stiffness of the axial spring was calculated, which compared reasonably well with the value calculated using the ALA (2005) design equation.

A few experimental studies are also available in literature where a sand box is moved in a horizontal plane keeping the pipe fixed. For example, Ge et al. (2023) investigated the resistance to axial movements of subsea on-bottom pipelines by laboratory shear tests. The effect of pipe surface curvature on the interface friction coefficient was discussed through the comparison with

results in direct planar interface shear tests. Alafari et al. (2021) studied the effect of lateral ground movement on a high-density polyethylene (HDPE) pipe by pulling a soil box in the lateral direction. The central section of the cell was placed on rollers in a track, allowing movement perpendicular to the testing cell length. A manual winch attached via cable was used to facilitate movement. The pipe was restrained inside the box using steel clamps at each end. Soil pressure sensors were also placed at distinct locations along the length of the pipe to measure soil pressure during testing.

2.4 Numerical Modelling

To accompany full-scale testing, numerical methods are often employed to investigate many parameters that would otherwise be too onerous to test at full-scale. A few numerical studies on axial pipe–soil interaction are available in literature (e.g., Wijewickreme et al. 2009; Meidani et al. 2017, 2018; Al-Khazaali and Vanapalli 2019a; Murugathasan et al. 2021; Saberi et al. 2022; Reza and Dhar 2024). Wijewickreme et al. (2009) employed a 2-D continuum-based finite difference method, using FLAC 2D, to study the effect of soil dilation on the normal stress increase on the pipe. Note that the study did not simulate the most realistic 3-D axial pullout condition due to its high computational cost. Therefore, soil dilation of the shear zone was mimicked by radially expanding the pipe (0.7 to 1 mm) instead of simulating the pullout directly. The soil was modelled using hyperbolic stress–strain relations with a Mohr-Coulomb (MC) failure criterion, as described by Duncan and Chang (1970). The pipe was modelled using beam elements. The pipe–soil interface was modelled using unbonded interface elements employing the Coulomb shear strength criterion. Normal soil stresses were calculated from numerical

analysis after expansion of the pipe by the predefined amount of 0.7 to 1 mm and compared with the measurements.

Meidani et al. (2018) used the 3-D discrete-element method (DEM) to study the axial pipe–soil response of a steel pipeline buried in granular material. Experimental results reported by Wijewickreme et al. (2009) were used to validate the numerical model. Using the validated model, parametric studies were performed to evaluate the factors that contributed to the axial soil resistance to movement. Finally, an expression of earth pressure coefficient was proposed using a multivariate regression analysis of the results of the parametric study to accurately predict the axial soil resistance.

Murugathasan et al. (2021) investigated the mechanism of axial pipe–soil interaction using three-dimensional finite-element analysis in Abaqus. The axial pullout force of ductile iron pipe buried in dense and loose sand was simulated by validating experimental results. Solid eight-node reduced integration brick elements (C3D8R) were used for both the soil and the pipe. The surface-to-surface contact approach available in Abaqus was used to simulate the contact between the pipe and the soil. The analysis was performed in two steps: first, the self-weight of soil and pipe were applied in the gravity step, and then the pipe was displaced from one end with the opposite end kept free. The built-in elastic-perfectly plastic Mohr–Coulomb (MC) plasticity model was employed to model the stress–strain behaviour of the sand while the pipe was modelled as purely elastic. It was found that to successfully simulate test results for dense sand, an interface friction angle equal to 95% of the angle of internal friction of the soil was required. Likewise, to simulate testing in loose sand, an interface friction angle equal to 78% of the angle

of internal friction of soil was required. Normal stresses around the pipe increased during axial pullout when it was buried in dense sand while no significant change was noted for loose sand. Results of the analyses confirm that normal stress increases during axial pullout were due to soil dilation, resulting in a higher pullout resistance in dense sand.

Recently, Reza and Dhar (2024) employed three-dimensional finite-element (FE) analysis to examine the mechanism for buried medium-density polyethylene (MDPE) pipes under axial loads. The study revealed that the effect of shearing-induced soil dilation at the pipe–soil interface could be insignificant for MDPE pipes. The reason was attributed to the small volumetric strains developed on interface soil elements, causing changes in pipe normal stresses. During initial loading of the pipe, soil dilation due to shearing tended to increase normal pressures acting on the pipe; however, reductions in pipe diameter acted in the opposite manner. It was also found that compaction-induced horizontal stress can significantly influence the axial pullout resistance of shallow buried pipes. Lateral pressure due to compaction effects was calculated from Duncan and Seed (1986) and modelled using equivalent temperature loads. These loads utilized in a FE analysis were successful in simulating the measured pipe responses.

A further simplification can be made whereby soil elements are not modelled. Instead, the resistance offered by the soil is simulated using a series of discrete independent Winkler springs in each direction (axial, lateral and vertical). The pipe is also simplified, being represented by beam elements. This method, the beam-on-spring method, is recommended by ALA (2005) and PRCI (2009), whereby the springs are defined as elastic-perfectly plastic models. The maximum force capable of transmission from soil to pipe is governed by one of four

equations: axial, lateral, vertical upward and vertical downward (bearing). Various studies have utilized the beam-on-spring method mainly to understand the likelihood of damage to pipelines in landslide regions (e.g., Ni et al. 2018 and Saberi et al. 2022). Ni et al. (2018) studied the effects of transverse permanent ground deformations on continuous buried steel pipes. To do this, they developed a simplified 2-D Winkler-based numerical model in Abaqus where the pipe was modelled using pipe elements (PIPE31) and the soil simulated using pipe–soil interaction elements (PSI34). Both lateral and axial spring elements were considered, with the vertical direction ignored. Behaviour of these springs was defined using the ALA (2005) equations, with K_0 conservatively taken as one in Eq. 2-1.

Saberi et al. (2022) introduced a numerical approach using beam-spring-interface elements to study the axial pipe–soil interaction during cyclic displacement. Their approach, termed the Hybrid-Winkler-Interface (HWI) model, uses beam elements to represent the pipe, nonlinear springs to represent the surrounding soil, and a layer of very thin, solid elements to represent the pipe–soil interface. The soil-interface elements were defined using the bounding surface plasticity constitutive model as described by others using a user subroutine and four-noded quadrilateral elements. These elements were capable of simulating various complex behaviours at the pipe–soil boundary such as stress hardening and softening, cyclic stress degradation, dilation, stress stabilization and particle breakage among others. Meanwhile, the soil-springs were defined using ALA (2005). The intent of the model was to simulate the stresses at the crown, springline and invert on a buried pipe subjected to cyclic axial movement.

2.5 Summary

Understanding the behaviour of buried steel pipes undergoing relative axial movement is an important endeavor as landslides, earthquakes, faults and other ground movement events have the ability to transfer axial force to buried pipelines in their vicinity. To this end, current pipeline design guidelines recommend an approach to estimate the peak force transferred from soil to pipe during relative ground movements. To date, various studies have been performed investigating the behaviour at the pipe–soil interface by pulling a pipe through a static soil mass. It has been shown that the relative density of soil greatly affects the pullout force. Further, the moisture content of cohesionless soil has also been shown to impact the pullout force via matric suction, with unsaturated soil provided two times more resistance to pullout than saturated ones. However, all the previous studies were performed using a testing setup that pulled a pipe through a soil mass and did not investigate the reverse; whether a difference exists if the soil is moved along a fixed pipe.

Soil normal stresses have also been captured during pipe pullout testing using pressure transducers situated on the pipe surface. From this, it has been shown that normal stresses increase during pipe movement due to shear-induced soil dilation. This effect is prevalent in steel pipes, however, reduces significantly in flexible pipes due to pipe diameteric reduction. Attempts have been made to incorporate this behaviour by increasing the lateral earth pressure coefficient used in guidelines, though this has not been successful in all burial condition. The effect of non-continuous pipe pulling on axial pullout has also been studied briefly; however the effect is not greatly understood. There is evidence that up to 30% of strains are “locked-in” even after pulling

load is removed however these findings are presented specifically for PVC piping, further testing on alternate pipe materials is recommended.

Lastly, to accompany full-scale testing, numerical analysis is often performed allowing for a deeper look at the parameters involved and their role. Various numerical modelling techniques have been used in analyses, such as three-dimensional continuum finite-element model and Winkler beam-on-spring model. The continuum model has the advantage of being able to simulate direct contact between pipe and soil, however is very complex and computationally expensive. Instead, Winkler beam-on-spring models can be developed to estimate the maximum soil resistance achieved during pipe or soil movement. The soil spring load-displacement responses are usually defined using existing guideline equations, however as mentioned previously, the equations set out in the guidelines do not adequately predict the maximum forces in all cases. This highlights a further need to study the pipe–soil interface.

2.6 References

- ALA (American Lifelines Alliance) 2005. *Guidelines for the design of buried steel pipe*. Washington, DC and Reston, VA, USA: Federal Emergency Management Agency (FEMA) and American Society of Civil Engineers (ASCE).
- Alarifi, H., Mohamad, H., Nordin, N. F., Yusoff, M., Rafindadi, A. D. U., and Widjaja, B. 2021. A large-scale model of lateral pressure on a buried pipeline in medium dense sand. *Applied Sciences*, 11(12): 5554.

- Ali-Khazaali, M., and Vanapalli, S. K. 2019. Axial force-displacement behaviour of a buried pipeline in saturated and unsaturated sand. *Géotechnique*, 69(11): 9861003.
- Banushi, G., and Squeglia, N. 2018. Seismic analysis of a buried operating steel pipeline with emphasis on the equivalent-boundary conditions. *Journal of Pipeline Systems Engineering and Practice*, 9(3): 04018005.
- Duncan, J. M., and Seed, R. B. 1986. Compaction-induced earth pressures under K 0-conditions. *Journal of Geotechnical Engineering*, 112(1): 1–22.
- Duncan, J. M., and Chang, C. Y. 1970. Nonlinear analysis of stress and strain in soils. *Journal of the soil mechanics and foundations division*, 96(5): 16291653.
- Hardin, B. O., and Black, W. L. 1966. Sand stiffness under various triaxial stresses. *Journal of the Soil Mechanics and Foundations Division*, 92(2): 27–42.
- Ge, B., Martin, G., Dietz, M. S., Mylonakis, G., and Diambra, A. 2023. A novel pipe-segment shear test apparatus: Polypropylene pipe behaviour over sand beds vs element interface tests. *Canadian Geotechnical Journal*, (ja).
- Janbu, N. (1963). Soil compressibility as determined by oedometer and triaxial tests. In *Proceedings, European Conference on Soil Mechanics and Foundations Engineering, Wiesbaden, Germany 1963 (Vol. 1, pp. 19–25)*.
- Liu, W., Huang, C., Zhang, S., and Song, Z. 2022. Centrifuge tests of large-diameter steel pipes crossing strike-slip faults. *Engineering Structures*, 279: 115124.
- Matymish, J., Moore, I. D., Woods, J. E., and Hault, N. A. 2023. Axial Pullout Behaviour of Fusible PVC Pipes and Fusion Weld Joints Assessed using Distributed Fibre Optic Sensors. *Canadian Geotechnical Journal*, (ja).

- Meidani, M., Meguid, M. A., and Chouinard, L. E. 2018. Estimating earth loads on buried pipes under axial loading condition: insights from 3D discrete element analysis. *International Journal of Geo-Engineering*, 9: 1–20.
- Morshed, M. A., Roy, K., and Hawlader, B. 2020. Modeling of buried pipelines in dense sand for oblique movement in vertical–lateral plane. *Journal of Pipeline Systems Engineering and Practice*, 11(4): 04020050.
- Muntakim, A. H. and Dhar, A. S. 2021. Assessment of Axial Pullout Force for Buried Medium-Density Polyethylene Pipelines. *Journal of Pipeline Systems Engineering and Practice*, 12(2):04020074.
- Murugathasan, P., Dhar, A. S., and Hawlader, B. C. 2021. An experimental and numerical investigation of pullout behavior of ductile iron water pipes buried in sand. *Canadian Journal of Civil Engineering*, 48(2): 134–143.
- Ni, P., Mangalathu, S., and Yi, Y. 2018. Fragility analysis of continuous pipelines subjected to transverse permanent ground deformation. *Soils and Foundations*, 58(6): 14001413.
- PRCI (Pipeline Research Council International). 2009. *Guidelines for constructing natural gas and liquid hydrocarbon pipelines through areas prone to landslide and subsidence hazards*. Report prepared for the Design, Material, and Construction Committee. Chantilly, VA: Pipeline Research Council International, Inc.
- Reza, A. and Dhar, A.S. 2024. Finite-element modelling of axial movements of polyethylene pipes in dense sand, (under review).
- Reza, A., and Dhar, A. S. 2021. Axial Pullout Behavior of Buried Medium-Density Polyethylene Gas Distribution Pipes. *International Journal of Geomechanics*, 21(7): 04021120.

- Rostami, H., Osouli, A., and Kumar, S. 2023. Experimental modeling of far-field effects in buried pipelines subjected to reverse faulting. *Soil Dynamics and Earthquake Engineering*, 164: 107561.
- Saberi, M., Annan, C.D. and Sheil, B.B. 2022. An efficient numerical approach for simulating soil-pipe interaction behaviour under cyclic loading. *Computer and Geotechnics*, 146, 104666.
- Saiyar, M., Moore, I. D., and Take, W. A. 2015. Kinematics of jointed pipes and design estimates of joint rotation under differential ground movements. *Canadian Geotechnical Journal*, 52(11): 1714–1724.
- Sheil, B. B., Martin, C. M., Byrne, B. W., Plant, M., Williams, K., and Coyne, D. 2018. Full-scale laboratory testing of a buried pipeline in sand subjected to cyclic axial displacements. *Géotechnique*, 68(8): 684–698.
- Wijewickreme, D., Karimian, H., and Honegger, D. 2009. Response of buried steel pipelines subjected to relative axial soil movement. *Canadian Geotechnical Journal*, 46(7): 735–752.
- Weerasekara, L., and Wijewickreme, D. 2008. Mobilization of soil loads on buried, polyethylene natural gas pipelines subject to relative axial displacements. *Canadian Geotechnical Journal*, 45(9): 1237-1249.

CHAPTER 3: Laboratory Investigation of Buried Small-Diameter Steel Pipes Subjected to Axial Ground Movement

3.1 Abstract

Small-diameter steel pipes are often used for the distribution of gas to residential homes. These pipelines must service the end-user, even if located in landslide-prone areas, necessitating the study of their response to ground movements. Many studies were conducted in the past by pulling a pipe through a static soil mass to investigate the behaviour of pipe subjected to axial ground movements. However, in a real landslide, the soil mass moves applying force to the pipe, restrained by stable ground. Soil movement may happen intermittently in a given direction with varying times of little change. The effects of soil movement around a restrained pipe are believed similar to that of pulling a pipe through static soil. A test facility was designed at Memorial University of Newfoundland, where a soil mass is pulled around a buried pipe fixed at one end, simulating the condition expected during ground movement. This paper presents the results of a test program undertaken using the test facility to investigate steel pipes subjected to axial ground movements. Pipes of different diameters (26.7, 60.3, and 114.3 mm) were buried in dense sand inside a moveable steel tank, they were anchored at one end and free at the other. The tank was pulled at a constant rate for multiple pulling phases and was held in place for varying times between each pull to investigate stress relaxation during ground movements. The cycle was repeated multiple times before pushing the tank back to its original position. Pipe axial force, axial strain and tank displacement were recorded during the tests. Results showed that axial force was higher during soil pulling than pipe pulling, particularly when normalized based on pipe burial depth, diameter, length and soil unit weight. No reduction of axial force was observed during relaxation period. The maximum axial force was found to reduce with repeated cycles of

ground movements due to the soil's critical state being reached. Measurements of axial strains along the length of the pipe indicated negligible pipe elongations during testing.

3.2 Introduction

Buried pipelines are essential to urban infrastructure, transporting oil, gas and water to residential and commercial properties. Typically, distribution lines connecting to the final destination, sometimes termed the “last mile,” are the smallest in the pipe network. Some case histories have been documented in different countries in which these pipelines have been adversely affected by permanent ground deformations due to landslides, ground subsidence, and earthquakes (Kishawy and Gabbar 2010; Weerasekara and Rahman 2019; Veseghi et al. 2021; Weerasekara et al. 2023). As many properties are developed within landslide and earthquake-prone areas, pipelines must be placed in these zones and designed to withstand such conditions. For these reasons, it is important to understand the pipe–soil behaviour during ground movement events. Previous studies available in the literature to understand the behavior of pipes undergoing permanent ground deformation can be categorized based on the position of the pipes relative to the direction of the ground movements. Many of them focused on the consequences of an axial ground movement where the pipes were buried parallel to the direction of the ground deformation. Rajani et al. (1995) developed two approaches for predicting the pipe loads for pipelines experiencing longitudinal ground movement: the limit equilibrium approach and the force–displacement approach. The limit equilibrium approach calculates the maximum axial load on a pipeline at the interface of moving–nonmoving soil masses, considering the failure takes place along a soil–soil interface and there is no slip between the soil and the pipe. The force–displacement approach estimates the net force at the moving–nonmoving soil mass interface by

examining the ongoing soil–pipe interaction resulting from the developed soil displacements. Current pipe design guidelines, such as ALA (2005) and PRCI (2009), recommend a similar pipe–soil interaction model as the force–displacement approach in Rajani et al. (1995) to estimate the ultimate axial soil resistance per unit length of the pipe. Elastic-perfectly plastic axial springs was proposed in the design guidelines to represent the surrounding soil. The axial spring’s maximum force can be calculated from the laboratory testing either pulling the pipes through static soil masses or displacing the soil masses around an anchored pipe.

Over the last few decades, many studies have been performed to evaluate the recommendations in the design guidelines for calculating the axial soil resistance for rigid pipes (mostly steel pipes) in different ground conditions. For example, Murugathan et al. (2021), Al-Khazaali and Vanapalli (2019), Sarvanis et al. (2017), Sheil et al. (2018), Bilgin and Stewart (2009), and Wijewickreme et al. (2009) have investigated axial pipe loading by pulling a pipe from one end, while keeping the other end free, in a large-scale soil box. Common findings were mentioned in all the studies, where the peak pullout forces in loose sand were predicted well using the pipe design guidelines; however, these guidelines underpredicted the behaviour in dense sand. Wijewickreme et al. (2009) proposed a new parameter K , an equivalent lateral earth pressure coefficient, instead of lateral earth pressure coefficient at-rest (K_0) in the design equation to account for the higher normal stress on the pipes in dense sand (because of shearing induced dilation at the pipe–soil interface). Sheil et al. (2018) investigated cyclic motion by pulling, then pushing, a large-diameter steel pipe through loose and dense soil, simulating thermal expansion and contraction during seasonal temperature changes. Results showed that peak force increased continually with loose sand, while dense sand weakened with repeated

cycles. They also highlighted shortcomings with ALA and PRCI guidelines, which neglect pipe self-weight, and simplify the normal stress distribution around the pipe in the calculation of the maximum axial soil resistance. Al-Khazaali and Vanapalli (2019) conducted experiments on saturated and unsaturated sand, concluding that matrix suction in unsaturated sands can greatly impact axial soil resistance. Those forces were 2.5 times greater than forces developed in the saturated condition. It is worth pointing out that all the studies assume that pipes in the unstable soil mass will behave similarly to those in the stable mass (i.e., symmetrical behavior about the moving–nonmoving soil interface). However, the soil in the stable mass may be different from that in the sliding mass.

Some studies have investigated the effects of moving soil on a static pipe; Oskouei et al. (2019) and Jalali et al. (2016) focus on soil bearing and pipe bending created during fault movements; both conducted full-scale testing on varying diameters of steel pipes in sandy soil. Oskouei et al. (2019) simulated strike-slip faulting by burying pipes of 19–, 63.4–, 88.9– and 168 mm diameters in two large steel boxes, fixing one and moving the other laterally left and right. Jalali et al. (2016) tested 114.3- and 168.3-mm diameter pipes buried in an 8.5 m testing box. Hydraulic actuators moved half of the soil box vertically at a 45-degree while maintaining the other half fixed to simulate reverse faulting. Pipe strain and movement were measured in both cases. Normal fault movement has also been well-researched, including Zhou et al. (2019) and Ni et al. (2018), while Demirci et al. (2018) examined reverse-faulting movement. HDPE piping was tested by Zhou et al. (2019), PVC by Ni et al. (2018) and model pipes made of aluminum and brass alloys tested by Demirci et al. (2018). The specifics of each testing programme differ, though the underlying principle remains that a split box moves one portion of

soil vertically (up or down), inducing stress, strain and displacements on the pipe. Soil movement laterally against a pipe has also been performed, such as by Alarifi et al. (2021). In their large-scale experiments, a 3 m long, 1 m wide and 1.6 m deep soil box was constructed to house a 3 m long, 90 mm diameter, high-density polyethylene (HDPE) pipe, supported on each end. Five earth pressure sensors were attached to the pipe surface to measure the variation in soil pressure along the pipe during soil box movement. The middle segment of the soil box was connected to a winch and supported on wheels in a track, allowing the center to displace laterally while keeping each end stationary and stable. The main objective of the research was to obtain lateral soil pressures along the length of an HDPE pipe during lateral ground movement. Others, such as Robert et al. (2016), have applied soil displacement to steel pipes in the lateral orientation. A 114.3 mm diameter pipe was buried in Chiba sand within a testing cell capable of movement. The pipe was connected to a load cell using a steel cable. As the tank moved, the soil applied pressure on the pipe and the load on the pipe was transferred through the tension in the cable and measured in the load cell. Yoshizaki et al. (2003) investigated a different scenario: a steel pipeline with an elbow connection was anchored at both ends while a soil box was pulled around it, simultaneously creating axial and lateral conditions. The 100 mm diameter pipe was buried at a depth of 0.95 m from surface to springline. The shorter length of pipe that underwent axial loading was 5.4 m, while the longer leg that developed lateral loading was 9.3 m. Although axial and lateral conditions were tested in this research, the main objective was to quantify the effect of permanent ground deformations on pipe-elbow connections. Overall, it can be said that neither study directly examines the axial soil displacement alone by pulling it.

At the time of writing, only one published literature outlined similar testing to the current test programme, Rostami et al. (2023). Their primary goal was to investigate the effects of soil–pipe interaction at far-field locations of pipelines crossing reverse faults. To do this, they constructed a split box with a stationary segment 180 cm long and a moving segment 60 cm long, which was raised at an angle using a hydraulic ram. A 1.5 cm copper pipe was used in the setup as a model, and scaling factors were applied to simulate the response of a steel pipe. Different pipe end conditions were set up to test the effect of far-field fixity, including vertical roller with unrestrained horizontal motion, vertical spring with restrained horizontal motion, and both vertical and horizontal springs. In the latter case, they performed a moving-soil test (where pipe was fixed at one end) to determine the pullout resistance of soil at the far-field location, as reverse fault movement locally will cause axial load on the pipe at far-field locations. The pullout resistance found was used to calibrate the stiffness of axial spring. Their testing parameters differed greatly from the current test programme, using a 1.5 cm diameter copper pipe buried 15 cm deep in a 120 cm long box and moving at a rate of 15 mm/min, scaled to simulate a steel pipe. They did not investigate intermittent soil movement cycles or the behaviour between movement events, nor did they include different diameters.

Despite its real-world application, there is limited research concerning the effect of non-continuous soil movement on buried pipelines. Wood Environment & Infrastructure Solutions (2021) collected ground movement data in the town of Quesnel, BC, over the course of 22 years and compiled their findings in a report for the town titled Monitoring Report 2020. Data from various GPS hubs and slope inclinometers are presented in the report. The data shows ground movement may occur in small bursts relatively close together or in larger single events further

spaced. The pipe and soil may relax between each intermittent movement, redistributing the stresses created on the pipe and resulting in a reduction of resistance and strain. Furthermore, not every movement event will shift in the same direction, though overall movement may trend in a particular direction. Once multiple non-continuous ground-movement events have occurred, the soil-pipe bond will undoubtedly have been disturbed and weakened. It is of interest to investigate the force generated during this condition to understand the full picture of soil-pipe interaction. Therefore, the research discussed herein attempts to close gaps in knowledge regarding the effects of the following on buried small-diameter steel pipes: a) non-continuous soil movement, b) relaxation period and c) soil push-back (in disturbed soil conditions).

This paper presents the results from a novel testing facility developed at Memorial University of Newfoundland, where a soil mass can be moved at a fixed rate along a pipe fully restrained at one end and unrestrained at the other. The axial force transferred from soil to pipe via the pipe-soil interaction was investigated, measuring the load at the pipe's fixed end and the strain along the pipe's full length. Multiple pipe sizes are considered in these tests, including 26.7-, 60.3-, and 114.3 mm outside diameter. The main objective is to confirm whether displacing the soil is comparable to pulling the pipe, as is widely performed, with a further aim to examine the effect of pipe diameter. In addition, successive soil pulls have been conducted, with relaxation periods between them, to observe pipe behaviour during simulated consecutive ground movement events.

3.3 Testing Methods

3.3.1 Apparatus

The testing facility was developed at Memorial University of Newfoundland by retrofitting an existing setup designed to pull a pipe through a static soil mass. The previous configuration was constructed to pull a pipe through a static soil mass, as reported in Murugathan et al. (2021), Reza and Dhar (2021ab), and Reza et al. (2023). The new setup was created to anchor the buried pipe while moving the soil tank (see Fig. 3-1). The setup consists of a 4.8 m base frame bolted to the floor and braced against the hydraulic ram's reaction frame, on which a 4.0×2.0 m ($L \times W$) carriage frame is placed. Six linear bearings (three along each side's length) are mounted on tracks between the carriage and base frame. The linear bearing tracks were bolted to the base frame, with the carriage bolted to sliding blocks, facilitating a virtually frictionless movement system. A 4.0×2.0×1.5 m ($L \times W \times D$) reinforced steel soil tank is then welded to the top of the carriage. Support arms are welded to the tank, as seen in Fig. 3-2(a), which connects the shaft of the hydraulic ram to the setup, allowing for movement up to 150 mm. The carriage has a travel limit of up to 300 mm, allowing for future development. To facilitate pipe entry through the tank, a 177 mm hole is cut into both tank walls, while two gasket plates, one steel and one rubber, are bolted over each hole. Each set of gaskets are sized corresponding to a specific pipe diameter. The rubber gaskets have a centre hole 3 mm larger than the pipe diameter, allowing for instrumented or non-instrumented pipe entry. Center holes of the steel gaskets are larger than those of the rubber gaskets to reduce the effects of any tank boundary conditions caused by the stiff walls. In addition, the rubber gaskets were used to reduce pipe–tank friction produced during tank movement. The pipe is pushed into the tank from the ram end, resting on a soil bed prepared to the desired condition. A sizeable vertical channel is welded vertically on the frame's

backstop with holes drilled in a rosette pattern securing a 22 kN (5,000 lb) capacity pancake load cell for use with the smallest pipe or an 88 kN (20,000 lb) capacity pancake load cell for the larger sizes. A custom-built connector is attached to the load cell at one end, with a clevis connection joining the pipe at the other, linking the pipe with the load cell. A photo of the connector attachment is shown in Fig. 3-2(b). A steel plate with a tab was welded to one end of each pipe to facilitate the clevis connection. The tab was fitted between the ears of the connector and was secured in place using a bolt of appropriate size as a shear pin. The other end of the pipe remains unrestrained, while a linear variable displacement transducer (LVDT) has been set up to measure pipe elongation (Fig. 3-2(a)).

To fill the tank with soil, an overhead crane of 10 T capacity was used to lift large sandbags, which were then emptied into the tank. The soil was placed in roughly 100 to 150 mm lifts and then compacted using a Wacker Neuson 1135e battery-powered vibratory plate tamper to obtain the required density of 18 kN/m^3 . To ensure the appropriate density conditions are met, sand-cone replacement tests are performed at the surface level prior to testing as per ASTM D1556 (2016).

3.3.2 Backfill Material

The backfill material used during testing was locally manufactured sand, classified as well-graded sand (SW) based on the Unified Soil Classification System (USCS). The soil contained a fines content of 1.3% and gravel content of 0.87%. The mechanical properties of the sand were determined earlier by conducting direct shear and triaxial tests at various normal stresses (Saha et al. 2019, 2020). At the stress level expected for the pipe based on the chosen soil density, the

internal angle of friction, ϕ' , and peak dilation angle, ψ_p , of the soil can be taken as 42° and 12° , respectively. Table 1 lists the backfill soil characteristics. The maximum dry unit weight of the sand is 18.8 kN/m^3 based on standard Proctor compaction tests (ASTM D698-12, 2021). Moisture content during the testing was limited to 3%, as this was not expected to contribute significantly to the axial pullout force obtained as per Saha (2021), who reported that suction force due to moisture content at that level has a negligible effect on the pipe–soil interaction.

3.3.3 Pipe Instrumentation

A fibre-optic strain sensor system was used on the pipes during the testing to capture detailed and continuous strain information along the length of the pipe. Fig. 3-3 shows the fibre-optic sensor and accompanying equipment used. The strain setup includes a multi-channel sensing platform by Luna Innovations Inc. called an optical distributed sensor interrogator (ODiSI), a laptop controller, a 10 m standoff cable, a remote module, and a fibre-optic strain sensor of 5 m length. As per Luna Innovations Inc. (2020) User Guide, the ODiSI system operates using “an optical frequency domain reflectometry (OFDR) technique to interpret the signal from the fibre optic sensors.” A laser is generated and shone through fibre-optic cabling to the end of the sensor, where there is a termination, which reflects the light to the sensing platform. Based upon the amount of light that has been reflected, differing due to backscatter, the system computes the amount of strain in the sensor and, thus, in the item it is bonded to.

Luna Innovations Inc. (2017) ODiSI Fiber Optic Sensor Installation Guide describes the recommended procedure for adhering a fibre-optic sensor to a material; first, the surface should be cleaned using an alcohol wipe and sanded with coarse, then finer, sandpaper. After sanding,

the material should be cleaned again before the strain sensor's path is laid out. The sensor must be temporarily held down using a Kapton dot every 300 mm, with a polyurethane epoxy applied to each end, anchoring the sensor in place. Once the epoxy has cured, a catalyst is applied between Kapton dots to speed up the curing process, and a cyanoacrylate adhesive is carefully spread to bond the sensor to the surface. After bonding, a thin layer of silicone caulking is added, protecting it from separation during testing and from rupture during soil compaction. An added safeguard against sensor failure not included in Luna's installation guide, sheathing tape was placed over the caulking to help prevent tearing of the sensor. This technique was used by Matymish et al. (2023) with success and was adopted here after multiple sensor failures before test completion. Fig. 3-4 shows photos of the pipe during various stages of instrumentation.

During testing, the ODiSI's gauge pitch was set to 2.6 mm, and the collection trigger was set to 2 data points every 1 second. Thus, the system was set to collect a strain reading every half second at 2.6 mm increments along the pipe. The fibre optic strain sensor has a strain limit of 3%; however, the system can only calculate strain up to 1.5%. It should be noted that a tare of sensor data was created before Pulling Phase 1 (described in the Test Programme section) of each test to ascertain that the strain induced solely by soil movement was captured.

3.3.4 Test Programme

The results presented in this paper cover six separate pipe tests. Three differing diameters were tested, 26.7–, 60.3– and 114.3 mm, where one pipe of each diameter was instrumented with a fibre-optic sensor and one left bare. All pipes tested were schedule 40 (SCH40) steel pipes with a

yield strength of 310 MPa or greater. Table 3-2 shows test names and associated testing parameters.

Tests ST-01 through ST-04 were performed using 650 mm burial depth, from top surface to pipe springline, while ST-05 and ST-06 were buried about 625 mm due to material quantity limits. Tests ST-04 and ST-06 had sheathing tape applied over the caulking to protect the instrumentation further, while ST-02 did not include tape. A pulling rate of 0.5 mm/min was chosen to simulate the speed of moderately slow moving landslides expected in the field. Cruden and Varnes (1996) presented a modified scale of landslide velocity classes, where slides between 0.005 and 0.5 mm/s (0.3 to 30 mm/min) are categorized as class 4 (moderate) slides. A higher pulling speed is not expected to produce different results due to steel being a strain-rate-independent material. However, moving the entire soil mass at a faster rate may cause shear stresses to peak faster, culminating in lower peak force developed in the pipe. The soil tank was moved by 35 mm at 0.5 mm/min to perform all tests. Once the tank reached the desired displacement of 35 mm (termed herein as Pulling Phase 1), the ram was stopped, and its position held constant for a given time, allowing the pipe and system to relax. After this, soil tank pulling continued until 70 mm of displacement was reached (termed herein as Pulling Phase 2) after which another relaxation period ensued. For tests ST-01 and ST-02, a third displacement phase continued up to 105 mm (termed herein as Pulling Phase 3), followed by another relaxation period. Finally, once all displacement phases for the given test were completed, the soil tank was pushed back to its original location. During each test, the axial load developed in the pipe was measured using a load cell at the fixed end. The load and the ram's displacement were recorded

using a Data Acquisition System (DAQ) running the Signal Express software. Strain distribution in the pipe was measured by the ODiSI system for instrumented samples.

3.4 Test Results

3.4.1 Load-displacement responses

Fig. 3-5 shows the force–soil displacement curves for each of the six tests, categorized by outside diameter and instrumentation status. Note that the axial soil forces shown in the figure are the shearing forces offered by the interface soil during tank displacement. It can be seen that the pipe diameter and instrumentation status both affect the peak force (i.e., full shear strength of the soil along the pipe length) developed in the pipe. Beyond the peak value, the pulling force on the pipe is slightly reduced or remains the same as the peak shearing resistance of the interface is reached. For the 26.7 mm diameter pipes (ST-01 and ST-02), the peak resistances were roughly 13 kN each, while for the 60.3 mm pipes (ST-03 and ST-04), the peak resistances were approximately 21 kN. Finally, the largest diameter, 114.3 mm, develops a peak force of 40 kN bare (ST-05) and 30 kN instrumented (ST-06). Table 3-3 shows the peak value reached by each test at the corresponding soil displacement. Although not anticipated, a potential reason for the same peak forces in 26.7 mm-diameter pipe tests (ST-01 and ST-02) could be that the shear failure occurred between soil particles surrounding the pipes instead of the pipe–soil interface. This does not happen with the other pipe diameters tested due to their larger size. The 25% decrease in peak force generated between tests ST-05 and ST-06 can be attributed to the use of polypropylene sheathing tape to further protect the fibre-optic sensor from frictional forces. The sheathing tape was smooth with a lower friction coefficient than the steel pipe. However, test ST-04 developed a peak load nearly equal to that of ST-03 despite the inclusion of sheathing tape

in the former. One possible reason may be that the reduced frictional coefficient of the sheathing tape counteracts the frictional resistance offered by an added ridge along the surface of the 60-mm diameter pipe due to the thickness of sensor application and caulking. The approach to cover the caulking with sheathing tape was adopted after sensors used in ST-02 and a previous trial of ST-04 were damaged following Pulling Phase 1 had concluded. The previous trial of ST-04, with no sheathing tape applied to the caulking, developed a peak force of roughly 24 kN (not shown in the figure). By applying the sheathing tape, the frictional increase from the caulking was essentially eliminated. Frictional increase in soft pipe material due to sand particle penetration was discussed by Scarpelli et al. (2003). Therefore, it can be assumed that the same phenomenon is applicable here since silicone caulking is more pliable, less stiff, and softer than steel. Another observation when comparing the bare and instrumented 26.7 mm pipe curves is that the instrumented curves have a slightly higher initial slope, indicating a more significant increase in force per soil displacement, likely due to the increased frictional coefficient of the caulking (without the application of sheathing tape). The other two sets of curves do not show this trend, whereby the initial slope of the bare pipes is nearly equal to the instrumented pipes.

Fig. 3-6 plots the non-dimensional force N_a against soil displacement for each test, again identified by pipe diameter and instrumentation. The force is normalized based on individual pipe diameter, burial depth, burial length, and soil density according to Eq. (3-1), as below.

$$.N_a = \frac{P}{\gamma' \pi D H L} \quad (3-1)$$

Where P is the pullout force developed in the pipe, γ' is the effective unit weight of soil, D is the pipe outside diameter, H is the burial depth from the pipe from surface to springline, and L is the buried length of the pipe. When normalized, the 26.7 mm pipes have the highest force at roughly

3.2, followed by the 60.3 mm pipes with about 2.4 for both instrumented and bare cases, and finally, the 114.3 mm pipes with 2.4 for bare and 1.6 for instrumented pipes. The larger normalized forces for smaller pipes compared to larger pipes indicates a higher interface frictional resistance for the smaller pipes. Note that shearing-induced dilation of the interface soil can increase the friction resistance. According to the elastic cavity expansion theory, the normal pressure increases on the pipe due to soil dilation is inversely proportional to the pipe diameter (Boulon and Foray 1986; Johnston et al. 1987) and therefore, the dilation-induced increase of frictional resistance can be higher for smaller pipes. A similar observation was found from numerical modelling performed by Meidani et al. (2018) and experiments with MDPE pipes (Reza et al. 2023). In addition, at a buried depth of 650 mm, a pipe of 26.7 mm diameter had a soil cover (distance from surface to pipe crown) of 636.7 mm, while a pipe of 114.3 mm diameter had a less soil cover of 592.9 mm. This increased cover for smaller diameter pipes, which may further restrain the thin soil layer around the pipe to dilate, causing higher normal loads on the pipe.

3.4.2 Comparison of Axial Forces

This section compares axial soil resistances between soil mass movement and pipe pullout tests. To the best of the authors' knowledge, no axial pullout tests are currently available in literature with the pipe diameter used in this study. Therefore, the normalized test results for tests ST01–06 have been compared with tests available in literature, as shown in Fig. 3-7. Note that the test geometry and soil conditions in literature sources also differ from those used in the present study; refer to Table 3-4 for a comparison of parameters. The nondimensional peak axial forces,

calculated using ALA (2005) and PRCI (2009) guidelines, are also included in the figure based on Eq. (3-2).

$$\frac{P_u}{\gamma' \pi D H L} = \frac{K_0 + 1}{2} \tan \delta \quad (3-2)$$

Where K_0 is the at-rest lateral earth pressure coefficient for the soil, and δ is the interface friction angle between the pipe and surrounding soil (equal to the pipe's coating-dependent factor times the friction angle of soil, ϕ). Note that PRCI (2009) recommends K (effective coefficient of lateral earth pressure) of 2 instead of K_0 in Eq. (3-2) for dense dilative soils. Values of $K_0 = 0.5$ and $K = 2.0$ were used during the comparison in Fig. 3-7.

When test results are normalized, see Fig. 3-7, the peak axial forces developed during pipe pull from literature are considerably lower than those produced by soil pull conducted in the current study. The highest being the pair of 26.7 mm pipe tests at ~ 3.2 , followed by both 60.3 mm pipe tests and the bare 114.3 mm at ~ 2.4 . The lowest of the current testing programme is the instrumented 114.3 mm pipe test at about 1.6. Both Murugathasan et al. (2021), who pulled a 178 mm diameter pipe, and Wijewickreme et al. (2009), who pulled a 457 mm diameter pipe, produced peak forces of roughly 0.95. The next lowest results are those from Bilgin and Stewart (2009) and Sarvanis et al. (2017), with a normalized peak force of around 0.65. Bilgin and Stewart (2009) tested a pipe of 175 mm diameter, while Sarvanis et al. (2017) used 219 mm diameter. The lowest normalized peak forces were developed by the 350 mm diameter pipe tested by Sheil et al. (2018) at 0.46. Peak forces calculated from the ALA (2005) guideline, using parameters corresponding to the current testing programme, equate to about 0.5 when normalized, lower than most current programme and literature results. Whereas, when a K -value of 2.0 is used, per PRCI (2009), the normalized peak force increases to just over 1.0, which

better predicts the forces from Murugathasan et al. (2021) and Wijewickreme et al. (2019), however, significantly unestimates the normalized results presented for the tests conducted herein. Each compared literature source used the pipe-pulling method and tested a larger diameter pipe than the present programme. The latter may also have contributed to the large difference seen in the figure. According to the elastic cavity expansion theory, the increase of normal stress on the pipe due to soil dilation is expected to be less for large diameter pipes (Johnston et al. 1987, Luo et al. 2000). This means that the higher normalized resistances of the current tests for the small diameter pipes in dense sand may be attributed to the higher soil dilation around the pipe. From discrete-element modelling study, Meidani (2018) also found that the increase in normal stress around a pipe during pullout decreased with increased pipe diameter. Finally, it can be said that both the soil pulling mechanism and small diameter pipes in this study yielded higher normalized pullout loads compared to the others available in literature.

3.4.3 Force-Time and Relaxation Response

Fig. 3-8 plots the axial force variation with time for tests ST-01 and ST-06 during loading and relaxation phases. In Fig. 3-8(a), Pulling Phase 1 (0–35 mm tank displacement), shown by a light blue line, starts at 0 kN, spikes quickly to ~13 kN and then decreases, leading to the orange line of Relaxation Phase 1 (no displacement of the tank). The first relaxation phase holds steady at 4 kN over the full ~72-hour period as a residual force on the pipe. Pulling Phase 2 (35–70 mm tank displacement), indicated by a purple line, starts just above 4 kN in force, increases quickly to about 12 kN, then back down to just under 4 kN for the start of Relaxation Phase 2 (again no displacement of the tank). The second relaxation phase, plotted in red, stays consistent at just under 4 kN for its 24-hour duration, leading to Pulling Phase 3 (70–105 mm tank displacement),

plotted in dark blue. This pulling phase starts close to 8 kN, peaks at just over 10 kN, and then decreases rapidly to the final relaxation phase, plotted in a dark yellow. Relaxation Phase 3 lasts around 12 hours, with the force recorded consistent at around 4 kN. Once the final relaxation phase is completed, the tank is pushed back to the starting position, shown by the green line. The force developed during the pushing phase quickly decreases, reaching a minimum close to -1 kN, indicating a compressive force on the pipe. The load does not decrease further than this as the bond between the soil and pipe has already been broken due to the previous pulling phases. Looking at the results presented by Sheil et al. (2018), a similar curve was plotted during the push-back of each cycle, as depicted in the pushing phases shown in Fig. 3-8, confirming the occurrence of this behaviour in both the pipe and soil pulling. Nevertheless, asymmetric pulling-pushing phase displacements in the current study seem to produce dissimilar peak forces, as Sheil et al. (2018) obtained peak forces of similar magnitude (yet opposite sign). They also noted that changes in peak axial resistance were minimal after five loading cycles. However, Sheil et al. (2018) considered 20 mm of pipe displacement for each cycle, whereas 70 mm of total soil displacement was considered for the presented testing programme (105 mm for tests ST-01 and ST-02). The effects of successive pulling on axial resistance are discussed in the following section. Note that the dashed lines shown in Fig. 3-8(a) between the pulling and relaxation phases have been added for plot continuity and were necessary due to loading and unloading events too fast for data to be captured. As the relaxation periods extended overnight, the hydraulic system was shutdown prior to each relaxation period for safety reasons.. Since the hydraulic pump did not pressurize the system, no pressure held the ram cylinder (or soil tank) in place, meaning no restraining force was maintained on the pipe by the soil during this time, causing quick unloading. The opposite effect occurred when transitioning from a relaxation

phase to a pulling phase, whereby the hydraulics were pressurized, causing sudden tension in the system, transferring force from soil to pipe.

Fig. 3-8(b) (for test ST-06) shows identical behaviour during Relaxation Phase 2 for the reasons previously mentioned. However, Relaxation Phase 1 differs as the hydraulic system remained on, maintaining ram loading on the tank. The 2 kN increase in load during this period was caused by ram movement of about 0.5 mm due to system capabilities. After this movement, the load remained consistent. Reversed relaxation period timings for test ST-06 are also indicated in Fig. 3-8(b), when compared to Fig. 3-8(a) for ST-01, whereby Relaxation Phase 1 was performed for two hours and Relaxation Phase 2 continued, with the hydraulic system off for a 24-hour period. In contrast, during test ST-01, Relaxation Phase 1 being conducted over a longer period (72 hours) and Relaxation Phase 2 a shorter period (24 hours). This means that, regardless of relaxation length, the force decreases rapidly to roughly 4 kN (a 6 kN reduction in this case) and remains steady following hydraulic system shutdown. On the other hand, there is a much smaller drop (about 2 kN at the onset of Relaxation Phase 1) if the hydraulic system is kept pressurized, which maintains the ram's position and the load constant. Moreover, the steady force-time responses in all the relaxation phases demonstrate no time-dependent behaviour exists for pipe or soil. Matymish et al. (2023) described the effect of releasing hydraulic pressure from the ram after pipe displacement, noting that the pipe unloads completely, meaning the force measured becomes 0 kN. However, this did not happen during the current testing. This is because of the difference in the two testing setups, pipe pulling and soil tank pulling. With pipe-pull testing, the pipe's leading-end is connected directly to a ram, with the trailing-end free. If the ram is de-pressurized and allowed to move unrestrained, the shear stresses developed in the

soil can dissipate freely from both ends of the pipe. However, when pulling the soil, one end of the pipe is permanently anchored to the load cell, meaning that if soil movement ceases, the soil will maintain some level of shear resistance while the end-fixity prevents the load from dissipating from that end. A pipeline experiencing an axial ground-movement event in the field can be considered fixed similarly to the current testing end configuration, given that the length of typical pipelines would be larger than the 4 m tested, indicating residual forces may be held after ground movement ceases.

3.4.4 Successive Pulling Tests

As mentioned in the test programme, each test was performed by pulling the soil a set amount, holding the soil at this location, and then pulling the soil further before pushing it back to the starting location. It can be seen from Fig. 3-8 that there is a reduction in peak axial force during each subsequent pulling phase. However, it is more clearly shown in Fig. 3-9(a), where the forces for each phase of test ST-01 are plotted with the soil tank movements. Note that relaxation phases are omitted for clarity. The figure shows the post-peak degradation of axial soil resistance between each phase, attributed to the wear and tear of sand grains and post-peak softening response of the dense sand. This reduction is evident in the graphs, for example, the ending load of Pulling Phase 1 is above 10 kN from the peak load of ~13 kN. Then, the Pulling Phase 2 starts at ~4 kN due to the unloading event caused by the hydraulic system shut-down for Relaxation Phase 1 (as discussed above). From the plot, it is clear that each subsequent pulling phase develops successively lesser peak forces. In test ST-01, the peak forces developed during Pulling Phase 1 was roughly 13 kN, which was reduced to 12 kN in Pulling Phase 2 and 10 kN in Pulling Phase 3. The peak force reduction in consecutive pulling phases indicates that the pipe–soil

interface bond has weakened, and the soil has reached its shearing limit, loosening the soil at the pipe–soil interface. The soil’s ability to transfer load to the pipe will continue to decrease as the interface bonding is released and soil particles rearrange. After the third pulling and relaxation phases, the soil was pushed back to its starting position, whereby the axial force dropped to a negative value, indicating compression. The large gap visible between the final pulling phase and the pushing phase is caused by a high unloading rate, faster than the collection rate of 2 data-points per second could record. Interestingly, this phase produces no significant compression force in the pipe, again indicating the broken pipe–soil bond.

From Fig. 3-9(a), further conclusions about successive pulling behaviour can be drawn that peaks from successive pulling phases will develop at vastly reduced displacements. The peak force during Pulling Phase 1 takes 14.2 mm of soil movement to develop, while Pulling Phase 2 starts at the soil tank displacement of 35 mm and reaches its peak after just 1.6 mm at a total displacement of 36.4 mm. Again, Pull 3 peaks after a short displacement, 2.5 mm. Thus, it is clear that intermittent soil-movement events cause lower peak loads to develop with each successive movement. In addition, each peak load develops in a fraction of the soil displacement, compared with a first-time movement event. As an example, Fig. 3-9(a) shows that Pull 1 produces peak force at 14.2 mm of soil displacement, whereas from the peak force from Pull 2 occurs at almost 1.0 mm, less than 10% of the first peak’s displacement.

The force–displacement responses for tests ST-03 and ST-04 (60.3 mm), along with tests ST-05 and ST-06 (114.3 mm), are plotted in Fig. 3-9(b). Relaxation phases are again omitted for clarity and were conducted with the hydraulic system pressurized as opposed to unpressurized.

Based on the post-peak nature of each curve, it is clear that force reduction behaviour was prevalent across all tests and diameters, indicating consistent initial soil condition (dense state) of the tests. It is important to note that these curves are continuous, except test ST-05 (bare 114.3 mm pipe); with no clearly discernable peak value visible in the second pulling phase following the initial peak in the first pulling phase. Nevertheless, a clear and distinct peak was observed in each pulling phase of test ST-01, wherein the hydraulic system became unpressurized through shut-down before each relaxation phase. Overall, successive peaks gradually decreased by about 10-15% for each subsequent movement-relaxation event, irrespective of pipe diameters and instrumentation conditions. This trend is illustrated in Fig. 3-10 by the discrete peak forces obtained during each test.

3.4.5 Strain Distributions

Strain distributions measured along the pipe length within the test box for each pipe diameter at the peak pulling force for different phases are presented in Fig. 3-11. The development of axial strains along the pipe depends on the axial stress/force, which in turn depends on the pipe–soil interface shear stress. Fibre-optic sensor data confirmed that shear stress at the interface was developed along the entire pipe length at a very small tank displacement (1 to 2 mm), as shown in Fig. 3-11(a) for test ST-02. This indicates an instant mobilization of soil resistance along the pipe. As the tank displacement increases (i.e., the relative displacement between the pipe and soil), the axial strains continue to increase linearly to a maximum when the shear strength of the soil is fully mobilized. Similarly, as seen in Fig. 3-5, the soil resistances (i.e., shear stresses) increase linearly to the peak value with the tank displacements. Therefore, it can be said that the mobilization of soil resistance is uniform along the pipe length, as expected for steel pipes.

Overall, the distribution of axial strain along the length of the pipe is essentially linear within the soil box, except near the ends. Fig. 3-11(a) shows the axial strain profiles obtained during Pulling Phase 1 of test ST-02 since no further strain data is available as the fibre-optic sensor was damaged following this phase. At tank displacement of 10.9 mm (displacement corresponding to the peak resistance), the 26.7 mm diameter pipe registers a strain of $\sim 25 \mu\epsilon$ at the fixed end, dips to zero, and then experiences its highest strain of $\sim 120 \mu\epsilon$ at roughly 750 mm from the fixed end. From here, strain decreases relatively linearly to $\sim -25 \mu\epsilon$ and finally zero. The dip in linear strain occurring just inside the fixed-end tank wall may be an artifact of the boundary of the tank. When the tank is pulled, the rubber gasket may push the pipe in front of it, compressing it slightly. Therefore, the reduction to zero strain shortly after the fixed end is thought to be due to the artifact of the tank's side wall and localized stiffness from the connection plate and tab. Alternatively, there may be a slight recess in the soil bed, causing bending and, thus, compression in the fibre optic sensors situated on the crown of the pipe. The same $25 \mu\epsilon$ difference found just inside the tank free-end wall might occur due to the rigid boundary of the tank. The tank wall's end opening supports more of the free-hanging pipe, pushing it slightly upwards in relation to the starting position causing compressive strain in the crown of the pipe.

The strain distribution for test ST-04 (60.3 mm diameter pipe) is shown in Fig. 3-11(b), which includes both the pulling and pushing phases. A similar trend is visible whereby strain is non-zero at the load-cell end during pulling phases, then reduces to roughly zero at 250 mm from the fixed end. After this, the strain climbs to its peak value ($\sim 60 \mu\epsilon$ for both pulls) and gradually decreases linearly to zero, as with the previous figure. Interestingly, negative strain values were recorded on the pipe portion outside the soil tank at the moment of peak force for pulling phase 1

and pushing as well as prior to test start, however, these changed to positive values at the instant of the peak force during pulling phase 2. As the fibre-optic sensor records negative linear strain values both prior to test start and during Pull 1's peak phase, a likely explanation could be that the pipe exited the tank at a slight upward angle, causing compressive strain at the pipe crown, where the sensor is affixed. For reference, roughly 300 mm of pipe remains outside the tank at the beginning of the test. Likewise, the positive strain values might be caused by the rigid tank boundary interacting with the pipe free-end, causing the pipe to bend downward, straightening out. This means that relative to the initial position, the new position of the pipe would produce tensile strain on the crown of the pipe, showing positive strain readings. Testing in the Pushing Phase behaves similarly to the pulling phases, except that strain is maintained negative for the entirety of the pipe. The strain linearly increases negatively, starting roughly 3 m from the fixed end, until peaking at nearly $-100 \mu\epsilon$ close to the fixed end.

Fig. 3-11(c) plots the strain distribution for test ST-06 (114.3 mm diameter pipe) and is the most unique. The highest strain values recorded near the fixed end during both pulling phases are $\sim 60 \mu\epsilon$ in Pulling Phase 1 and $\sim 30 \mu\epsilon$ in Pulling Phase 2, whereas the highest values along the buried length are $\sim 30 \mu\epsilon$ during Pulling Phase 1 and just above $20 \mu\epsilon$ for Pulling Phase 2. Once these values are reached, the distribution linearly decreases to -20 and $-30 \mu\epsilon$ for the respective phase and remains consistent. It can be seen that the strain values at the fixed end prior to testing start are also negative. Since the soil remained stationary, unable to transfer load to the pipe, a likely explanation for this would be an initial out-of-straightness of the pipe. During placement, the pipe required multiple longitudinal shifts to align the tab and clevis properly, which might have caused settlement in the pipe. The settlement would occur between

the soil tank walls, with little vertical displacement at these points, thus allowing bending in the pipe, causing compression (negative bending strain) in the pipe's crown prior to testing. Further testing is recommended to explain the mechanisms.

Despite variations, the strain values remain low and are below the typical allowable strain limit of 0.2% for steel pipes (e.g., Chan and Wong 2004; Weerasekara and Rahman 2019) for longitudinal ground movement. The low strain value indicates negligible elongation in the pipe. In other words, the steel pipes behaved as rigid bodies during tests. For the 26.7 mm pipe, if the strain distribution is approximated as a triangle of height 130 $\mu\epsilon$ and length 4.0 m, the area under the curve will approximate the elongation as 0.52 mm. Assuming a linear strain distribution along the pipe length, the total elongation of the pipe can also be calculated using the equation proposed in Reza and Dhar (2021b) as follows:

$$\Delta = \frac{PL}{2AE} \quad (3-3)$$

Where P is the peak pullout force in the pipe, L is the length of the pipe, A is the pipe's cross-section area, and E is the Young's Modulus of the pipe. With P taken as P_u (peak load), L taken as the total length of the pipe (4.6 m), and E taken as 200,000 MPa, the total elongation is 0.54 mm. This value is close, as calculated above (0.52 mm). Similarly, elongation can be estimated for the 60.3- and 114.3-mm pipes. Using the strain distribution associated with Pulling Phase 1 as it develops the highest strain, elongations of the pipes are calculated as 0.11 mm and 0.07 mm for the 60.3 and 114.3-mm pipes, respectively. The theoretical elongations are 0.16 mm and 0.12 mm using Eq. (3-3) for the 60.3- and 114.3-mm pipes, respectively. Given the magnitudes involved, these values are relatively close; however, the theoretical values are still roughly 30% higher. This difference is likely caused by the idealization of a linear strain distribution spanning

the entire length of the pipe and a consistent force throughout. In reality, the strain distribution is not captured for the entire 4.6 m length of pipe but for 4.2 m, and the distribution is not uniform from the fixed to the free end. These results indicate that steel pipes behave as rigid bodies with negligible elongation during the experiment.

Fig. 3-12 plots the axial strain distributions along the length of the pipe during ST-04 (60.3 mm diameter) to better understand the residual axial strain in the pipe. Residual strains and stresses are important in the context of buried pipes when considering the stress and strain limits of pipes that may have previously been subjected to permanent ground deformations (Matymish et al. 2023). In this regard, Fig. 3-12(a) shows the axial strain distributions at the start of the test, at the soil displacement corresponding to the peak load of Pull1 (10.2 mm) and the distribution recorded during the middle of Relaxation Phase 1, and Fig. 3-12(b) plots the axial strain distributions of the pipe at displacements corresponding to the Pull2 peak force (31.1 mm) and the middle of Relaxation Phase 2 along with the start of the test at 0 mm of soil displacement. The result shows a small decrease in axial strain upon removal of the axial force from pulling phase 1 to relaxation phase 1. This is mainly because the hydraulic system was kept running during the Relaxation Phase 1, similar to that shown in Fig. 3-8(b) for test ST-06, which results in a lower drop in the axial load and the axial strains. Besides, the relaxation period was performed for only 2 hours. On the other hand, unlike the first relaxation period, the second relaxation period was performed over roughly 20 hours, requiring the hydraulic system to be shut off. As seen in Fig. 3-12(b), the larger reduction in strain indicates that hydraulic shutoff allows a greater redistribution of stresses in the soil and the pipe, lowering the pipe strain. In contrast, holding the soil tank in place with a pressurized system allows for a much smaller redistribution,

as in Fig. 3-12(a). It is interesting to note that although the measured maximum strains during the tests were significantly lower than the expected yield strain of steel, the pipe strain did not revert to its pre-testing condition in either case. This indicates that some strains in the pipe are permanently “locked-in” due to the residual shear stresses remaining along the pipe length. While these remaining strains are likely much less than the allowable strain limit of the pipeline, they can potentially reduce the pipeline’s resilience to future ground deformation events.

3.5 Conclusions

This paper presents results from a novel testing setup developed at Memorial University of Newfoundland to investigate steel pipe behaviour during ground movement events. Six full-scale axial tests were performed, where the pipes, anchored at one end and free on the other, were buried inside a moveable steel tank filled with sandy soil. Once the tank was pulled up to a certain displacement, the system relaxed for varying time frames, and the pull-relax cycle started anew. The final testing phase pushed the tank back to its starting position. During testing, pipe axial force, soil tank displacement, and strain along the pipe were recorded. The key findings from the experiments are summarized below.

- 1) Pulling a pipe axially through a static soil mass may produce a different response than pulling the soil mass against a pipe fixed at one end. Pipe pulling results are considerably lower than soil pulling when force is normalized based on the unit weight of soil, pipe length, pipe diameter, and burial depth. It is important to note that different pipe diameters may contribute to this large difference in the normalized loads since no literature sources tested pipes of the same size in the current study.

- 2) The normalized axial force is higher for smaller diameter pipes, due to a larger effect of dilation-induced frictional resistance (consistent with the cavity expansion theory) for the smaller diameter pipe.
- 3) The measured axial soil resistance is underpredicted by the current design guidelines for the soil pulling tests presented. Similar findings were also reported by previous studies for pipe pulling in dense sand. Although the underprediction using the design equation can be partially reduced by choosing the modified earth pressure coefficient ($K=2$) recommended in the PRCI guideline, other factors, such as backfill compaction and testing methods (soil pull vs. pipe pull), may influence the test results that are not considered in the current guidelines.
- 4) A larger decrease in force was noted during the onset of relaxation phases where the hydraulic system was shut off compared to those where the system was kept running at a constant position. Axial load captured during the relaxation phases (varied between 24 to 72 hours) was steady and consistent, implying no time-dependent behaviour by either the pipe or the soil.
- 5) Peak forces developed during consecutive pull-relax cycles decrease consistently by around 10 to 15%, with consecutive peak forces developing in a fraction of the displacement. This reduction occurs because the interface soil has reached its limiting shear strength (i.e., achieved the maximum strength) during the first pull. Thus, the soil–pipe bond has been disturbed and weakened for the subsequent pulls.
- 6) Fibre-optic sensor data confirmed that shear stress at the interface was developed along the entire pipe length at a very small tank displacement (1 to 2 mm), indicating instant mobilization of soil resistance along the pipe. The linear strain distribution along the pipe

implies that the mobilization of soil resistance (axial force) is uniform per unit length of the pipe.

- 7) The recorded strains were negligible during the tests, meaning the pipe behaves as a rigid body. Assuming the linear strain profile, the total elongation of the pipe at peak load in pulling phase 1 was calculated to be less than a millimeter for all tests.
- 8) Similar to force reduction, strain reduction along the pipe length was higher during relaxation phases where the hydraulic system was shut off versus those where the system was left running. It is interesting to note that although measured maximum strains were significantly lower than the expected yield strain of steel, the pipe strain did not revert to its pre-testing condition in either case. This permanently “locked-in” strain in the pipe may be attributed to the presence of residual shear stresses that remain along the pipe length.

3.6 Acknowledgements

The authors would like to gratefully acknowledge the financial support and/or in-kind support provided by the Alliance Grants program of the National Science and Engineering Research Council of Canada, FortisBC Energy Inc., SaskEnergy Canada Inc., and WSP Canada Inc. for conducting this research.

3.7 References

- ALA (American Lifelines Alliance) 2005. *Guidelines for the design of buried steel pipe*. Washington, DC and Reston, VA, USA: Federal Emergency Management Agency (FEMA) and American Society of Civil Engineers (ASCE).
- Alarifi, H., Mohamad, H., Nordin, N. F., Yusoff, M., Rafindadi, A. D. U., and Widjaja, B. 2021. A large-scale model of lateral pressure on a buried pipeline in medium dense sand. *Applied Sciences*, 11(12): 5554.
- Ali-Khazaali, M., and Vanapalli, S. K. 2019. Axial force-displacement behaviour of a buried pipeline in saturated and unsaturated sand. *Géotechnique*, 69(11): 986–1003.
- ASTM (2015) D 1556: *Standard test method for density and unit weight of soil in place by the sand-cone method*. ASTM International, West Conshohocken, PA, USA.
- Bai, Y., Knauf, G., and Hillenbrand, H. G. 2000. Materials and design of high strength pipelines. *ISOPE International Ocean and Polar Engineering Conference* (pp. ISOPE-I). ISOPE.
- Boulon, M., and Foray, P. 1986. Physical and numerical simulation of lateral shaft friction along offshore piles in sand. In *Proceedings of the 3rd International Conference on Numerical methods in Offshore piling*, Nantes, France, 21–22 May 1986. Institut Francais du Petrole, Nantes, France. pp. 127–147.
- Bilgin, Ö., and Stewart, H. E. 2009. Pullout resistance characteristics of cast iron pipe. *Journal of Transportation Engineering*, 135(10): 730–735.
- Chan, P. D., and Wong, R. C. 2004. Performance evaluation of a buried steel pipe in a moving slope: a case study. *Canadian Geotechnical Journal*, 41(5): 894–907.

- Cruden, D.M. and Varnes, D.J. 1996. Landslide Types and Processes, *Transportation Research Board*, US National Academy of Sciences, Special Report, 247: 36–75. *Landslides Eng. Pract*, 24: 20–47.
- Cullin, M. J., Petersen, T. H., and Paris, A. 2015. Corrosion fatigue failure of a gray cast iron water main. *Journal of Pipeline Systems Engineering and Practice*, 6(2): 05014003.
- Demirci, H. E., Bhattacharya, S., Karamitros, D., and Alexander, N. 2018. Experimental and numerical modelling of buried pipelines crossing reverse faults. *Soil Dynamics and Earthquake Engineering*, 114: 198–214.
- Jalali, H. H., Rofooei, F. R., Attari, N. K. A., and Samadian, M. 2016. Experimental and finite element study of the reverse faulting effects on buried continuous steel gas pipelines. *Soil Dynamics and Earthquake Engineering*, 86: 1–14.
- Johnston, I.W., Lam, T. S. K., and Williams, A. F. 1987. Constant normal stiffness direct shear testing for socketed pile design in weak rock. *Géotechnique*, 37(1): 83–89.
- Kishawy, H. A., and Gabbar, H. A. 2010. Review of pipeline integrity management practices. *International Journal of Pressure Vessels and Piping*, 87(7): 373–380.
- Luna Innovations Inc. 2020. *User's Guide ODiSI 6*, Luna Innovations Inc., Blacksburg, VA, USA.
- Luna Innovations Inc. 2017. *ODiSI Fiber Optic Sensor Installation Guide*, Luna Innovations Inc., Blacksburg, VA, USA.
- Luo, S. Q., Tan, S. A., and Yong, K. Y. 2000. Pull-out Resistance Mechanism of a Soil Nail Reinforcement in Dilative Soils. *Soils and Foundations Japanese Geotechnical Society*, 40(1): 47–56.

- Matymish, J., Moore, I. D., Woods, J. E., and Hoult, N. A. 2023. Axial Pullout Behaviour of Fusible PVC Pipes and Fusion Weld Joints Assessed using Distributed Fibre Optic Sensors. *Canadian Geotechnical Journal*, (ja).
- Meidani, M., Meguid, M. A., and Chouinard, L. E. 2018. Estimating earth loads on buried pipes under axial loading condition: insights from 3D discrete element analysis. *International Journal of Geo-Engineering*, 9: 1–20.
- Murugathan, P., Dhar, A. S., and Hawlader, B. C. 2021. An experimental and numerical investigation of pullout behavior of ductile iron water pipes buried in sand. *Canadian Journal of Civil Engineering*, 48(2): 134–143.
- Ni, P., Moore, I. D., and Take, W. A. 2018. Distributed fibre optic sensing of strains on buried full-scale PVC pipelines crossing a normal fault. *Géotechnique*, 68(1): 1–17.
- Oskouei, A. V., Tamjidi, A., and Pourshabani, P. 2019. Effects of burial depth in the behavior of buried steel pipelines subjected to strike-slip fault. *Soil Dynamics and Earthquake Engineering*, 123: 252–264.
- PRCI (Pipeline Research Council International). 2009. *Guidelines for constructing natural gas and liquid hydrocarbon pipelines through areas prone to landslide and subsidence hazards*. Report prepared for the Design, Material, and Construction Committee. Chantilly, VA: Pipeline Research Council International, Inc.
- Rajani, B. B., Robertson, P. K., and Morgenstern, N. R. 1995. Simplified design methods for pipelines subject to transverse and longitudinal soil movements. *Canadian Geotechnical Journal*, 32(2): 309–323.
- Reza, A., Dhar, A. S. and Rahman, M. 2023. Strain assessment of polyethylene pipes in dense sand subjected to axial displacement. *Geosynthetics International*, 00(0): 1–18.

- Reza, A., and Dhar, A. S. 2021a. Effects of Axial Relative Ground Movement on Small Diameter Polyethylene Piping in Loose Sand. *Infrastructures*, 6(12): 168.
- Reza, A., and Dhar, A. S. 2021b. Axial Pullout Behavior of Buried Medium-Density Polyethylene Gas Distribution Pipes. *International Journal of Geomechanics*, 21(7): 04021120.
- Robert, D. J., Soga, K., O'Rourke, T. D., and Sakanoue, T. 2016. Lateral load-displacement behavior of pipelines in unsaturated sands. *Journal of Geotechnical and Geoenvironmental Engineering*, 142(11): 04016060.
- Rostami, H., Osouli, A., and Kumar, S. 2023. Experimental modeling of far-field effects in buried pipelines subjected to reverse faulting. *Soil Dynamics and Earthquake Engineering*, 164: 107561.
- Saha, R.C., Dhar, A.S., and Hawlader, B.C. 2019. Shear strength of a well-graded clean sand, Geo St. John's 2019, *Canadian Geotechnical Society*, St. John's, NL, CA.
- Sarvanis, G. C., Karamanos, S. A., Vazouras, P., Mecozzi, E., Lucci, A., and Dakoulas, P. 2017. Permanent earthquake-induced actions in buried pipelines: Numerical modeling and experimental verification. *Earthquake Engineering & Structural Dynamics*, 47(4): 966–987.
- Scarpelli, G., Sakellariadi, E., and Furlani, G. 2003. Evaluation of soil-pipeline longitudinal interaction forces. *Rivista Italiana di Geotecnica*, 37(4): 24–41.
- Sheil, B. B., Martin, C. M., Byrne, B. W., Plant, M., Williams, K., and Coyne, D. 2018. Full-scale laboratory testing of a buried pipeline in sand subjected to cyclic axial displacements. *Géotechnique*, 68(8): 684–698.
- Vasseghi, A., Haghshenas, E., Soroushian, A., and Rakhshandeh, M. 2021. Failure analysis of a natural gas pipeline subjected to landslide. *Engineering Failure Analysis*, 119: 105009.

- Weerasekara, L., and Rahman, M. 2019. Framework for assessing integrity of natural gas distribution pipes in landslide areas. In Proc., *72nd Canadian Geotechnical Conf.: Geo St. John's*.
- Wijewickreme, D., Karimian, H., and Honegger, D. 2009. Response of buried steel pipelines subjected to relative axial soil movement. *Canadian Geotechnical Journal*, 46(7): 735–752.
- Wijewickreme, D., Monroy, M., Honegger, D. G., and Nyman, D. J. 2017. Soil restraints on buried pipelines subjected to reverse-fault displacement. *Canadian Geotechnical Journal*, 54(10): 1472–1481.
- Wood Environment and Infrastructure Solutions 2021. Monitoring Report 2020, West Quesnel Land Stability Program (Project No. KX0439755).
- Yoshizaki, K., O'Rourke, T. D., and Hamada, M. 2003. Large scale experiments of buried steel pipelines with elbows subjected to permanent ground deformation. *Structural Engineering/Earthquake Engineering*, 20(1): 1s–11s.
- Zhou, M., Moore, I. D., and Lan, H. 2019. Experimental study of structural response of lined-corrugated HDPE pipe subjected to normal fault. *Journal of Geotechnical and Geoenvironmental Engineering*, 145(12): 04019117.

Table 3-1. Backfill soil parameters

Parameter	Values
Median particle size, D_{50} (mm)	0.742
Coefficient of uniformity, C_u	5.81
Coefficient of curvature, C_c	2.04
Fines content (%)	1.3
Gravel content (%)	0.87
Specific gravity, G	2.63
Minimum void ratio, e_{\min}	0.32
Maximum void ratio, e_{\max}	0.56
Minimum Dry Unit Weight, $\gamma_{d-\min}$	16.58
Maximum Dry Unit Weight, $\gamma_{d-\max}$	19.62

Table 3-2. Test programme

Parameter	ST-01	ST-02	ST-03	ST-04	ST-05	ST-06
Burial Depth, H (mm)	650				625	625
Pipe Diameter, D (mm)	26.7	26.7	60.3	60.3	114.3	114.3
H/D	24.34		10.78		5.47	
Buried Length, L (m)	4.0					
Dry Unit Weight, γ (kN/m ³)	18.1				18.8	
Avg. Relative Compaction, R (%)	96				99	
Pull rate (mm/min)	0.5					
Instrumentation	N	Y	N	Y	N	Y

Table 3-3. Soil displacement at corresponding peak load for first pull

Test	Peak load P_u (kN)	Soil displacement at P_u (mm)
ST-01 ($D=26.7$ mm Bare)	13.25	14.2
ST-02 ($D=26.7$ mm Instrumented)	13.18	10.9
ST-03 ($D=60.3$ mm Bare)	21.40	9.2
ST-04 ($D=60.3$ mm Instrumented)	21.59	10.2
ST-05 ($D=114.3$ mm Bare)	39.75	15.3
ST-06 ($D=114.3$ mm Instrumented)	28.80	12.6

Table 3-4. Testing parameter comparisons

Parameter	Current Test Programme			Murugathasan et al. (2021)	Bilgin and Stewart (2009)	Sheil et al. (2018)	Wijewickreme et al. (2009)
	ST-01-02	ST-03-04	ST-05-06				
Test number	ST-01-02	ST-03-04	ST-05-06	T3	N/A	K3	AB-4
Pull rate (mm/min)	0.5			0.5	N/A	N/A	2-50
Pipe Diameter, D (mm)	26.7	60.3	114.3	178	175	350	457
Burial Depth, H (mm)	650		625	831	760	1180	1140
H/D	24.34	10.78	5.47	4.67	4.34	3.37	2.50
Burial Length, L (m)	4.0			2.70	3.05	1.31	3.80
Dry Unit Weight, γ (kN/m ³)	18.1		18.8	17.17	14.76	16.40	15.70
Avg. Relative Compaction, R (%)	96		98	88.4	95.0	75.0	75.0

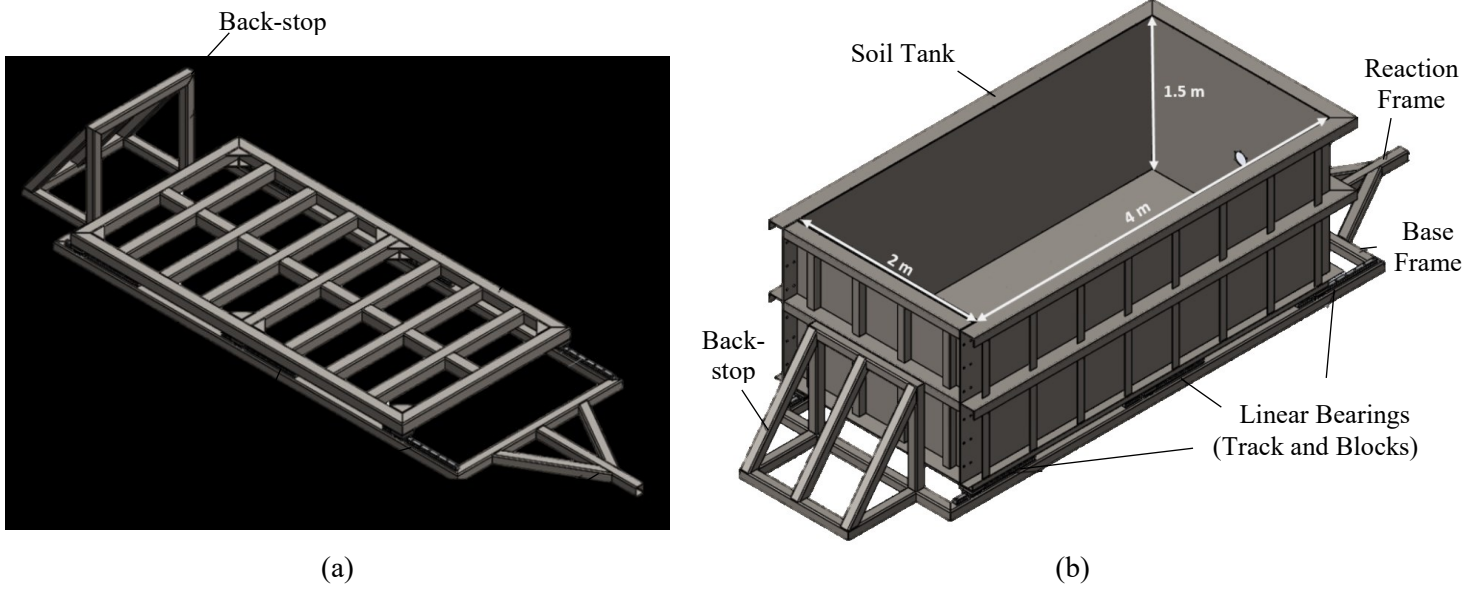
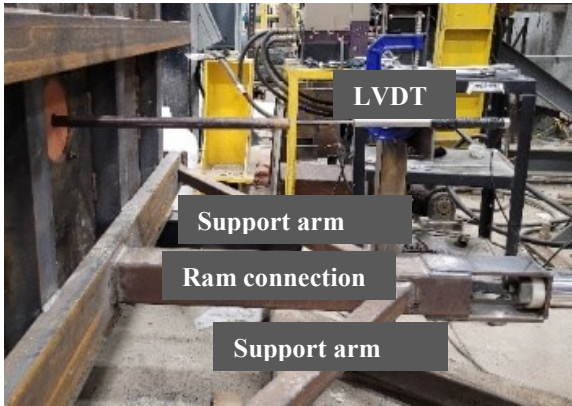
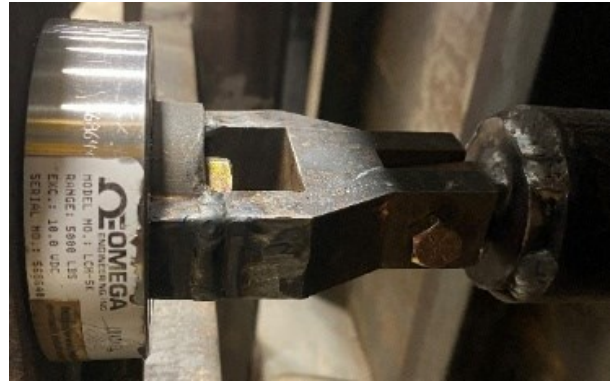


Fig. 3-1. Testing facility frame configuration: (a) without soil tank, and (b) with soil tank



(a)



(b)

Fig. 3-2. (a) Tank ram-end view with LVDT and tank-ram connection; (b) Connection between the load cell and pipe

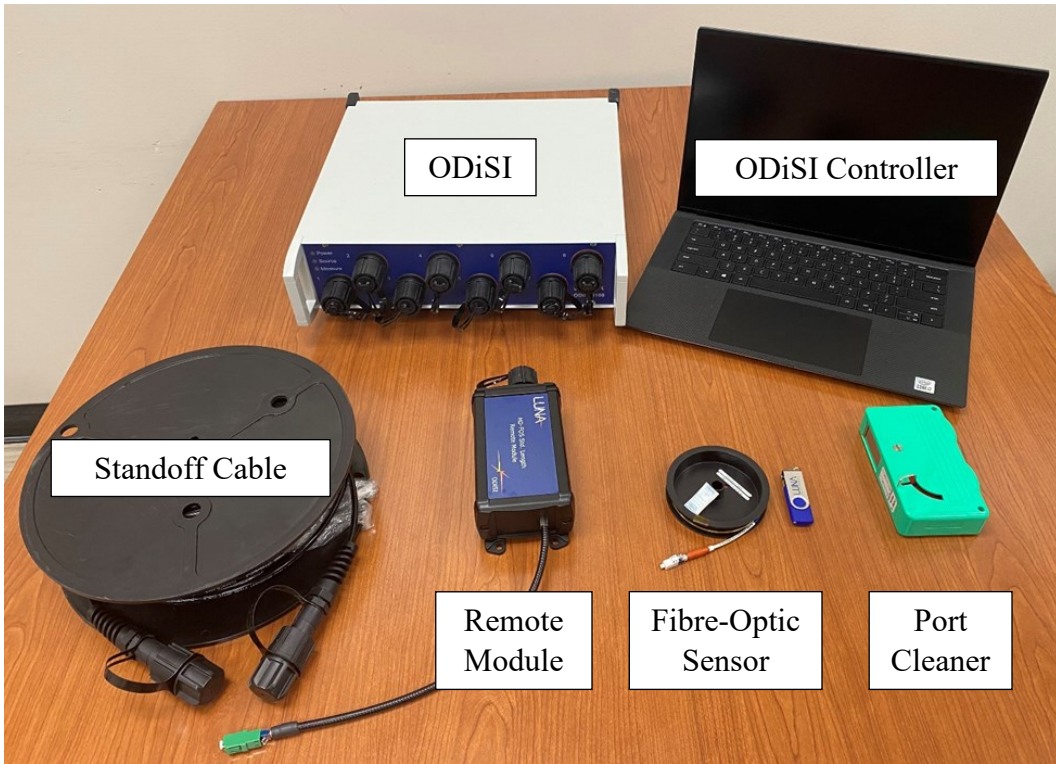


Fig. 3-3. Fibre-optic strain sensing equipment



(a)



(b)



(c)



(d)

Fig. 3-4. Fibre-optic strain sensor application: (a) Strain sensor path mapped and temporarily adhered using Kapton dot; (b) Application of cyanoacrylate adhesive between Kapton dots; (c) Silicone caulking applied to pipe after adhesive curing; and (d) Sheathing tape covering pipe to protect caulking and reduce friction increase.

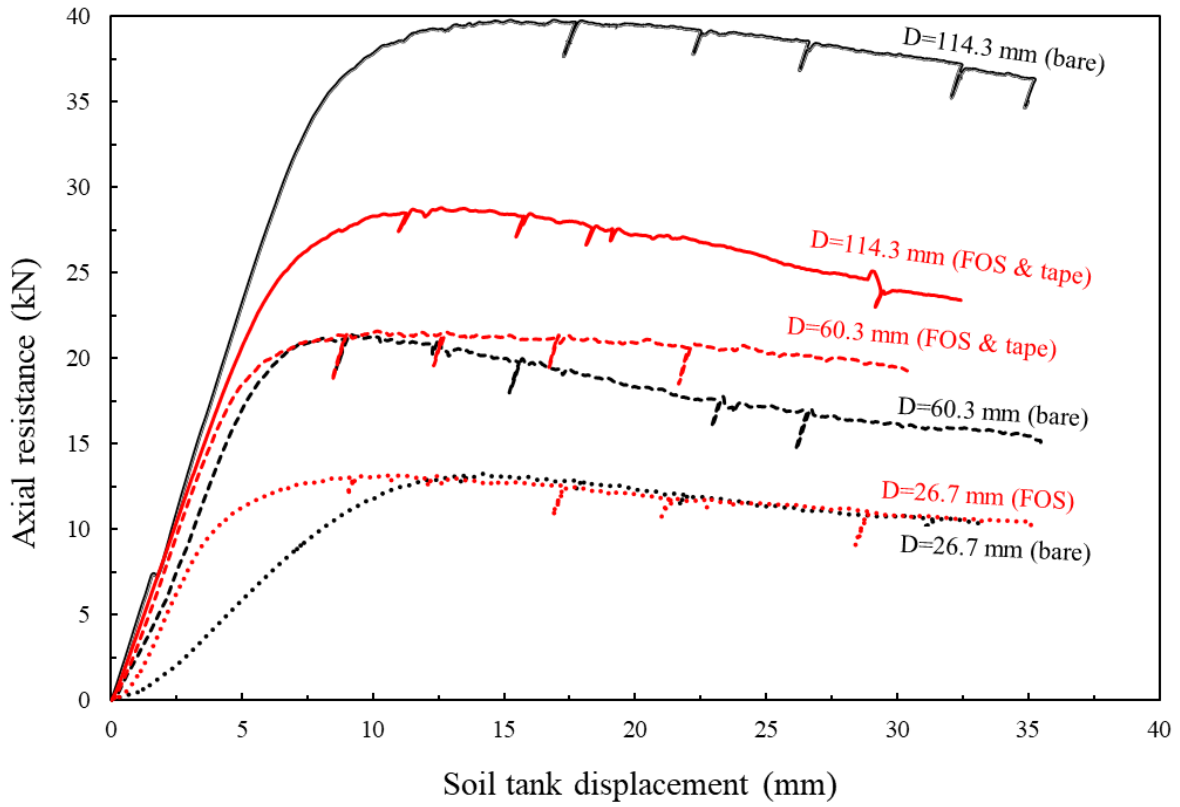


Fig. 3-5. Axial soil resistance with tank displacement for Pulling Phase 1

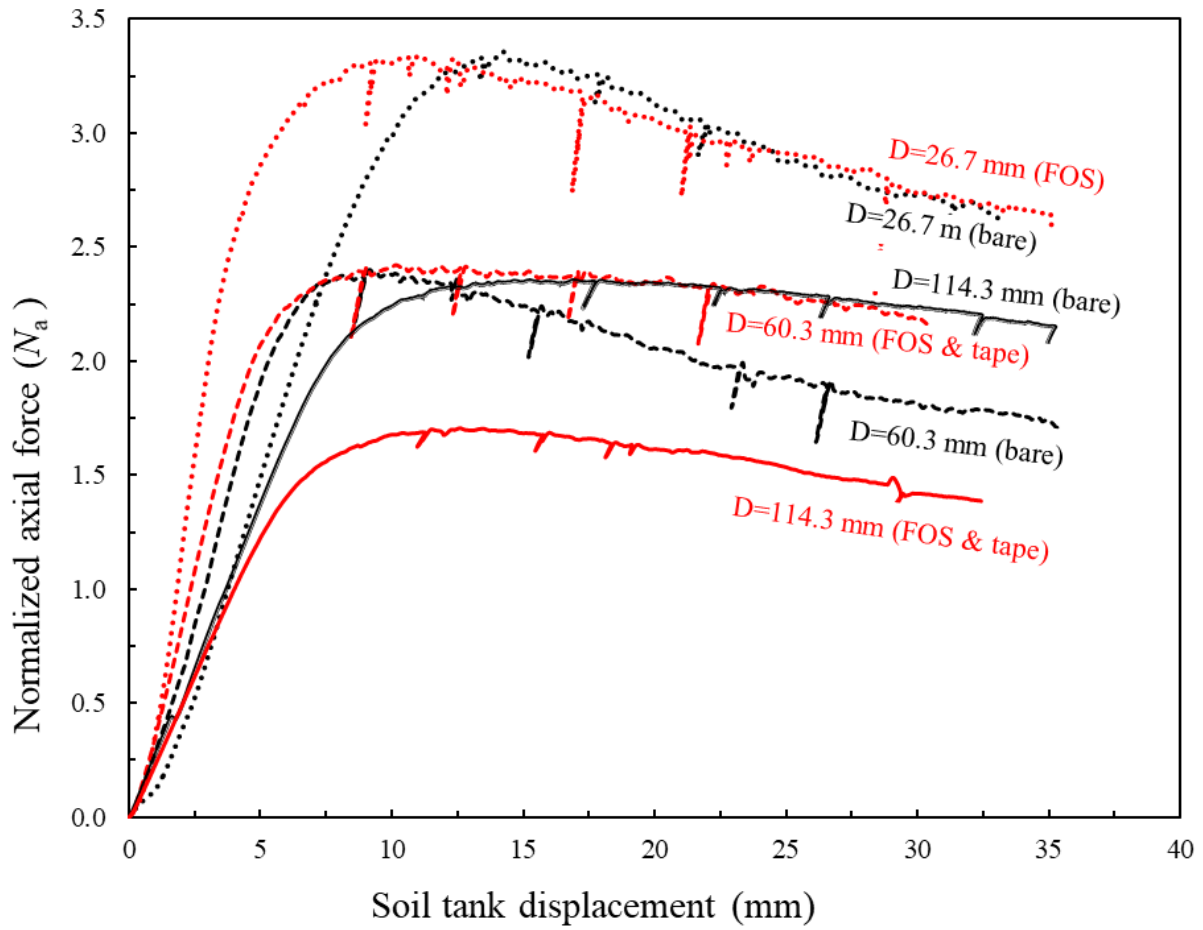


Fig. 3-6. Normalized axial soil resistance with tank displacement

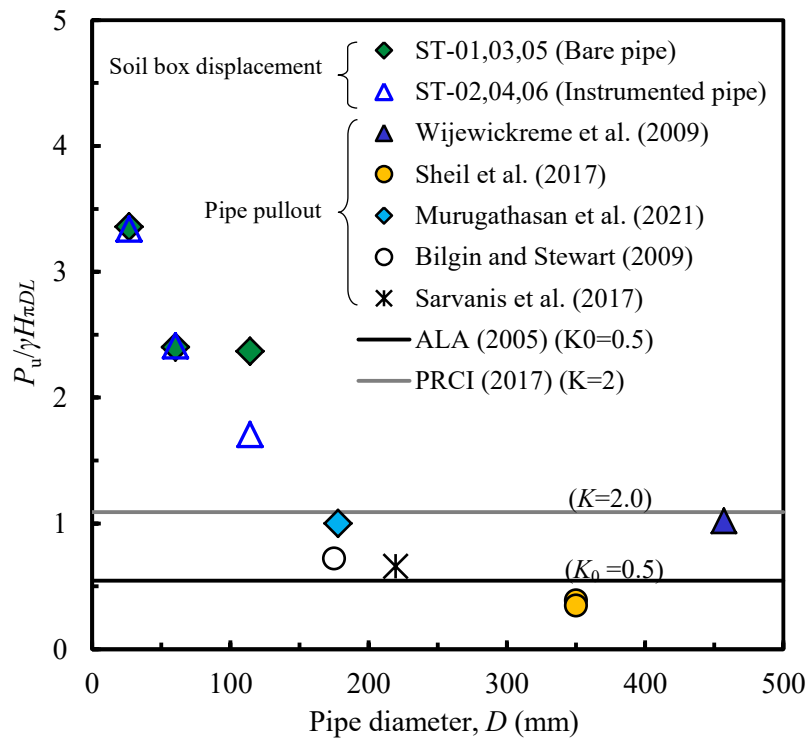
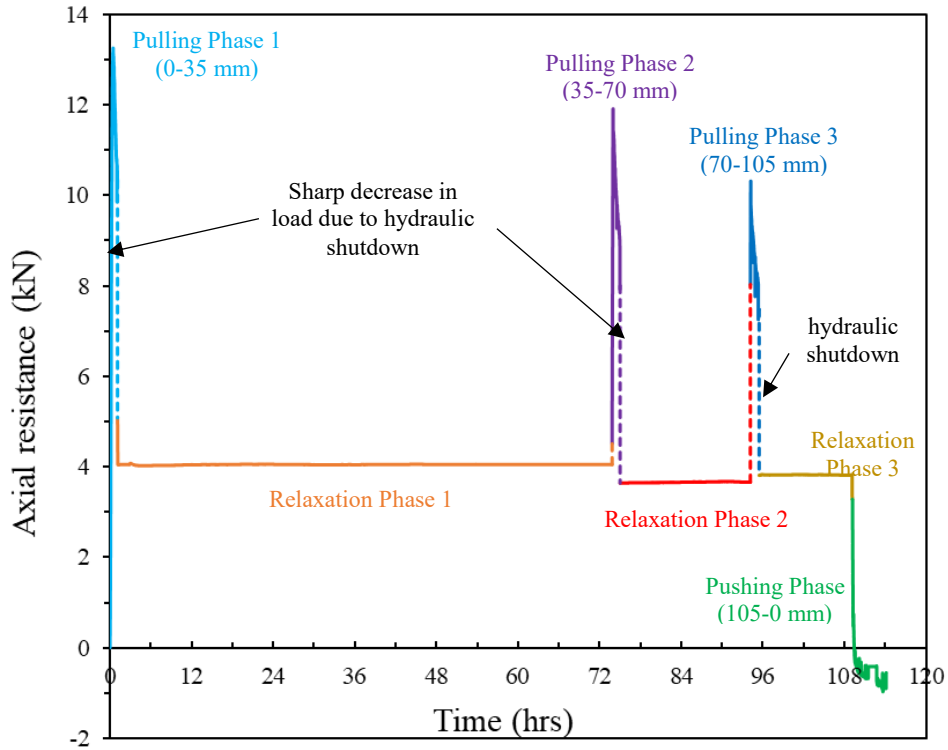
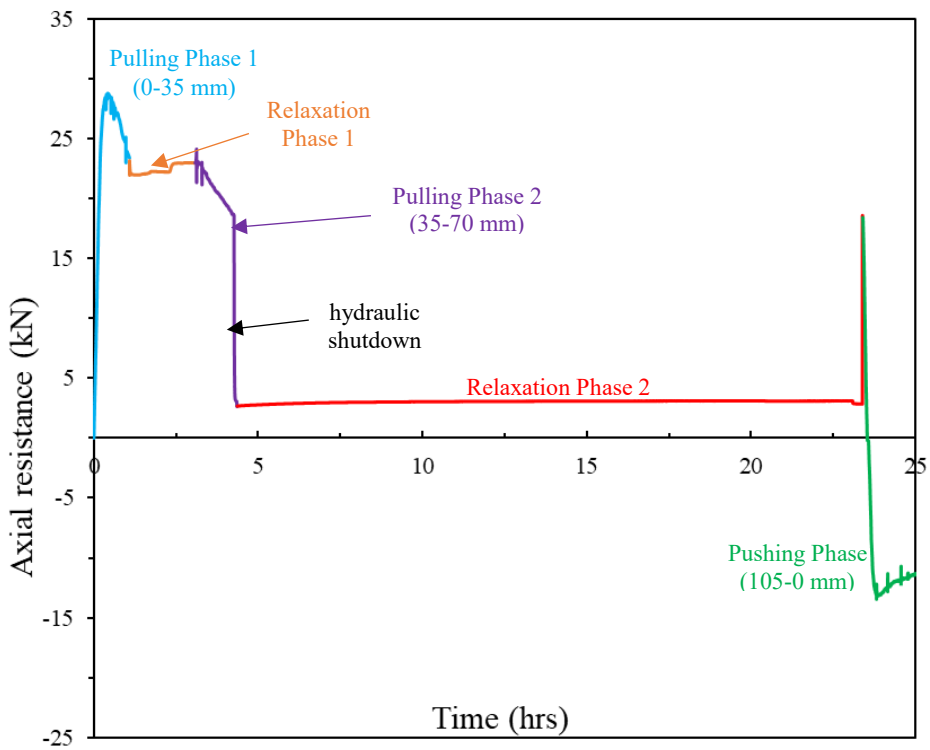


Fig. 3-7. Normalized peak axial resistance by pipe diameter (including both the soil box displacement and pipe pullout tests)

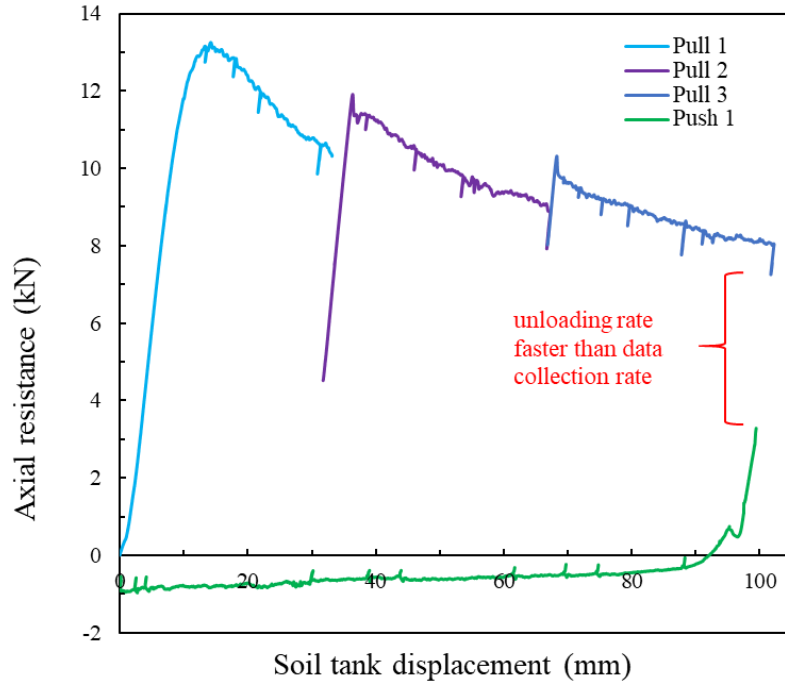


(a)

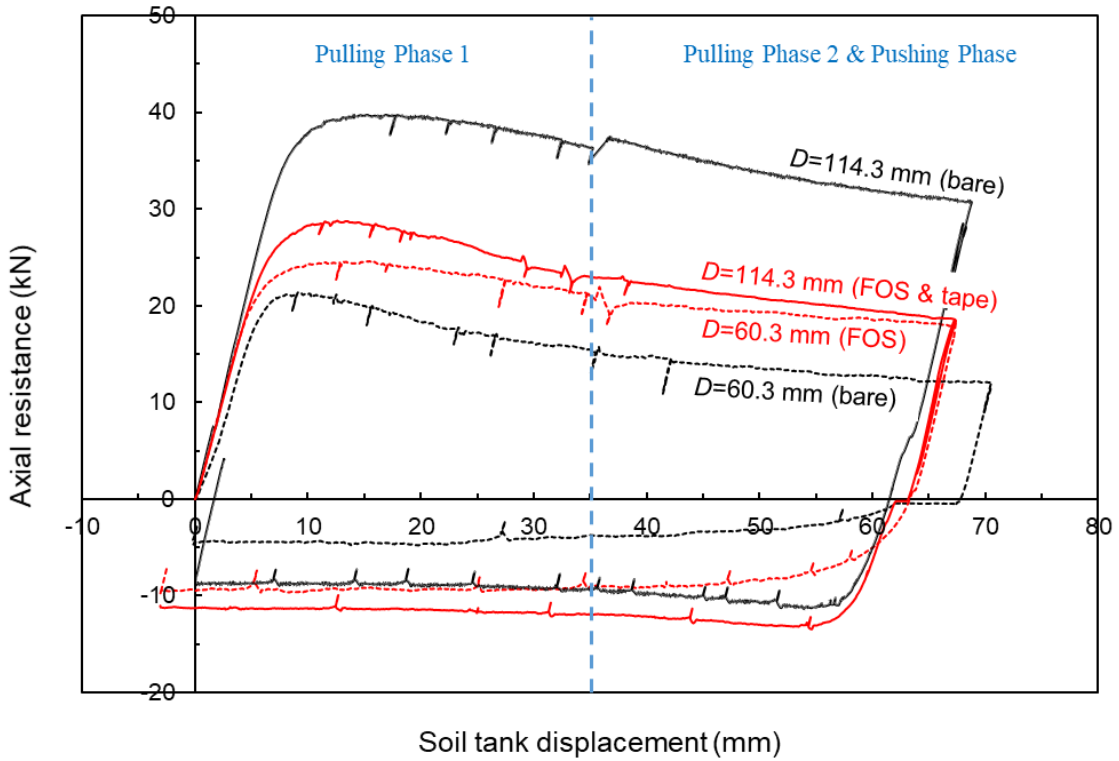


(b)

Fig. 3-8. Pipe axial force variation, with time, during each phase for: (a) Test ST-01; (b) Test ST-06



(a)



(b)

Fig. 3-9. Axial soil resistance with tank displacement: (a) Test ST-01 ($D=26.7$ mm); (b) Tests ST-03-04 ($D=60.3$ mm) and ST-05-06 ($D=114.3$ mm)

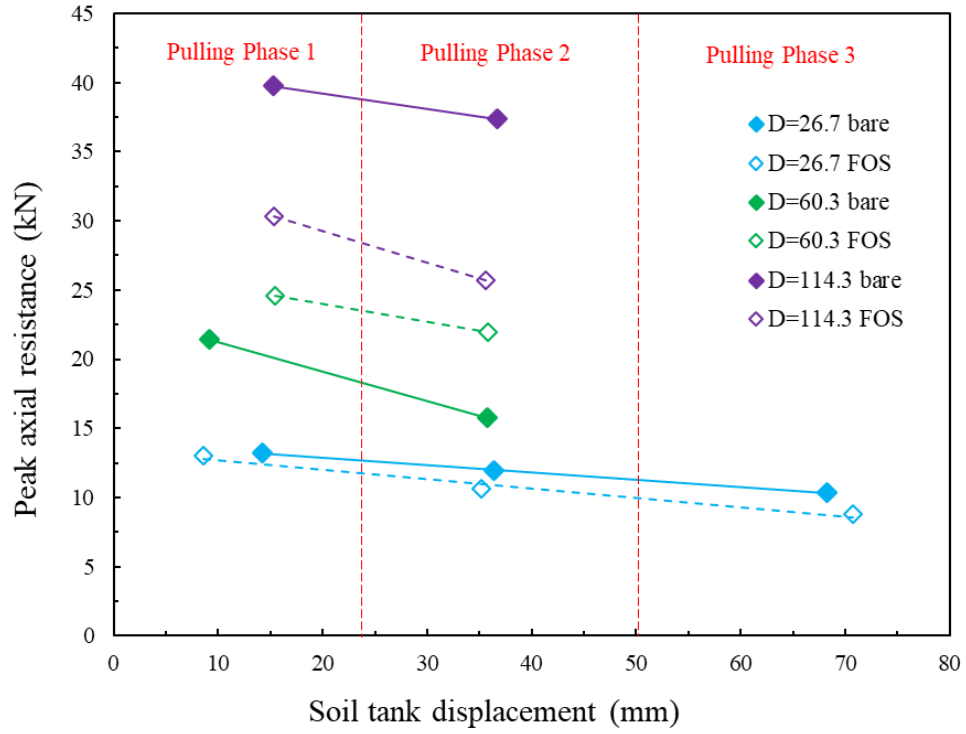
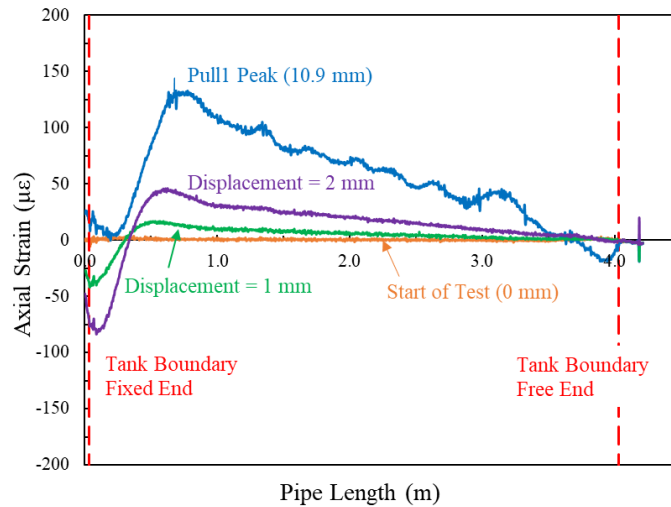
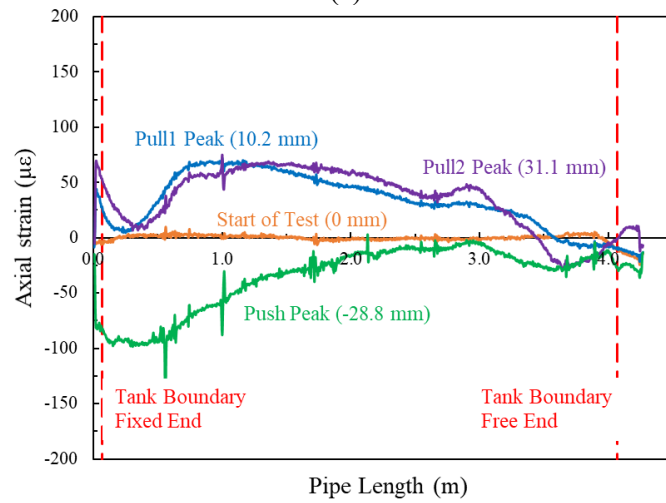


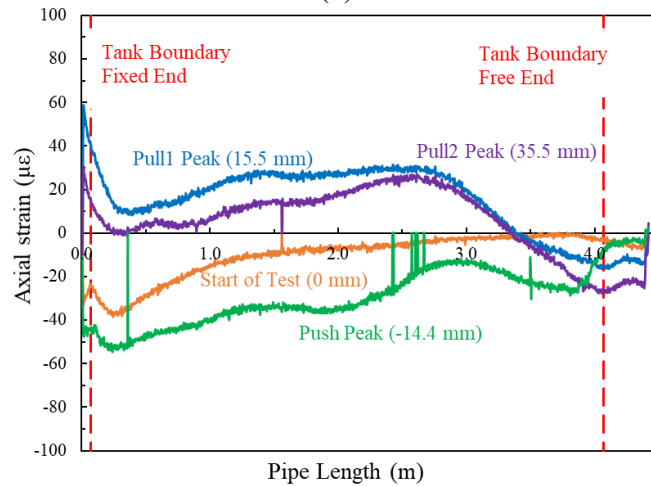
Fig. 3-10. Peak soil resistances in different pulling phases with tank displacement



(a)

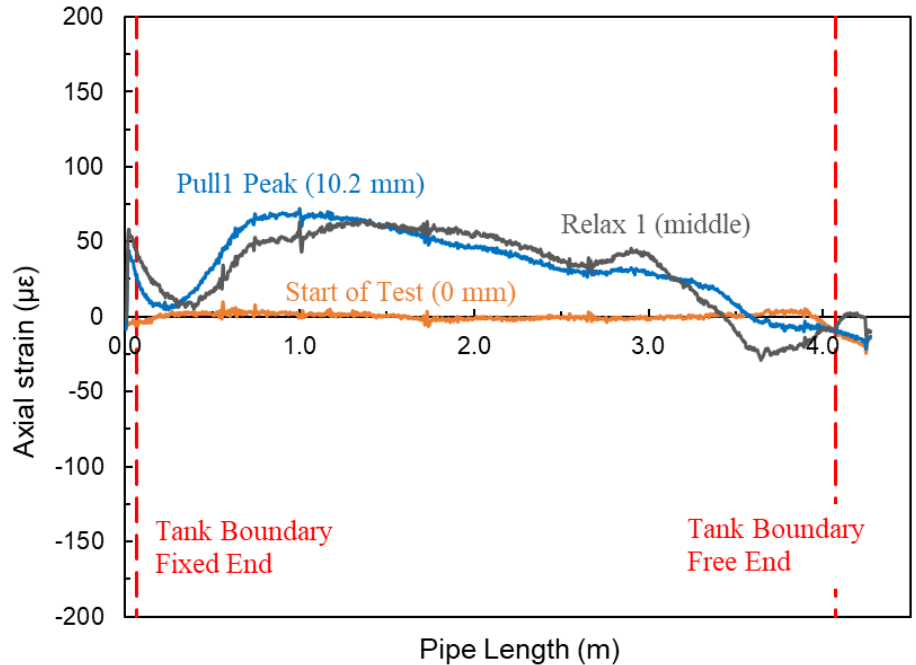


(b)

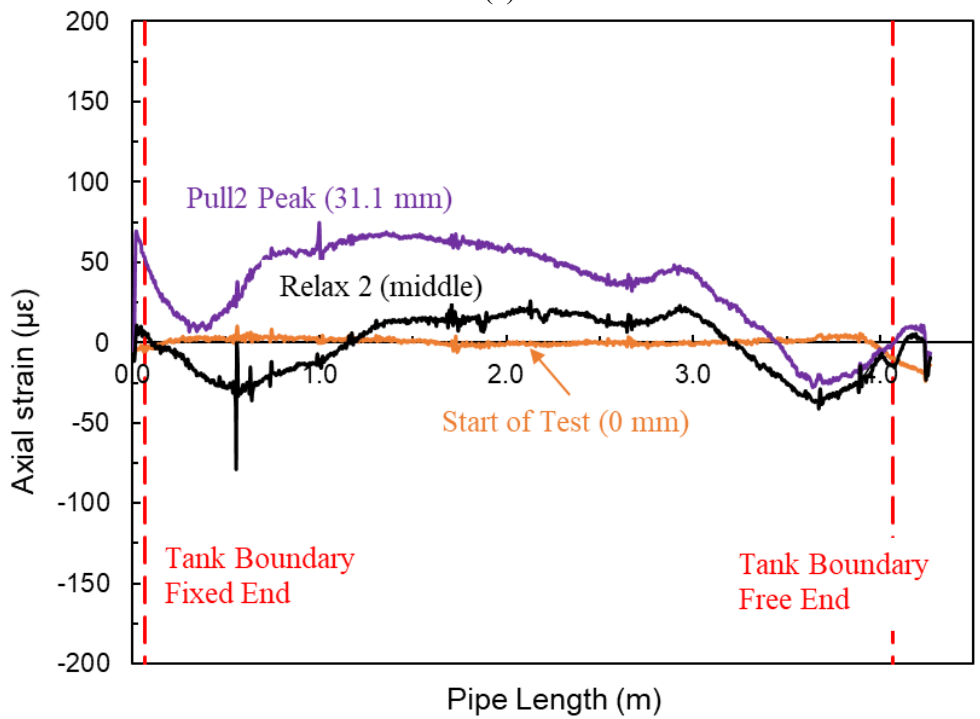


(c)

Fig. 3-11. Strain distribution along the length of the pipe at beginning of test and displacement corresponding to the peak load for each pulling and pushing phase: (a) $D=26.7$ mm pipe (ST-02); (b) $D=60.3$ mm pipe (ST-04); (c) $D=114.3$ mm pipe (ST-06).



(a)



(b)

Fig. 3-12. Axial strain distribution at various stages of the test ST-04: (a) Start of test, Pull1 peak load and middle of Relax1; (b) Start of test, Pull2 peak load and middle of Relax2.

CHAPTER 4: Beam-on-Spring Modelling of Buried Steel Pipes in Sand Subjected to Axial Loads

4.1 Abstract

Finite-element (FE) analysis is often used to assess the pipe conditions for buried pipes undergoing ground movements. Current design guidelines recommend simplified beam-on-spring analysis to assess buried pipes subjected to ground movements by calculating the pipe strains and comparing them to allowable strain limits. Elastic-perfectly-plastic springs are used to simulate the resistances provided by soil in three orthogonal directions while the pipe is modelled as a beam. To determine the magnitude of peak axial spring force, the normal stress is taken as the average of the vertical overburden pressure and the lateral earth pressure at the springline level of the pipe. To this end, the design equation generally uses the lateral earth pressure coefficient at-rest (K_0) or the effective lateral earth pressure coefficient (K , as high as 2.0) in defining the spring parameter. This chapter evaluates the applicability of the existing design guidelines by performing beam-on-spring analysis for small-diameter steel pipes experiencing relative axial ground movements. The present study reveals that K_0 or K recommended in the design guidelines are not applicable to predict the maximum axial soil resistance measured during the full-scale tests. Then, the K -values were back-calculated for the tests using the design equation and applied to the beam-on-spring analysis to simulate the test results. A correlation was found between the back-calculated K -value and pipe diameter, where a larger diameter pipe corresponds to a smaller K -value. Finally, a beam-on-spring analysis was conducted for a one-kilometer-long pipeline subjected to relative axial ground movement using different values of K , which reveals that the current guidelines may permit greater ground movement before the pipes reach the yield or fail.

4.2 Introduction

Understanding the behaviour of buried pipelines during ground movement events is an important part of pipeline design and management. Compiled data regarding pipeline incidents in the US and Europe showed that 37% of pipelines affected by natural hazards in the US were geological in nature (Girgin and Krausmann 2014). The European Gas Pipeline Incident Data Group (2015) reported that 85% of pipeline accidents attributed to geohazards in Europe between 2004 and 2013 occurred due to landslides. Clearly pipelines throughout a network may run through areas where ground movement is expected or common, and thus must be designed to withstand soil movement. Depending on the direction of the movement relative to the pipe, the behaviour of the pipe will change. The movement parallel to the pipe length will cause axial loads, while a perpendicular movement will cause lateral loads and induce bending. Ground movement at an angle between 0 and 90° can develop a combination of the two and is termed oblique. Due to these various loads from ground movements, large pipe deformations and even ruptures may occur. Considering the importance of the pipe–soil interaction during movement events, there are currently guidelines to assist with design in this area. The American Lifelines Association (ALA) published a guideline in 2001, updated in 2005, titled *Guidelines for the Design of Buried Steel Pipe*. Another, titled *Guidelines for Construction Natural Gas and Liquid Hydrocarbon Pipelines through Areas Prone to Landslide and Subsidence Hazards*, was published by Pipeline Research Council International in 2009.

These design guidelines, such as ALA (2005) and PRCI (2009), state that evaluating pipeline response to ground movement requires finite-element (FE) analyses that account for

nonlinear soil and pipeline behaviour. They mention the applicability of a three-dimensional (3-D) continuum model and a simple soil spring model to compute the response. The guidelines present equations for calculating the maximum soil resistance per unit length of the pipes in the axial, lateral, and vertical directions during ground movements. These resistances are used to define the soil spring stiffness, which characterizes the behaviour of spring elements in a beam-on-spring analysis. In current guidelines, all springs (axial, lateral and vertical) are uncoupled or independent of one another. However, these springs may influence the behaviour of each other. To study this interaction and to further explore underlying mechanisms, 3-D models are often employed. To this end, Barrett and Phillips (2020) conducted continuum-based 3-D finite-element (FE) modelling. They developed a system that linked axial, lateral and vertical soil-spring behaviour to more accurately predict the pipes behaviour. While continuum analyses show potential in overcoming the limitations of simplistic soil springs analysis, practical considerations such as large model size, limited relative pipe displacement, challenges in capturing non-continuum behavior, demands for more detailed soil property, and limited validation suggest that the use of a simple soil spring model is practical for routine engineering applications. Various researchers have used soil spring analysis to predict the forces that develop during ground or pipe movements. Liu and Wang (2018) used soil-spring analysis to study the global lateral buckling of buried submarine pipelines. They considered all three directional springs: vertical, axial, and lateral, each defined by varying methods. The vertical springs were defined using bilinear elastic-perfectly plastic spring models (ALA 2005). Behaviour of axial springs were defined by curve-fitting results from White et al. (2011) producing an elastic-perfectly-plastic spring. Lastly, lateral springs were defined using both an ideal elastic-perfectly-plastic spring and a multi-linear spring including post-peak softening as per DNV (2009). The

models were coupled with the modified RIKS algorithm, which uses the load magnitude as an unknown, solving for both force and displacement results simultaneously. According to Liu and Wang (2018), it is a generalized displacement control method and is useful for decreasing convergence time of some stable problems. Jung et al. (2016) performed 2D continuum analysis and developed new sets of hyperbolic force versus displacement relationships to define the spring parameters. Results calculated using the proposed method were compared to results from ALA (2005) guidelines and the results of full-scale experimentation with High-Density Polyethylene (HDPE) pipes.

Beam-on-spring can be performed either using discrete spring elements or special-purpose pipe–soil interaction (PSI) elements connected to the pipe. Sun et al. (2011) used PSI elements to model upheaval buckling in pipelines subjected to high temperatures and pressures. Liu and Wang (2018) also used PSI elements to predict global lateral buckling responses of submarine pipelines buried in sand. More recently, Sinha and Dhar (2023) investigated the soil resistance at the junction of a Medium-Density Polyethylene (MDPE) pipe using the PSI elements. Traditional non-linear springs have also been used in various studies. Kouretzis and Wu (2021) performed nonlinear beam-on-spring analysis using discrete spring elements for a buried steel pipe crossing an oblique normal fault. Saberi et al. (2022) developed a Hybrid-Winkler-Interface (HWI) model with nonlinear Winkler springs oriented in the vertical-uplift, vertical-bearing and lateral directions and an added ‘thin-layer’ of interface elements in the axial direction to capture the pipe–soil interface behaviours. The directions of the Winkler springs were chosen corresponding to the normal stresses at the pipe’s crown, invert and springline locations. Spring parameters were defined as per ALA (2005), while interface elements used an

advanced constitutive model based on bounding surface plasticity theory and critical state soil mechanics (CSSM). Using the HWI, they were able to simulate the cyclic axial pipe–soil interaction behaviour measured during full-scale testing. While both elements may produce similar results, one drawback of using discrete spring elements is associated with their distribution density in the model (Liu et al. 2015). Stress concentrations may develop at spring nodes under significant load when springs are sparsely distributed along the pipeline. In the present study, both approaches of beam-on-spring modeling are considered for buried steel pipes subjected to axial loads only.

Full-scale experiments are generally conducted to investigate the axial soil reaction developing on a pipe as a result of relative ground movements. Most often, the results of full-scale axial testing do not coincide with results calculated using previously mentioned guidelines, particularly when dense cohesionless soil is used as a backfill material (Murugathasan et al. 2021, Al-Khazaali and Vanapalli 2019, Sheil et al. 2018, Bilgin and Stewart 2009, and Wijewickreme et al. 2009). These discrepancies are also shown by Andersen et al. (2024), which is presented in Chapter 3. In calculating the maximum force (per unit length) for an axial spring, the ALA guideline considers normal stress as the arithmetic mean of the vertical overburden pressure and the at-rest lateral earth pressure at the springline level of the pipe. However, PRCI (2009) adopts K (effective coefficient of horizontal earth pressure) from the study of Wijewickreme et al. (2008), instead of K_0 (at-rest coefficient of horizontal earth pressure) to calculate the normal stresses on the pipe in dense sand. The K in the PRCI guideline is attributed to the normal stress increase due to the shear-induced dilation of the interface soil. However, a fixed value of K (as high as 2) cannot predict the peak soil resistance in all test conditions

(Meidani et al. 2018, Andersen et al. 2024). For instance, Andersen et al. (2024) found that the measured axial peak forces, depending on pipe diameter, were 3 to 6 times larger than those calculated by ALA (2005) and 1.5 to 3 times larger than those calculated by PRCI (2009), when pulling a soil tank over a restrained pipe. For pulling a pipe through static soil mass, the peak forces obtained by Murugathasan et al. (2021) were about two times higher than the ALA (2005) prediction but agreed well with PRCI (2009) calculations. Both the studies (Murugathasan et al. 2021 and Andersen et al. 2024) were conducted on shallow buried depths (600 mm from the pipe springline). On the other hand, for deep burial pipes, ALA can predict the peak resistance well for the tests conducted in Sheil et al. (2018), whereas PRCI significantly overestimate the peak load. Meidani et al. (2018) used three-dimensional discrete element analysis to create an expression for estimating the modified earth pressure coefficient (K^*). This parameter can be used to calculate the maximum axial soil resistance for steel pipes buried in dense sand for different ground conditions and pipe diameters. However, when calculating K^* using the proposed equation, one must exercise caution in selecting the parameters involved, otherwise, the peak axial force could be substantially overestimated or underestimated.

This chapter aims to select spring parameters to accurately predict tests results from full-scale axial testing performed by Andersen et al. (2024). In this regard, two-dimensional (2D) nonlinear beam-on-spring Winkler models were developed using the finite-element software Abaqus. Two types of soil-spring elements were employed in developing the model: traditional discrete spring elements and specialized Pipe–Soil Interaction (PSI) elements to investigate their respective effects on the results. In the current analysis, different K -values were considered when defining the soil spring sparameters, including K_0 as per ALA (2005), $K = 2.0$ as per PRCI

(2009), K^* as per Meidani et al. (2018) (discussed later in the chapter), and a back-calculated value termed K -fit which is the K -value required to produce the peak soil resistance. From this, an attempt was made to develop an equation, linking K -fit to pipe diameter regardless of setup (soil-pull or pipe-pull). In addition to the models simulating testing of Andersen et al. (2024), models were also developed to simulate testing by Murugathan et al. (2021), Sheil et al. (2018), Bilgin and Stewart (2009) and Wijewickreme et al. (2009). For these models, parameters set out in ALA (2005) were used along with K -fit. Finally, an example is presented, comparing the maximum pipe wall strains to allowable strain recommendations employing the current guidelines and the K -fit value for a 1 km long buried pipeline subjected to axial ground movement.

4.3 Full-scale Testing

Full-scale testing of small-diameter steel pipes subjected to axial ground movement was investigated by Andersen et al. (2024). They outlined the development of a testing facility at Memorial University of Newfoundland, where the tank can move to represent the displacement of the ground. The setup included a steel base-frame bolted to the floor and a steel carriage on which the 4 x 2 x 1.5 m soil tank is mounted. Six linear bearing tracks and slides were mounted between the base frame and steel carriage, allowing smooth system movement. The tank was connected to a hydraulic ram capable of moving the system up to 150 mm. Steel pipes were placed in the tank through 177 mm diameter holes at either end, with rubber gaskets fitted to the pipe diameter to prevent soil leakage and reduce pipe-tank friction. Pipes were 4.5 m long to maintain a constant 4 m burial length during testing. Pipes were connected at one end to a load

cell of appropriate capacity for different pipe diameters, fixed to a rigid backstop. The opposite end of the pipe was left unrestrained outside the tank. See Fig. 4-1 for the layout.

Using the setup described, Andersen et al. (2024) performed multiple tests on 26.7-, 60.3- and 114.3 mm diameter pipes by pulling the testing cell 35 mm at a rate of 0.5 mm/min. After each pulling phase, a relaxation phase was performed for varying time periods, between 1 and 3 days. The soil tank was held in place during these phases while data was recorded. The final phase pushed the testing cell back to its original location. One pipe of each diameter was instrumented with a fibre-optic strain sensor, capable of capturing real-time strain data along the length of the pipe during testing. The instrumented pipes corresponded to tests ST-02, ST-04 and ST-06 for the 26.7-, 60.3- and 114.3 mm diameter pipes, respectively, while ST-01, ST-03 and ST-05 remained bare.

Each pipe was buried in a well-graded, locally manufactured sand with a burial depth of 650 mm from surface to pipe springline. Saha (2021) performed direct shear and triaxial tests on the test soil to determine its mechanical properties. Table 4-1 lists the backfill soil parameters, after Saha (2021). Soil was lifted into the tank in large sandbags using an overhead crane, while each lift was compacted using an electric vibratory plate tamper. Sand-cone testing as per ASTM D1556 (2007) was used to confirm soil density before testing, with the average value being 18.1 kN/m³. Full testing results are not included in this chapter, though some results have been compared to FEA results in subsequent sections. Further details and results of the testing programme can be found in Andersen et al. (2024).

4.4 Finite-Element Model

4.4.1 Modelling Techniques

A total of 26 analyses were performed using a dynamic implicit modelling technique in Abaqus. See Table 4-2 for a model matrix. As mentioned earlier, current design practices for pipe–soil interaction primarily rely on force–displacement responses in each direction (lateral, vertical, and axial). Therefore, all models were created using axial and vertical spring elements to simulate the axial soil resistance in a 2-D environment. In the case of pure axial loading (presented herein), vertical springs were added for the convergence purposes only. First, three models were created using PSI elements simulating testing performed by Andersen et al. (2024) on three differing pipe diameters. ALA (2005), PRCI (2009), recommendations of Meidani et al. (2018), and the findings of Andersen et al. (2024) were used to define the axial spring parameters for each pipe. Analyses were performed by displacing the PSI element’s far end nodes while keeping one end of the pipe fixed. Alternatively, three additional analyses were conducted by pulling the pipe’s leading end and fixing the far-end nodes. Parameters recommended by ALA were considered here. The aforementioned six analyses were performed to examine potential differences between the soil-pull and pipe-pull methods in FE. Furthermore, three models were developed using SPRING2 elements (discrete spring between two nodes, acting in a fixed direction) for three sizes of pipes. Models P01–P15 and S01-S03 were created to simulate the axial soil resistance for the pipes tested in Andersen et al. (2024). Finally, another four models were created using PSI elements to simulate results published in Murugathan et al. (2021), Sheil et al. (2018), Bilgin and Stewart (2009) and Wijewickreme et al. (2009). These studies were chosen as they investigated the response of steel pipes during axial ground movement by way of axial pull-out testing such that a comparison could be drawn between pull-out and soil-pulling. For these

models, spring parameters were set out according to ALA (2005) along with back-calculated K -fit value (discussed in the following section).

Each model used the same pipe material properties: Young's Modulus, E , of 200 GPa with a Poisson's ratio ν of 0.3. No plastic material properties were included, as the pipe was not expected to develop plastic deformation for the applied displacement, as shown in Andersen et al. (2024). The pipe is modelled using linear B21 beam elements, which uses Timoshenko beam theory. They can resist axial and bending forces and include transverse shear deformations. Models employing cubic beam elements (B23) not allowing transverse shear deformations, as per Euler-Bernoulli beam-theory, were also used to simulate Andersen et al. (2024) tests; these elements did not produce significantly different results from the B21 elements. Uniformly sized elements of 0.001 m were used to discretize the beam for all models. A mesh sensitivity study was performed using element sizes of 0.002, 0.004, 0.05, 0.1 and 1 m, see Fig. 4-2, although this had no effect when using PSI elements to simulate the particular test conditions (4 m of pipe length). Note that the width of the PSI elements is the same as the length of the pipe element, as the PSI elements share the same nodes with the pipe elements (as discussed later). When traditional SPRING2 elements were used, decreased spring density also had no impact on the axial force. The total pipe length was modelled per the full-scale tested length for each test obtained from published literature. See Table 4-3 for full-scale testing parameters.

All analyses were performed using two steps: first, a gravity step, where gravity was applied to the model in the Y direction. Then a pulling step, which displaced either the soil nodes or the pipe as required in the +x direction. During the gravity step for soil-pulling, the pipe fixed-end node and each far-field soil node was restrained in both the x and y directions. During the

pulling step, the far-field soil nodes were released in the X direction, and displaced constantly for 0.035 m. For the pipe-pulling case, the far-field soil nodes were fixed in both X and Y directions during both steps, while the pipe was allowed to translate 0.035 m during the pulling step.

4.4.2 PSI Elements

The PSI element defines the soil as a Winkler media. The element interacts with the structural beam element, as illustrated in Fig. 4-3. Two-dimensional 4-noded PSI 24 elements were used for the analyses. At one end, the element shares a node with the pipeline (beam element) while nodes on the opposite end represent a far-field surface, such as the ground surface. The pipe's burial depth from springline to surface (H) is modelled using the PSI element's length. Each node has only displacement degrees of freedom, with the relative displacement between them transmitting force to the pipeline in relation to their stiffness. The force–displacement relationship used to represent soil spring characteristics was defined using a bilinear elastic-perfectly plastic spring model. Fig. 4-4 shows the typical force–displacement relations recommended in design guidelines (e.g., ALA 2005). The ultimate axial spring force per unit length was defined using Eq. (4-1).

$$T_u = \pi DH\gamma \frac{1+K}{2} \tan \delta \quad (4-1)$$

Where D is the pipe outside diameter, H is the burial depth, γ is the effective unit weight of soil, K is the lateral earth-pressure coefficient, and δ is the interface friction angle obtained from the multiplication of the pipe coating factor and soil interface friction angle ϕ' . The ultimate axial spring force per unit length (T_u) was calculated using Eq. (4-1) with an ultimate relative displacement (x_u) of 3 mm considered for dense sand. Four different lateral earth pressure coefficient values were used in Eq. (4-1) during the analysis: K_0 (ALA 2005), $K = 2.0$ (PRCI

2009), K^* (Meidani et al. 2018), and K -fit (back-calculated to fit experimental data). Note that the K value in Eq. (4-1) accounts for lateral normal stresses on the pipe at the peak pullout loads; however, the normal stresses surrounding the pipe may be different (as shown in Wijewickreme et al. 2009). Meidani et al. (2018) proposed an equation for K^* (modified earth pressure coefficient) to calculate the ultimate axial resistance of pipes in dense sand as below.

$$K^* = 2.75 \times K_0 \times \left(\frac{E_s}{\gamma H} \right)^{0.38} \times \left(\frac{\phi}{45} \right)^{1.39} \times \left(\frac{\Delta t}{D} \right)^{0.42} \quad (4-2)$$

where E_s is the Young's Modulus of soil calculated using Eq. (4-3), as given by Hardin and Black (1966) and Janbu (1963).

$$E = K p_a \left(\frac{p'}{p_a} \right)^n \quad (4-3)$$

Where K is a material parameter that determines the scale of E_s , p_a is the atmospheric pressure taken as 101.3 kPa, p' is the initial confining pressure at the pipe springline, and n is an exponent. The value of K is taken as 150 for dense sand, and n is taken as 0.5, per Roy et al. (2016). In Eq. (4-2), Δt is the thickness of the active shearing zone, which is calculated as ten times the median particle size (d_{50}) initially proposed by Roscoe (1970) and Bridgewater (1980), later confirmed by Scarpelli and Wood (1982) and Karimian (2006). Finally, the back-calculated K -fit value was determined by applying Eq. (4-1) to the maximum measured soil resistance per unit length obtained from the full-scale tests.

As the current study focuses on purely axial loads, only the parameters for axial springs are relevant. However, vertical spring parameters were needed since the model was developed in a two-dimensional environment. The vertical spring models were defined using Eq. (4-4), as recommended in the current design guidelines.

$$Q_d = N_c Dc + N_q \bar{\gamma} H D + N_y \frac{D^2}{2} \quad (4-4)$$

Where N_c , N_q , and N_y are bearing factors. Eq. (4-4) represents the ultimate vertical bearing force per unit length of pipe that the soil will produce at a given displacement ($0.1D$ for granular soils). Since there was no perceivable vertical motion during full-scale testing, the ultimate downward and upward displacements were set to 0.0001 m for convergence purposes. A value of exactly 0 m would result in an error.

4.4.3 Nonlinear Springs

As mentioned above, beam-on-spring analyses were also performed using the discrete nonlinear springs defined as SPRING2 in Abaqus. Fig. 4-5 presents the typical spring elements attached to the pipe. Each spring element was attached to two nodes set an arbitrary 10 mm apart. Note that this distance does not impact the analysis, as spring length is irrelevant to spring displacement. The one node of the spring was that of the beam element (the pipe), and the other node was a fixed point, simulating stable soil at the far-field condition. Depending on the analysis, the pipe end node or the soil nodes were displaced. Behaviour of the nonlinear springs was defined using force–displacement pairs. The ultimate axial force was calculated using Eq. (4-1) and the corresponding displacement was given as 3 mm for dense sand (ALA 2005). Beyond 3 mm of displacement, the force remained constant to simulate elastic-perfectly plastic behaviour. Note that initial forces in the nonlinear springs were defined by providing a nonzero force, at zero relative displacement. Vertical springs were attached to the axial springs by connecting one end to the pipe element nodes and the other to a fixed node directly above it.

4.5 Model Results

4.5.1 Load–Displacement Responses

Fig. 4-6 shows force–displacement plots for models P01 through P15, compared against the full-scale test results reported in Andersen et al. (2024). Fig. 4-6(a) presents the plot for analyses P01–P05 for the 26.7 mm diameter pipe. Each of the analyses was performed for different axial spring parameters by changing the K -values from Eq. (4-1), except P01 and P02; the same stiffness was used for these models using $K_0 = 0.43$. Instead the displacement method was altered; with P01 moving the soil nodes while P02 moved the pipe’s leading end. Both models produced identical results, showing the pulling method does not matter when performing a beam-on-spring analysis. Both P01 and P02 developed a peak force of just under 2 kN in this configuration. While setting $K = 2$ as per PRCI (2009), produces peak loads of 4 kN and setting $K = K^* = 4.51$ (as suggested by Meidani et al. 2018) produces a peak load of about 7 kN. Finally, the peak force obtained from Test ST01 in Andersen et al. (2024), 13.25 kN, is entered into Eq. (4-1) and a K -value of 9.10 is back-calculated. This result produces a peak force equaling that of the full-scale testing. Thus, the required K -value to produce the experimental peak load is much higher than either value proposed currently. Note that there are differences in the initial slope of the curves in Fig. 4-6, because the maximum elastic displacement of the spring model was defined 3 mm according to the guidelines. On the other hand, the peak force occurred at a higher tank displacement during the tests. This is because the shear strength of all soil particles along the pipe length did not fully mobilize at the same tank displacement. Also, the post-peak softening response of the measured force–displacement curve could not be simulated due to the use of elastic perfectly-plastic spring model. The goal of this analysis was to achieve the peak force, thus, no attempt was made to simulate post-peak behaviour.

Similarly, Fig 4-6(b) and 4-6(c) plot the force–displacement results of the analyses (P06 to P15) with the measured responses for 60.3– and 114.3 mm-diameter pipes, respectively. As seen in the figures, no differences in the results were observed for the soil node displacement and pipe node pulling in the beam-on-spring analysis. Again, four different K -values were used to calculate the ultimate axial spring force for each pipe diameter, with $K_0 = 0.43$, $K = 2.0$, $K^* = 3.20$ ($D = 60.3$ mm) and 2.45 ($D = 114.3$ mm), and back-calculated $K = 6.22$ ($D = 60.3$ mm) and 6.11 ($D = 114.3$ mm). Results show that the K -values recommended by both guidelines and literature failed to predict experimental peak axial resistances. The back-calculated K -values required to produce peak loads are significantly higher for all pipes tested. It should be noted that there is some sensitivity when calculating K^* using Eq. (4-2). Due to the uncertainty in parameters, such as soil modulus (E_s) and shear zone thickness (Δt), Eq. (4-2) might produce varying values of K^* . Consequently, the peak axial spring force per unit length could be overestimated or underestimated. As an example, E_s is calculated as per Eq. (4-3), which uses a coefficient K (modulus number) having a wide range of values. Fellenius (2009) shows a range for the material constant, K , of 150 to 400 for compact to dense sand. Using a value of $K = 250$ produces an $E_s = 7.0$ MPa, almost double that $K = 150$ produces. When input into Eq. (4-2), $E_s = 7.0$ MPa will result in more than 20% higher K^* which will reduce the underestimation of the peak loads of the present test results. Although K^* values see an increase, they still fall short of the back-calculated K -fit values. On the other hand, the selection of Δt depends on the median soil particle size (d_{50}), which is approximately 5–10 times d_{50} as recommended in Roscoe (1970), Bridgewater (1980), Scarpelli and Wood (1982), DeJong et al. (2006), and Karimain (2006). This range of Δt results in significant differences in the calculated K^* . For example, keeping all

other parameters the same for test ST01 ($D = 26.7$ mm), Eq. (4-2) calculates a $K^* = 4.51$ for $\Delta t = 10d_{50}$, but a $K^* = 3.37$ for $\Delta t = 5d_{50}$ (a 35% difference). Although Eq. (4-2) failed to predict the measured peak responses for the tests reported herein, it is better than the currently used approach in the pipeline design.

As previously mentioned, three additional models (S01–03) using traditional discrete springs were created to compare results to those of PSI elements. Fig 4-7 presents a comparison of results between the two methods. Each method produced the same results given a total element count of 4,000 for both the beams and springs. Even if half that number is used (2,000) for each element (beam and spring), there is no effect on the axial load for the test conditions simulated. While both element types produced similar results, stress concentrations may arise at the spring nodes under certain loading scenarios if the springs are sparsely distributed along the pipe (Liu et al. 2015).

A beam-on-spring analysis was also conducted in some of the previous studies to determine axial spring parameters. Models P16, P18, P20, and P22 simulate literature-based tests in which axial spring parameters were defined using Eq. (4-1), with K specified as K_0 based on the parameters of each experiment. Subsequently, a K -value was back-calculated for each test and defined in models P17, P19, P21, and P23 to satisfy the experimental results (Fig. 4-8). A list of relevant model parameters is presented in Table 4-4. As expected, the results from models P17, P19, P21, and P23, employing back-calculated K -values, align with the experimental peak loads, as illustrated in Fig. 4-7(b). Notably, the K -values corresponding to peak forces for tests reported by Murugathan et al. (2021), Sheil et al. (2018), Bilgin and Stewart (2009), and

Wijewickreme et al. (2009) were 2.09, 0.24, 2.10, and 1.76, respectively. These values are significantly higher than the recommended K_0 (ALA 2005) but very close to the value (2.0) suggested in PRCI (2009), except for Sheil et al. (2018). This discrepancy can be attributed to the fact that the test by Sheil et al. (2018) was conducted at much higher burial depths than the others, where the dilative effects of dense sand could be suppressed due to the higher overburden pressure. Consequently, the K value is much lower and approaches K_0 .

It should be noted that, as seen in the previous chapter, the normalized peak axial resistances developed by pulling a soil mass axially along a pipe were greater than those developed by pulling a pipe directly through a stationary soil mass. However, all the current understandings mentioned above are developed for pulling the pipe through the soil. In summary, the higher K -value with the present study may be attributed to the combined effects of three factors: (1) higher compaction of the backfill soil, (2) higher soil dilation on small diameter pipes, and (3) higher loads on pipes due to tank displacement. Further study is required to examine the soil stress on the pipes either experimentally or numerically to explore the mechanism.

4.5.2 K -Value Comparisons

Fig. 4-9 plots the back-calculated K -fit values for the previous studies and the tests performed by Andersen et al. (2024), against pipe outside diameter. The trendline, plotted using Eq. (4-5) below, fits the data moderately well, with an R^2 value of 0.63.

$$K_{\text{fit}} = 315.87D^{-0.982} \quad (4-5)$$

The parameter D in the equation is the pipe outside diameter, in mm. It should be noted that any differences arising from soil-pulling versus pipe-pulling have been ignored for the sake of analysis, as these differences are not well-understood at this time. The trend shows that as pipe diameter increases, the K -fit value decreases, although there are some distinct differences when calculating K -fit from the equation, as seen in Table 4-5. However, there is a correlation between the K -value and pipe diameter with a larger pipe diameter corresponding to a smaller K -value. Obviously, additional research is needed on large-diameter pipes to confirm the trend for tank displacement.

4.6 Pipe Axial Strain

To compare the effects of different K -values in pipeline design subjected to axial ground movements, beam-on-spring analysis was performed on a one-kilometer-long steel pipeline. Similar to the full-scale testing previously mentioned, an axial ground displacement of 70 mm was applied over the full pipe length. The boundary conditions and displacement methods were similar to models in Table 4-2, with one end of the pipe being fixed and the PSI far-nodes being displaced by 70 mm. Burial depths and pipe diameters were assumed to be 600 and 60 mm, respectively. The pipe was discretized using a uniform element size of 1 m. Note that to be conservative, no joints were considered in the pipeline as it was assumed any joints would be stiffer than the pipe itself. Three analyses were performed, one using $K = K_0 = 0.5$ as per ALA (2005), one using $K = 2.0$ as per PRCI (2009) and the other using $K = K$ -fit in Eq. (4-1) as presented earlier. Results of the analysis showed that at 70 mm of soil displacement, using a K -fit value of 6.22, the maximum axial strain of 0.23% was developed at the fixed-end of the pipe (Fig. 4-10). This is greater than the allowable limit of 0.2% strain in steel pipes (Chan and Wong

2004 and Weerasekara and Rahman 2019). In contrast, 70 mm of displacement only caused 0.1% and 0.15% of axial strain when using ALA and PRCI, respectively. These findings suggest that following the current guidelines may permit greater ground movement before the pipes yield or fail, potentially causing damage to the pipeline sooner than expected.

Fig. 4-10 plots the axial strain distribution along the pipeline length for 70 mm of soil displacement. As the axial strain depends on the axial stress/force, it can be said from the distribution that the interface shear stress mobilizes gradually from the fixed end to the free end of the pipe. The linear strain profile along the pipeline length indicates that the maximum shearing resistance of the soil is fully mobilized and experiences sliding at the interface over this distance. Whereas the nonlinear strain distribution indicates soil resistance is not fully mobilized and the pipeline remains ‘bonded’ to the interface soil. Beyond this, to the free end of the pipe, soil frictional resistance is not mobilized at all, resulting in zero strain. It is evident from Fig. 4-10 that as the value of the peak axial spring force (spring stiffness) increases via K -value increases, the length of the pipeline along which the axial strain (or force) is distributed significantly decreases. As seen in the figure, this length (a.k.a “mobilized frictional length”) is significantly lower (60% to 120%) when using K -fit in Eq. (4-1) instead of the ALA or PRCI recommended values. Thus, a shorter length of the pipeline experiences the effects of sliding. The determination of mobilized frictional length is of considerable importance, especially because pipe connections are common in distribution networks. If connections experience soil friction, they can create large, localized strains in the main pipe (Weerasekara et al. 2006, Chakraborty et al. 2020). Therefore, accurate determination of the mobilized frictional length is

important, and a useful metric to ascertain whether the frictional resistance of a pipe connection is mobilized.

4.7 Conclusions

This chapter evaluates the beam-on-spring method used to calculate axial forces in buried steel distribution lines subjected to axial ground movements. Full-scale pipe tests conducted by various researchers were simulated using FE analysis by idealizing the pipes as beam elements and the pipe–soil interaction as spring elements. The study reveals that while beam-on-spring analysis can be used to simulate the test results, the spring parameters recommended by the design guidelines are not suitable for the test condition presented in this study. Axial springs stiffer than those recommended in the design guidelines, or available literature, was required to simulate the test results. The main conclusions reached from the analyses are presented below.

- 1) ALA (2005) and PRCI (2009) guidelines underpredicted the maximum spring force required for the test conditions. The only difference between these two guidelines is the coefficient of lateral earth pressure, which accounts for normal stresses on the pipe. ALA (2005) recommends K_0 (lateral earth pressure coefficient at rest), whereas PRCI (2009) uses K (effective lateral earth pressure coefficient) to calculate the peak axial spring force. Between the two design guidelines, the peak spring force given by PRCI (2009) is higher; however, still falls short of the values needed to simulate the test results.
- 2) The modified earth pressure coefficient proposed by Meidani et al. (2018) did not produce the desired peak force, although it performed better than others.

- 3) Using the design equation, K -values for all the tests were back-calculated to simulate the pipe's behaviour. These back-calculated K -values are moderately higher than the values recommended in the guidelines and reported by other researchers. This may be attributed to the combined effects of three factors: (a) compaction of the backfill soil, (b) shear-induced soil dilation, and (3) higher loads on pipes during tank displacement than pipe pullout.
- 4) Using the test results presented in Chapter 3 and data available in literature, a correlation between the back-calculated K -value and pipe diameter was found. A larger diameter pipe corresponds to a smaller K -value.
- 5) Beam-on-spring analysis was also performed for a 1 km long pipeline subjected to axial ground movement using different axial spring parameters. The maximum pipe strain is higher if using a higher K , ie K -fit, than ALA (2005) and PRCI (2009) recommended values. Also, the length along the pipe which the axial strain (or force) distributes decreases when the K -value is increased.

The method of obtaining spring parameters for steel pipes presented in this study was developed for the test conditions discussed in the paper. Further research is needed to investigate the correlation between the axial soil resistance and pipe diameter for other burial conditions and loading scenarios.

4.8 Acknowledgements

The authors would like to gratefully acknowledge the financial support and/or in-kind support provided by the Alliance Grants program of the National Science and Engineering Research

Council of Canada, FortisBC Energy Inc., SaskEnergy Canada Inc., and WSP Canada Inc. for conducting this research.

4.9 References

- ALA (American Lifelines Alliance) 2005. *Guidelines for the design of buried steel pipe*. Washington, DC and Reston, VA, USA: Federal Emergency Management Agency (FEMA) and American Society of Civil Engineers (ASCE).
- Al-Khazaali, M., and Vanapalli, S. K. 2019. Axial force-displacement behaviour of a buried pipeline in saturated and unsaturated sand. *Géotechnique*, 69(11): 986–1003.
- Andersen et al. 2024. Full-scale testing of small-diameter steel pipes buried in dense sand, subjected to axial loading using a moving soil tank. (not submitted yet)
- ASTM (2015) D 1556: Standard test method for density and unit weight of soil in place by the sand-cone method. *ASTM International*, West Conshohocken, PA, USA.
- Barrett, J., and Phillips, R. 2020. Formulation of 3D Soil Springs for Pipe Stress Analyses. *In International Pipeline Conference* (Vol. 84454, p. V002T02A012). American Society of Mechanical Engineers.
- Bilgin, Ö., and Stewart, H. E. 2009. Pullout resistance characteristics of cast iron pipe. *Journal of Transportation Engineering*, 135(10): 730–735.
- Chan, P. D., and Wong, R. C. 2004. Performance evaluation of a buried steel pipe in a moving slope: a case study. *Canadian Geotechnical Journal*, 41(5): 894–907.
- Chakraborty, S., Dhar, A. S, Talesnick, M., and Muntakim, A. H. Behavior of a branched buried MDPE gas distribution pipe under axial ground movement. Proc., 73rd Canadian Geotechnical Conf., Canadian Geotechnical Society, GeoVirtual 2020.

- European Gas Pipeline Incident Data Group. 2015. *Gas Pipeline Incidents. 9th EGIG Report 1970–2015, No EGIG 05-R-0002.*
- Girgin, S., and Krausmann, E. 2014. Analysis of pipeline accidents induced by natural hazards. European Union: Brussels, Belgium.
- Hardin, B. O., and Black, W. L. 1966. Sand stiffness under various triaxial stresses. *Journal of the Soil Mechanics and Foundations Division*, 92(2): 27–42.
- Janbu, N. (1963). Soil compressibility as determined by oedometer and triaxial tests. *In Proceedings, European Conference on Soil Mechanics and Foundations Engineering, Wiesbaden, Germany 1963 (Vol. 1, pp. 19–25).*
- Jung, J. K., O'Rourke, T. D., and Argyrou, C. 2016. Multi-directional force–displacement response of underground pipe in sand. *Canadian Geotechnical Journal*, 53(11): 1763–1781.
- Karimian, S. A. 2006. Response of buried steel pipelines subjected to longitudinal and transverse ground movement, Doctoral dissertation, University of British Columbia.
- Liu, R., and Wang, X. Y. 2018. Lateral global buckling of submarine pipelines based on the model of nonlinear pipe-soil interaction. *China Ocean Engineering*, 32(3): 312–322.
- Meidani, M., Meguid, M. A., and Chouinard, L. E. 2018. Estimating earth loads on buried pipes under axial loading condition: insights from 3D discrete element analysis. *International Journal of Geo-Engineering*, 9: 1–20.
- Murugathasan, P., Dhar, A. S., and Hawlader, B. C. 2021. An experimental and numerical investigation of pullout behavior of ductile iron water pipes buried in sand. *Canadian Journal of Civil Engineering*, 48(2): 134–143.
- PRCI (Pipeline Research Council International). 2009. *Guidelines for constructing natural gas and liquid hydrocarbon pipelines through areas prone to landslide and subsidence hazards.*

Report prepared for the Design, Material, and Construction Committee. Chantilly, VA:
Pipeline Research Council International, Inc.

Roy, K., Hawlader, B., Kenny, S., and Moore, I. 2015. Finite element modeling of lateral pipeline–soil interactions in dense sand. *Canadian Geotechnical Journal*, 53(3): 490–504.

Saberi, M., Behnamfar, F., and Vafaeian, M. 2013. A semi-analytical model for estimating seismic behavior of buried steel pipes at bend point under propagating waves. *Bulletin of Earthquake Engineering*, 11(5): 1373–1402.

Saberi, M., Annan, C. D., and Sheil, B. B. 2022. An efficient numerical approach for simulating soil-pipe interaction behaviour under cyclic loading. *Computers and Geotechnics*, 146: 104666.

Saha, R.C., Dhar, A.S., and Hawlader, B.C. 2019. Shear strength of a well-graded clean sand, Geo St. John's 2019, *Canadian Geotechnical Society*, St. John's, NL, CA.

Scarpelli, G., and Wood, D. M. 1982. Experimental observations of shear patterns in direct shear tests. In *IUTAM Deformation and Failure of Granular Materials Conference* (pp. 473–483).

Sheil, B. B., Martin, C. M., Byrne, B. W., Plant, M., Williams, K., and Coyne, D. 2018. Full-scale laboratory testing of a buried pipeline in sand subjected to cyclic axial displacements. *Géotechnique*, 68(8): 684–698.

Sinha, T., and Dhar, A. S. 2023. Beam-on-Spring Modeling of Buried MDPE Pipes in Sand Subjected to Lateral Loads at Pipe Junction. *Journal of Pipeline Science and Engineering*, 100125.

- Sun, J., Shi, H., and Jukes, P. 2011. Upheaval buckling analysis of partially buried pipeline subjected to high pressure and high temperature. *In International Conference on Offshore Mechanics and Arctic Engineering* (Vol. 44366: pp. 487–494).
- Wang, Z., Chen, Z.H., and Liu, H.B. 2015. On lateral buckling of subsea pipe-in-pipe systems. *International Journal of Steel Structures*, 15(4), 881–892.
- Weerasekara, L., Wijewickreme, D., and Mitchell, A. (2006). “Response of tee-junctions in buried polyethylene natural gas distribution piping subject to ground movement.” Proc., 59th Canadian Geotechnical Conf., Canadian Geotechnical Society, Richmond, BC, Canada, 321–329.
- Weerasekara, L., and Rahman, M. 2019. Framework for assessing integrity of natural gas distribution pipes in landslide areas. In Proc., *72nd Canadian Geotechnical Conf.: Geo St. John's*.
- Wijewickreme, D., Karimian, H., and Honegger, D. 2009. Response of buried steel pipelines subjected to relative axial soil movement. *Canadian Geotechnical Journal*, 46(7): 735–752.

Table 4-1. Backfill soil parameters (Saha 2021)

Parameter	Values
Median particle size, d_{50} (mm)	0.742
Coefficient of uniformity, C_u	5.81
Coefficient of curvature, C_c	2.04
Fines content (%)	1.3
Gravel content (%)	0.87
Specific gravity, G	2.63
Minimum void ratio, e_{min}	0.32
Maximum void ratio, e_{max}	0.56

Table 4-2. Model matrix

Model Name	Test Reference	D (mm)	Size Pipe Elements	# Spring Elements	Element Type	K -ref	K -value	k (N/m)	Disp. (Pipe/Soil)
P01	Andersen et al. (2024) [ST-01]	26.7	0.001	4000	PSI	K_0	0.33		Soil
P02						K_0	0.33		Pipe
P03						PRCI	2.0		Soil
P04						K^*	4.51		Soil
P05						Fit	9.10		Soil
P06	Andersen et al. (2024) [ST-03]	60.3	0.001	4000	PSI	K_0	0.33		Soil
P07						K_0	0.33		Pipe
P08						PRCI	2.0		Soil
P09						K^*	3.20		Soil
P10						Fit	6.22		Soil
P11	Andersen et al. (2024) [ST-05]	114.3	0.001	4000	PSI	K_0	0.33		Soil
P12						K_0	0.33		Pipe
P13						PRCI	2.0		Soil
P14						K^*	2.48		Soil
P15						Fit	6.08		Soil
P16	Murugathan et al. (2021) [Test T3]	178	0.001	2700	PSI	K_0	0.38		Pipe
P17						Fit	2.09		
P18	Sheil et al. (2018) [Test K3]	350	0.001	1310	PSI	K_0	0.40		Pipe
P19						Fit	0.22		
P20	Bilgin and Stewart (2009)	175	0.001	3050	PSI	K_0	0.43		Pipe
P21						Fit	2.09		
P22	Wijewickreme et al. (2009) [Test AB-4]	457	0.001	3800	PSI	K_0	0.38		Pipe
P23						Fit	1.56		
S01	Andersen et al. (2024) [ST-01]	26.7	0.001	4000	Spring	ALA		436	Soil
S02	Andersen et al. (2024) [ST-03]	60.3	0.001	4000	Spring	ALA		985	Soil
S03	Andersen et al. (2024) [ST-05]	114.3	0.001	4000	Spring	ALA		1860	Soil

Table 4-3. Testing parameter comparisons (Andersen et al. 2024)

Parameter	Current Test Programme			Murugathasan et al. (2021)	Bilgin and Stewart (2009)	Sheil et al. (2018)	Wijewickreme et al. (2009)
	ST-01-02	ST-03-04	ST-05-06				
Test number	ST-01-02	ST-03-04	ST-05-06	T3	N/A	K3	AB-4
Pull rate (mm/min)	0.5			0.5	N/A	N/A	2-50
Pipe Diameter, D (mm)	26.7	60.3	114.3	178	175	350	457
Burial Depth, H (mm)	650		625	831	760	1180	1140
H/D	24.34	10.78	5.47	4.67	4.34	3.37	2.50
Burial Length, L (m)	4.0			2.70	3.05	1.31	3.80
Dry Unit Weight, γ (kN/m ³)	18.1		18.8	17.17	14.76	16.40	15.70
Avg. Relative Compaction, R (%)	96		98	88.4	95.0	75.0	75.0

Table 4-4. Model parameter comparisons

Parameter	Andersen et al. (2024)			Murugathasan et al. (2021)	Bilgin and Stewart (2009)	Sheil et al. (2018)	Wijewickreme et al. (2009)
	ST-01	ST-03	ST-05	Test T3	N/A	Test K3	Test AB-4
Pipe Diameter, D (mm)	26.7	60.3	114.3	178	175	350	457
Burial Depth, H (mm)	650		625	831	760	1360	1140
Burial Length, L (m)	4.0			2.70	3.05	1.31	3.80
Dry Unit Weight, γ (kN/m ³)	18.10		18.75	17.17	14.76	16.40	15.70
Earth-Pressure Coeff, K_0	0.43			0.38	0.43	0.20	0.29
Modified Earth-Pressure Coeff, K^*	4.51	3.20	2.45	N/A	N/A	N/A	N/A
Back-calculated K , K -fit	9.10	6.23	6.10	2.09	2.10	0.24	1.76
Interface friction angle, ϕ (deg)	42			38	35	36.8	45.5
Pipe–soil friction angle, δ (deg)	33.6			30.4	31.5	24.4	36

Table 4-5. *K*-fit values calculated using Equation 5

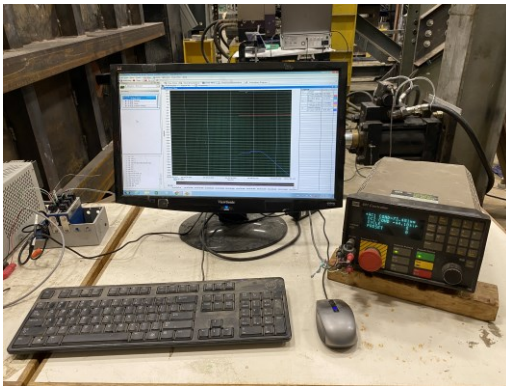
Literature Source	Back-Calculated <i>K</i> -fit	Equation 5	
		<i>K</i> -fit	Error (%)
Andersen et al. (2024) – $D = 26.7$ mm	9.10	12.55	38
Andersen et al. (2024) – $D = 60.3$ mm	6.22	5.64	-9
Andersen et al. (2024) – $D = 114.3$ mm	6.11	3.01	-51
Murugathasan et al. (2021) – $D = 178$ mm	2.09	1.95	-7
Sheil et al. (2018) – $D = 350$ mm	0.22	1.00	354
Bilgin and Stewart (2009) – $D = 175$ mm	2.09	1.98	-5
Wijewickreme et al. (2009) – $D = 457$ mm	1.76	0.77	-56



(a)



(b)



(c)



(d)

Fig. 4-1. Full-scale testing layout: (a) Pipe fixed-end connection to load cell and back-stop, (b) Pipe free-end with ram connection to tank, (c) Data acquisition system for pipe load and tank position, (d) Axial strain recording setup including controller, signal interrogator, standoff cable, remote module, sensor and port cleaner (Andersen et al. 2024)

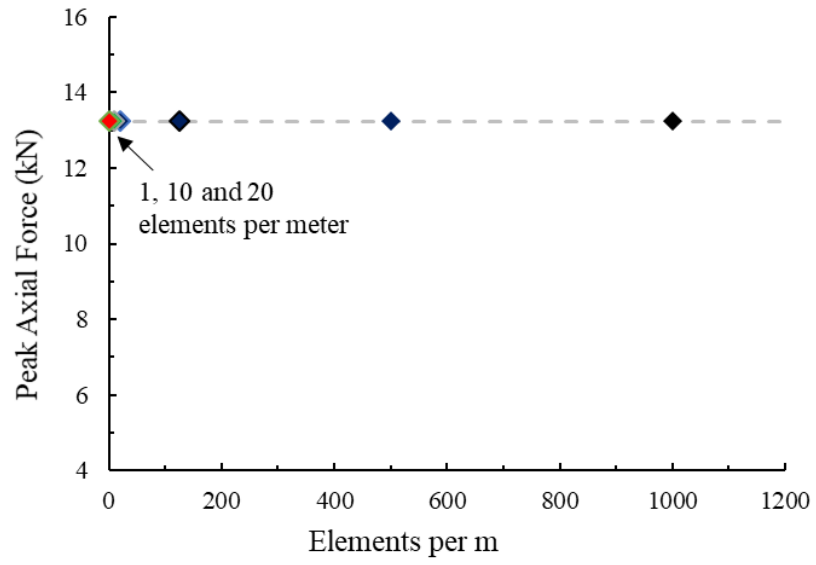


Fig. 4-2. Mesh convergence analysis for PSI elements

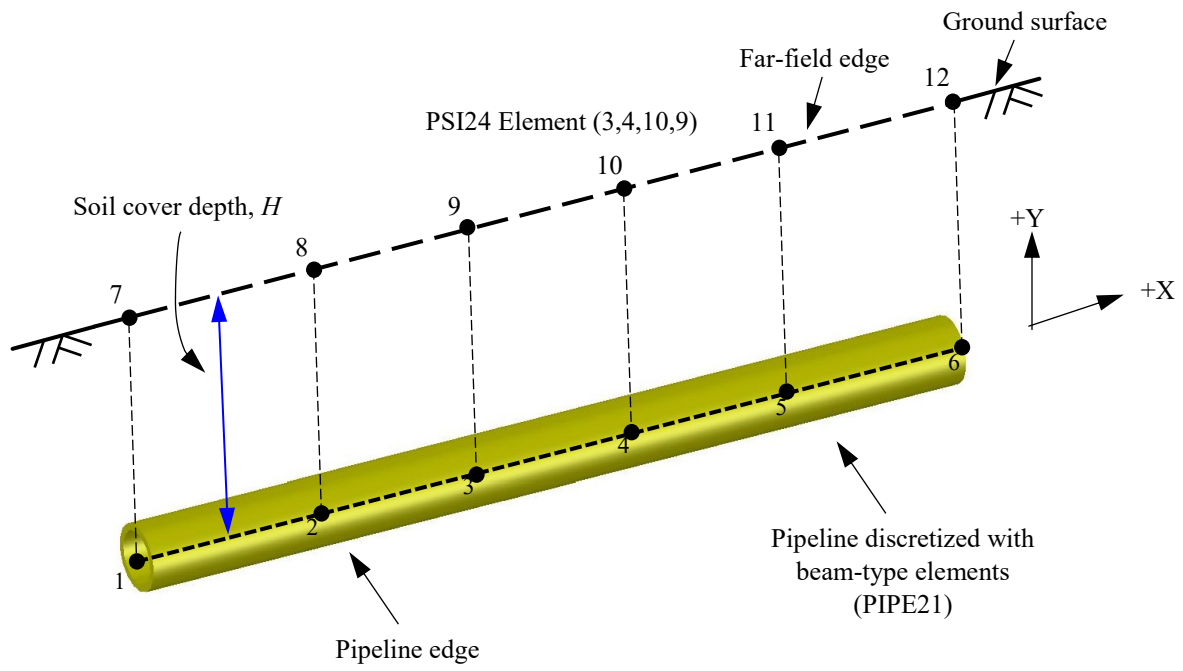


Fig. 4-3. Pipe–soil interaction (PSI) model

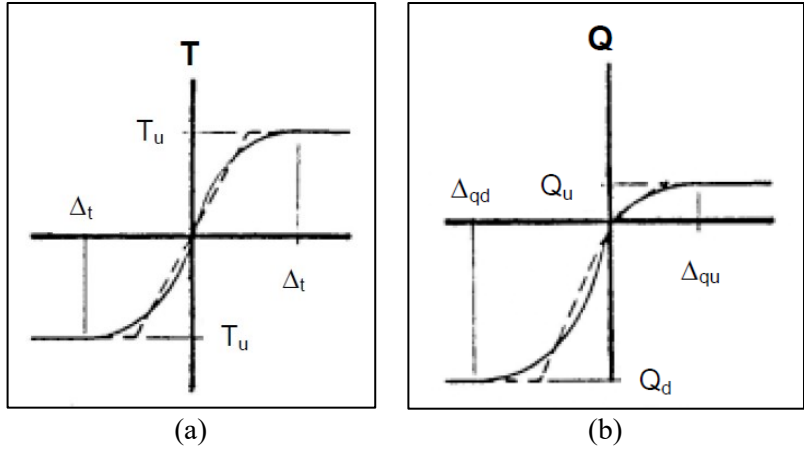


Fig. 4-4. Current design guidelines: (a) Axial loading; (b) Vertical loading (ALA 2005).

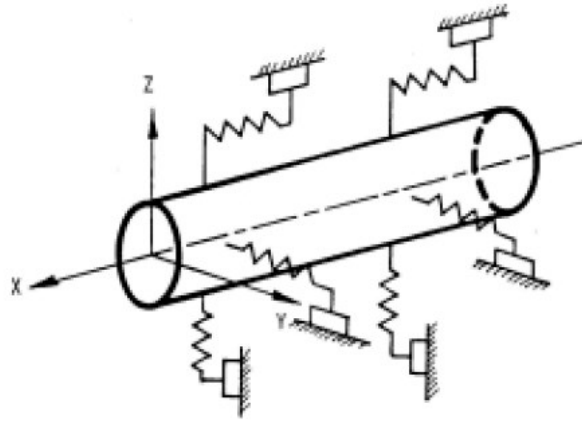
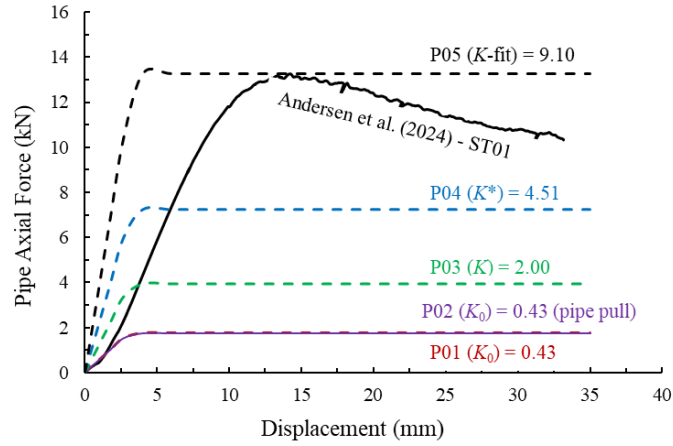
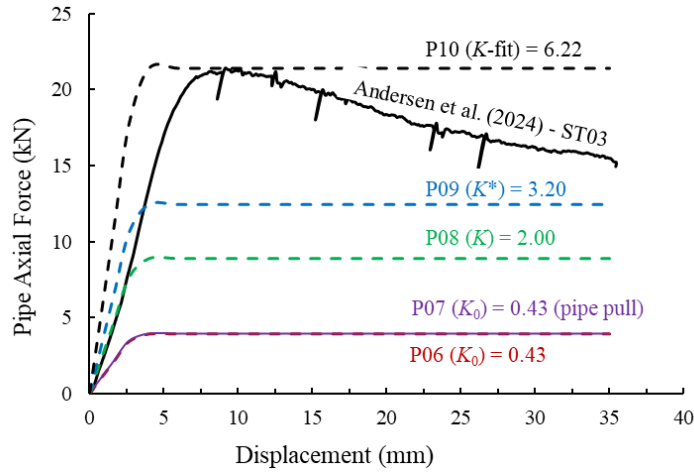


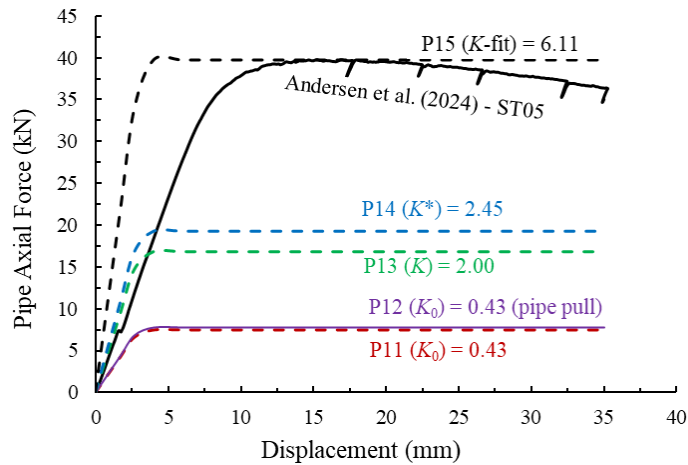
Fig. 4-5. Idealized representation of soil using discrete springs connected to a buried pipe (ALA 2005).



(a)



(b)



(c)

Fig. 4-6. Comparison of force–displacement plots with the measurements: (a) $D=26.7$ -mm, (b) $D=60.3$ -mm, (c) $D=114.3$ -mm.

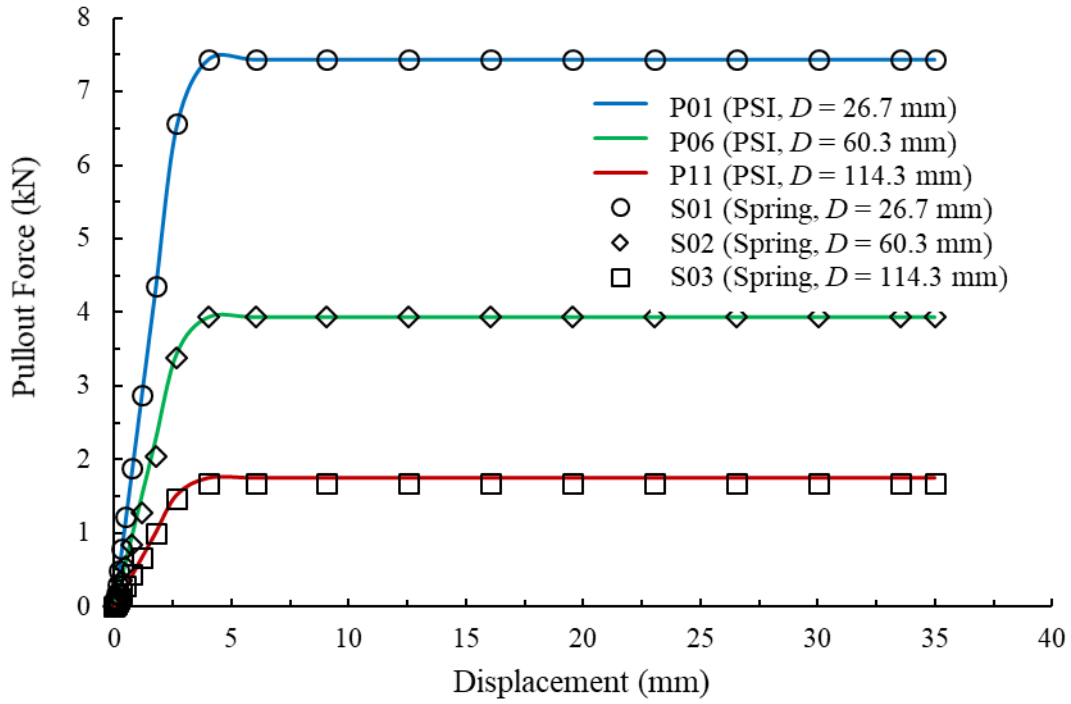
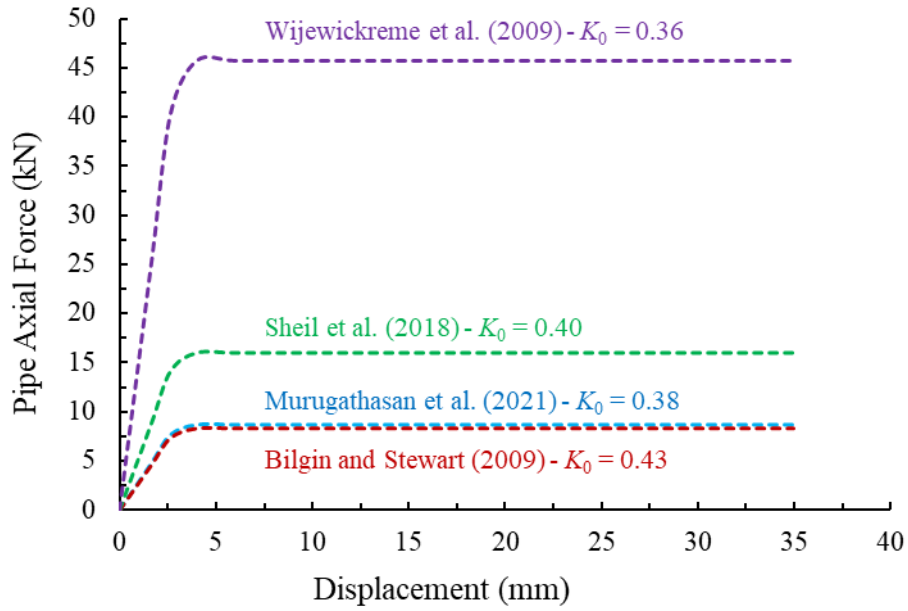
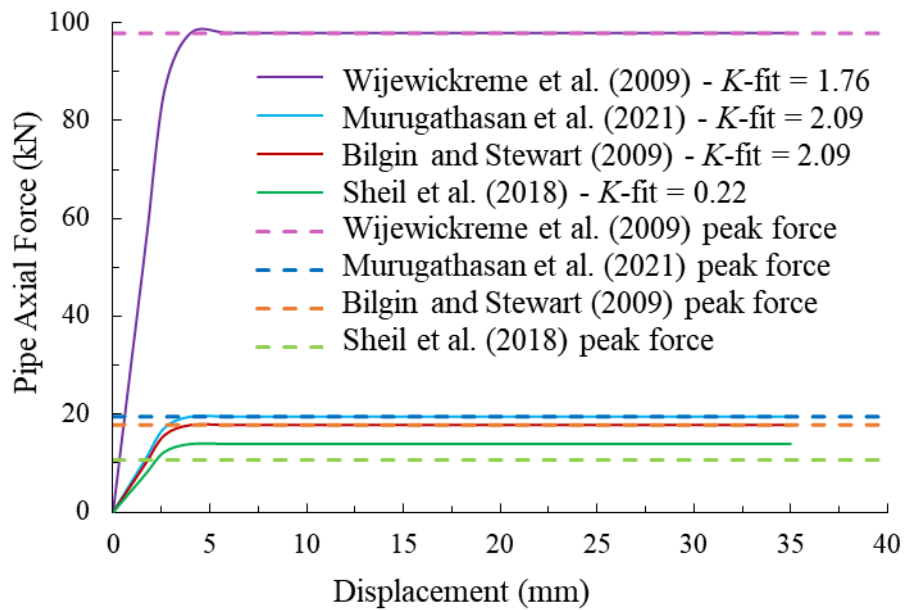


Fig. 4-7. Force–displacement plots comparing results from PSI elements to traditional nonlinear spring elements.



(a)



(b)

Fig. 4-8. Force–displacement results for analyses P16, P18, P20 and P22 using: (a) $K=K_0$, and (b) K =Back-calculated K -fit value in Eq. (4-1).

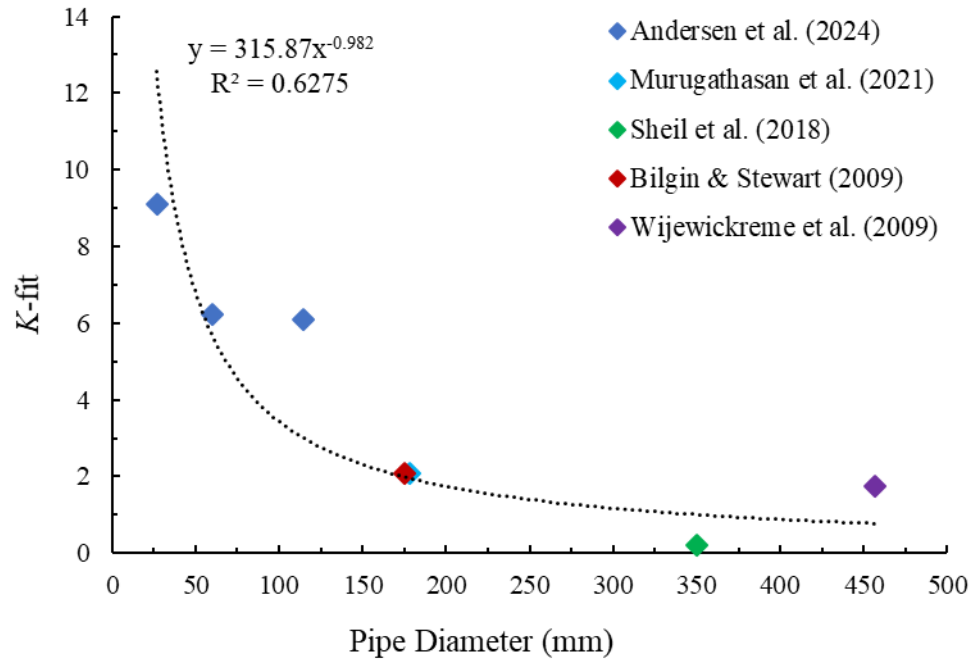


Fig. 4-9. Variation of K with pipe diameter.

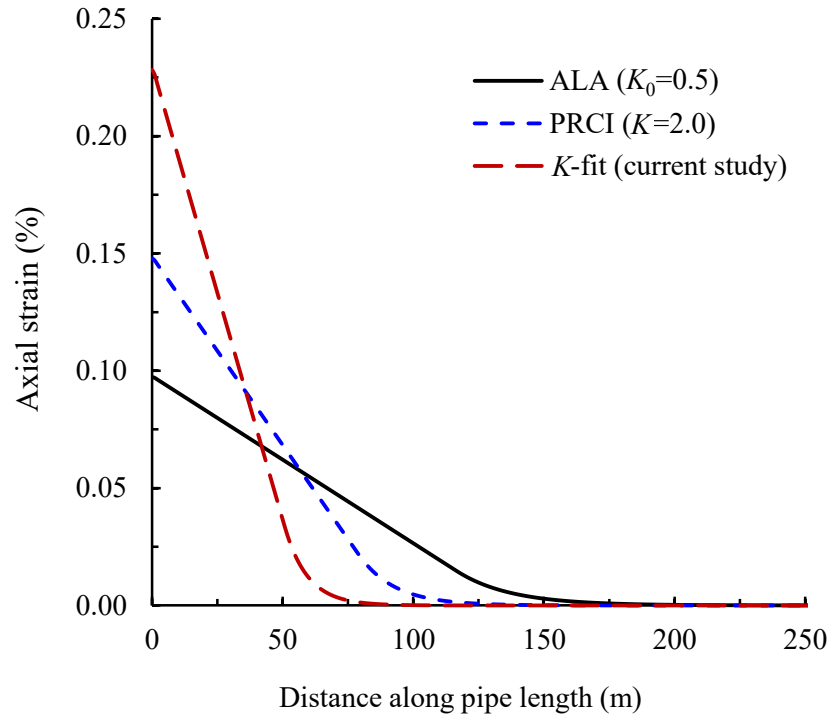


Fig. 4-10. Strain distributions along the length of the pipes

CHAPTER 5: Conclusions and Recommendations for Future Research

5.1 Conclusions

Pipelines are an important part of modern infrastructure, utilized to transport water, oil, gas and other essential products for society across wide geographic areas. Most land-based pipelines are buried underground to protect against external interference. However, different ground movement sources can still impact pipeline integrity. Proper route selection is the most efficient strategy to avoid potential ground movement; however, there may be situations where it is impossible to avoid geotechnically unstable areas. As a result, a pipeline may experience stresses/strains which can eventually lead to failure of the pipeline. For this reason, there is a need to better understand the buried pipe's response during ground-movement events. During ground movements in the field, soil mass moves when the pipe can be restrained in the stable ground. No study investigates the responses of static small-diameter steel pipe against moving soil. With this background, this thesis focused on the behaviour of small-diameter steel pipes buried in sand and loaded axially by a moving sand mass. In this chapter, the overall findings from the full-scale testing and finite-element (FE) modelling simulating the test conditions using beam-on-spring model are discussed. The specific conclusions related to different aspects are presented in Chapters 3 and 4:

5.2 Major Findings from the Full-Scale Testing Programme

Six axial tests are conducted under the full-scale testing program on three different diameters of steel pipe buried in dense sand. Pipe responses due to the tank's applied displacement are investigated in the current study while the results of pulling a pipe axial through static soil were examined from literature. The major findings are as follows;

- Pulling a pipe axially through a static soil may produce a different response than pulling the soil mass along a pipe fixed at one end. The normalized axial force was found to be higher during soil pulling. It should be noted that differing pipe diameters may contribute to this difference as the tested pipes are not of the same size as those used in literature sources.
- The axial forces developed during testing are much greater than the forces predicted using current design guidelines, such as ALA (2005) and PRCI (2009). This discrepancy can be explained due to the omission of compaction-induced loads by the guidelines when calculating the axial pullout resistance. Additionally, the design equation is derived from laboratory investigations where a pipe is pulled through a fixed soil mass, as opposed to the presented method.
- Differences in pipe response were found depending on the functional state of the hydraulic system. A complete shut-off of the system caused quick unloading in the measured load while the load remained constant when maintaining hydraulic system power during the relaxation phase.
- The axial load captured during relaxation phases remained steady and consistent, regardless of relaxation time, implying no time-dependent behaviour by either pipe or soil.
- Fibre-optic sensor placed along the length of the pipe confirmed that shear stress at the interface was developed along the entire pipe length at a very small tank displacement (1 to 2 mm), confirming a rigid body motion of soil over the pipe.

- Strains recorded during testing were negligible in magnitude and roughly linear in nature, with the peak force during pulling phase 1 yielding less than 1 mm in total elongation. This indicates rigid body motion of the pipe.

5.3 Major Findings from the Beam-on-Spring Analysis

Full-scale pipe tests previously conducted were simulated using FE analysis through idealizing the pipe using beam elements and the pipe–soil interaction using spring elements. The study reveals:

- Spring parameters presented in current guidelines (ALA 2005; PRCI 2009) are not suitable for the test condition presented in this study.
- The modified earth pressure coefficient, K^* , proposed by Meidani et al. (2018) produced peak forces closer to those measured in laboratory tests, although results were still underpredicted.
- Using the design equation, a K -value representing the normal stress on the pipe was back-calculated for all tests simulated. These were moderately higher than the values ascribed by both the guidelines and literature sources likely due to pipe backfill compaction, soil dilation and higher loads during the soil-displacement setup.
- A correlation exists between the back-calculated K -values and pipe diameter whereby a larger diameter corresponds to a smaller K -value.
- Using the higher K -values for a long pipeline subjected to axial ground movement, a spring analysis was performed. Results showed that use of a higher K value will cause the

axial load to distribute over a shorter distance along the pipe's length from the pipe's anchored location.

5.4 Recommendations

The following are recommendations for future research:

- The full-scale experiments presented herein effectively considered a single burial depth (25 mm in the difference) and a single movement rate for a particular soil type. These parameters should be altered for a more robust understanding of how they impact the behaviour of steel pipes subjected to axial soil-pulling.
- During testing, the moisture content of the soil was kept at a low value, 3% and lower, to negate the effect of matric suction on the axial force. Higher moisture contents could be tested to investigate its effect on results.
- Relaxation phases were implemented only after the peak force in a pipe was developed; however, a single ground-movement event may not fully develop the peak force. Therefore, soil-pulling intervals at varying stages of force development should be considered.
- This thesis investigated the effect of axial loading exclusively on a buried steel pipe, however, landslides often cause lateral and vertical loading on pipelines. A similar full-scale setup should be adopted to test these loading scenarios with the soil-pulling method.

- To understand the soil dynamics at the interface, discrete-element modelling of axial pipe–soil interaction with the moving soil box could be performed.
- A single definition of spring behaviour, namely elastic-perfectly-plastic, was utilized in the FE study. Additional definitions of the spring elements, which considers soil-softening with reduced resistance after peak, could be implemented to simulate real-world behaviour more closely.

5.5 References (General)

- American Gas Association (AGA) (2019). Get the Facts: Pipeline Safety. https://www.aga.org/wp-content/uploads/2019/02/2019-pipeline-safety_final.pdf
- ALA (American Lifelines Alliance) 2005. *Guidelines for the design of buried steel pipe*. Washington, DC and Reston, VA, USA: Federal Emergency Management Agency (FEMA) and American Society of Civil Engineers (ASCE).
- Alarifi, H., Mohamad, H., Nordin, N. F., Yusoff, M., Rafindadi, A. D. U., and Widjaja, B. 2021. A large-scale model of lateral pressure on a buried pipeline in medium dense sand. *Applied Sciences*, 11(12): 5554.
- Ali-Khazaali, M., and Vanapalli, S. K. 2019. Axial force-displacement behaviour of a buried pipeline in saturated and unsaturated sand. *Géotechnique*, 69(11): 9861003.
- Andersen, D., Reza A., and Dhar, A. S. 2024. Laboratory Investigation of Buried Small-Diameter Steel Pipe Subjected to Axial Ground Movement. (to be submitted)
- Ansari, Y., Kouretzis, G., and Sloan, S. W. 2021. Physical modelling of lateral sand–pipe interaction. *Géotechnique*, 71(1): 60–75.

- Bain, C. A., O'Rourke, T. D., and Bray, J. D. 2024. Pipeline Response to Seismic Displacement at Balboa Boulevard during the 1994 Northridge Earthquake. *Journal of Geotechnical and Geoenvironmental Engineering*, 150(2): 04023139.
- Banushi, G., and Squeglia, N. 2018. Seismic analysis of a buried operating steel pipeline with emphasis on the equivalent-boundary conditions. *Journal of Pipeline Systems Engineering and Practice*, 9(3): 04018005.
- Bilgin, Ö., and Stewart, H. E. 2009. Pullout resistance characteristics of cast iron pipe. *Journal of Transportation Engineering*, 135(10): 730–735.
- Cevik, E., and Topal, T. 2003. GIS-based landslide susceptibility mapping for a problematic segment of the natural gas pipeline, Hendek (Turkey). *Environmental geology*, 44: 949962.
- Duncan, J. M., and Seed, R. B. 1986. Compaction-induced earth pressures under K 0-conditions. *Journal of Geotechnical Engineering*, 112(1): 1–22.
- Duncan, J. M., and Chang, C. Y. 1970. Nonlinear analysis of stress and strain in soils. *Journal of the soil mechanics and foundations division*, 96(5): 16291653.
- Ge, B., Martin, G., Dietz, M. S., Mylonakis, G., and Diambra, A. 2023. A novel pipe-segment shear test apparatus: Polypropylene pipe behaviour over sand beds vs element interface tests. *Canadian Geotechnical Journal*, (ja).
- Gupta, K., and Satyam, N. 2022. Co-seismic landslide hazard assessment of Uttarakhand state (India) based on the modified Newmark model. *Journal of Asian Earth Sciences*: X, 8, 100120.
- Hara, T., Kagawa, T., and Iide, J. 2020. Case Studies of Hazard Resilient Ductile Iron Pipe Withstanding Natural Hazards in Japan. In *Pipelines 2020* (pp. 294303). Reston, VA: American Society of Civil Engineers.

- Hardin, B. O., and Black, W. L. 1966. Sand stiffness under various triaxial stresses. *Journal of the Soil Mechanics and Foundations Division*, 92(2): 27–42.
- Hungr, O., Evans, S. G., and Hazzard, J. 1999. Magnitude and frequency of rock falls and rock slides along the main transportation corridors of southwestern British Columbia. *Canadian Geotechnical Journal*: 36(2), 224238.
- Janbu, N. (1963). Soil compressibility as determined by oedometer and triaxial tests. In Proceedings, European Conference on Soil Mechanics and Foundations Engineering, Wiesbaden, Germany 1963 (Vol. 1, pp. 19–25).
- Karimian, S. A. 2006. LONGITUDINAL, AND TRANSVERSE GROUND MOVEMENT (Doctoral dissertation, University of British Columbia).
- Los Angeles Times. (2019, January 16). The Northridge earthquake. Los Angeles Times. <https://www.latimes.com/local/lanow/la-me-northridge-earthquake-photos-20190116-photogallery.html>
- Lee, E. M., Audibert, J. M. E., Hengesh, J. V., and Nyman, D. J. 2009, May. Landslide-related ruptures of the Camisea pipeline system, Peru. *Geological Society of London*.
- Liu, W., Huang, C., Zhang, S., and Song, Z. 2022. Centrifuge tests of large-diameter steel pipes crossing strike-slip faults. *Engineering Structures*, 279: 115124.
- Matymish, J., Moore, I. D., Woods, J. E., and Hault, N. A. 2023. Axial Pullout Behaviour of Fusible PVC Pipes and Fusion Weld Joints Assessed using Distributed Fibre Optic Sensors. *Canadian Geotechnical Journal*, (ja).
- Meidani, M., Meguid, M. A., and Chouinard, L. E. 2018. Estimating earth loads on buried pipes under axial loading condition: insights from 3D discrete element analysis. *International Journal of Geo-Engineering*, 9: 1–20.

- Morshed, M. A., Roy, K., and Hawlader, B. 2020. Modeling of buried pipelines in dense sand for oblique movement in vertical–lateral plane. *Journal of Pipeline Systems Engineering and Practice*, 11(4): 04020050.
- Muntakim, A. H. and Dhar, A. S. 2021. Assessment of Axial Pullout Force for Buried Medium-Density Polyethylene Pipelines. *Journal of Pipeline Systems Engineering and Practice*, 12(2):04020074.
- Murugathan, P., Dhar, A. S., and Hawlader, B. C. 2021. An experimental and numerical investigation of pullout behavior of ductile iron water pipes buried in sand. *Canadian Journal of Civil Engineering*, 48(2): 134–143.
- Ni, P., Mangalathu, S., and Yi, Y. 2018. Fragility analysis of continuous pipelines subjected to transverse permanent ground deformation. *Soils and Foundations*, 58(6): 14001413.
- Ni, P., Moore, I. D., and Take, W. A. 2018. Numerical modeling of normal fault-pipeline interaction and comparison with centrifuge tests. *Soil Dynamics and Earthquake Engineering*, 105: 127–138.
- PRCI (Pipeline Research Council International). 2009. *Guidelines for constructing natural gas and liquid hydrocarbon pipelines through areas prone to landslide and subsidence hazards*. Report prepared for the Design, Material, and Construction Committee. Chantilly, VA: Pipeline Research Council International, Inc.
- Reed, M., Lee, R., and Coote, B. 2012, September. Development of Pipeline Integrity Performance Indicators for Canadian Energy Pipelines. In International Pipeline Conference (Vol. 45158, pp. 789799). American Society of Mechanical Engineers.
- Reza, A. and Dhar, A.S. 2024. Finite-element modelling of axial movements of polyethylene pipes in dense sand, (under review).

- Reza, A., and Dhar, A. S. 2021. Axial Pullout Behavior of Buried Medium-Density Polyethylene Gas Distribution Pipes. *International Journal of Geomechanics*, 21(7): 04021120.
- Rostami, H., Osouli, A., and Kumar, S. 2023. Experimental modeling of far-field effects in buried pipelines subjected to reverse faulting. *Soil Dynamics and Earthquake Engineering*, 164: 107561.
- Saberi, M., Annan, C.D. and Sheil, B.B. 2022. An efficient numerical approach for simulating soil-pipe interaction behaviour under cyclic loading. *Computer and Geotechnics*, 146, 104666.
- Saiyar, M., Moore, I. D., and Take, W. A. 2015. Kinematics of jointed pipes and design estimates of joint rotation under differential ground movements. *Canadian Geotechnical Journal*, 52(11): 1714–1724.
- Sheil, B. B., Martin, C. M., Byrne, B. W., Plant, M., Williams, K., and Coyne, D. 2018. Full-scale laboratory testing of a buried pipeline in sand subjected to cyclic axial displacements. *Géotechnique*, 68(8): 684–698.
- Vasseghi, A., Haghshenas, E., Soroushian, A., and Rakhshandeh, M. 2021. Failure analysis of a natural gas pipeline subjected to landslide. *Engineering Failure Analysis*, 119: 105009.
- Wijewickreme, D., Karimian, H., and Honegger, D. 2009. Response of buried steel pipelines subjected to relative axial soil movement. *Canadian Geotechnical Journal*, 46(7): 735–752.
- Weerasekara, L., and Wijewickreme, D. 2008. Mobilization of soil loads on buried, polyethylene natural gas pipelines subject to relative axial displacements. *Canadian Geotechnical Journal*, 45(9): 12371249.

Wood Environment and Infrastructure Solutions 2021. Monitoring Report 2020, West Quesnel
Land Stability Program (Project No. KX0439755).

Appendix A: Challenges and Issues During Full-Scale Testing

Laboratory testing has the potential to provide researchers with important data pertaining to the pipe–soil interaction. However, full-scale testing is not without its challenges. This appendix describes several challenges encountered during testing and the results obtained due to those issues.

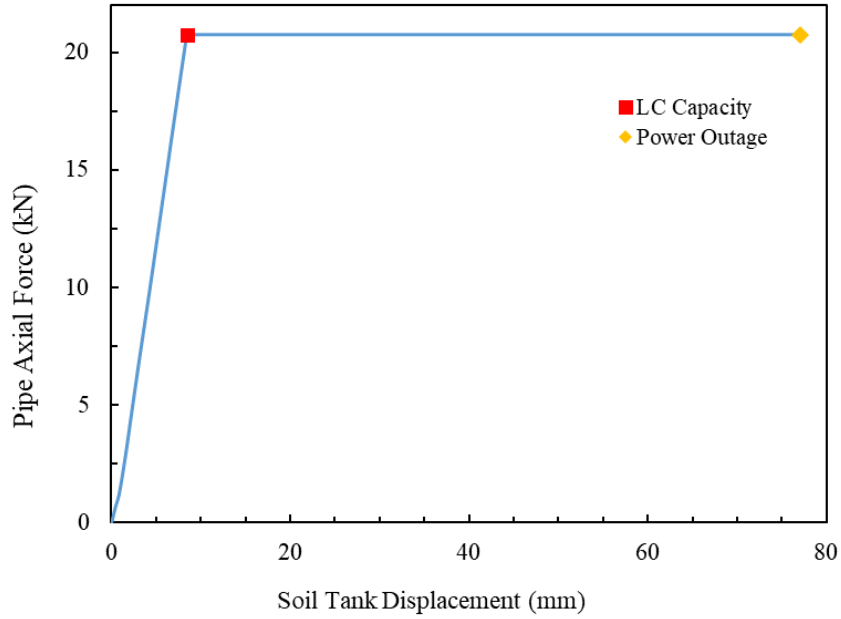
Before the first scheduled steel pipe test, the laboratory hydraulic system was Locked-Out and Tagged-Out due to required safety reviews and upgrades. As such, the hydraulic system required for soil-tank displacement was inoperable for several months with no recourse.

The first testing performed on a steel pipe was that of a 60.3 mm pipe instrumented with a fibre-optic strain sensor buried in sand of roughly 85% relative compaction. The soil was moved at a rate of 0.5 mm/min for 120 mm of total soil displacement. This test encountered several issues. First, the load cell's capacity was exceeded, causing damage to the equipment and necessitating its replacement. This set-back testing of the two larger diameter pipes (60.3 and 114.3 mm) for months while a higher capacity (20 kips / 88 kN) load cell was procured and the smallest pipe testing while a replacement 5 kips was ordered. Secondly, a power outage caused the test to stop early at 76 mm of tank displacement instead of 120 mm. Finally, due to a learning curve with the new fibre-optic sensor, the strain data was erroneously collected at a lower rate than required to compare with axial force data. Fig. A-1(a) shows the force–displacement plot from this test with points indicating the load cell's capacity and power outage. Fig A-1(b) shows the strain distribution along the pipe, plotted at discrete soil displacements. Both hydraulic ram

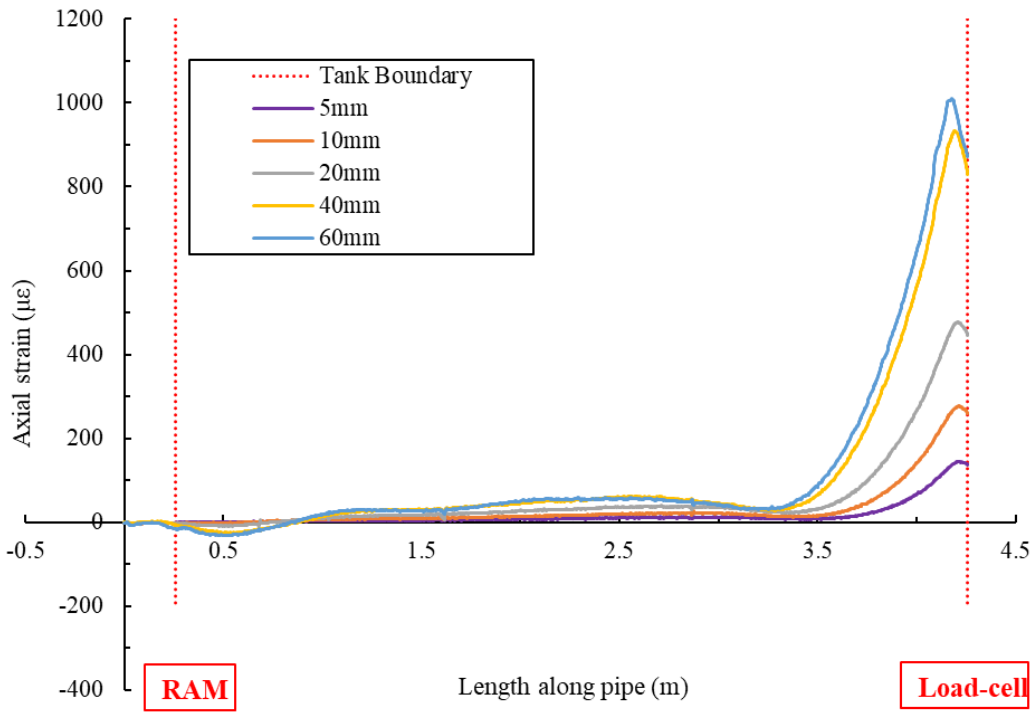
(free-end of pipe) and load-cell (fixed-end of pipe) locations are identified. Results of this test are at odds with later tests performed, as the axial strain continued to increase with soil displacement, far beyond any strains recorded during later tests.

Further challenges arose after the first test when the hydraulic ram's controller ceased functioning. The controller is the only device capable of giving displacement instructions to the ram and thus moving the soil tank, as well as sending displacement data to the data logger. The controller had to be shipped to the manufacturer for several months to be repaired. Once the controller returned, it malfunctioned again, with the ultimate cause for both incidents being a faulty solenoid in the hydraulic manifold. After manifold repairs were completed, a spare controller was located and set up with mixed results. During testing on the 60.3 mm diameter steel pipe, saw-tooth results were obtained during Pull 1 and the end of Pull 2 (Fig A-2). Additionally, the controller malfunctioned between Relax 1 and Pull 2, causing the soil tank's return to its pre-testing displacement before moving back to the required starting point (35 mm). Fig. A-2 (a) shows force versus time behaviour during this test. The saw-toothed behaviour during Pull 1 and Pull 2, along with the short reduction to compressive force after Relax 1, is visible. Fig. A-3 plots the force–displacement behaviour for the test and more clearly shows the soil tank's travel to its original position. During this test, a loud bang was heard just before the first saw-toothed peak and upon further investigation, it was found that the backstop of the testing frame was not bolted at the end. It is believed that this led to the backstop rotating slightly about the next bolt group, causing uplift in the frame and lateral translation of the load cell and pipe, which sharply decreased the load causing the saw-toothed plot. Interestingly, no noise was heard during the test presented in Fig. A-2, although a similar response was obtained.

Lastly, Fig. A-3 presents the force–displacement plot of an unsuccessful 26.7 mm pipe test whereby the controller malfunctioned, causing the ram, and thus soil tank, to move at a higher rate than intended. It can be seen from the figure that from 0 to roughly 7 mm of tank displacement, the slope is flatter, indicating a faster tank displacement per load development. After this the tank is stopped, shown by the reduction of force, and once again started at the intended, slower, rate.

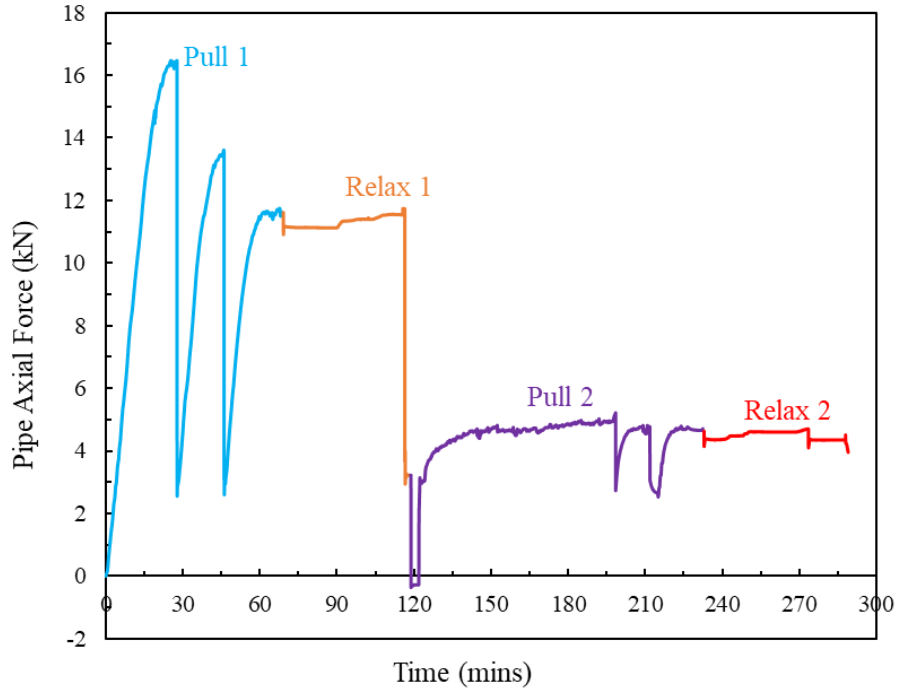


(a)

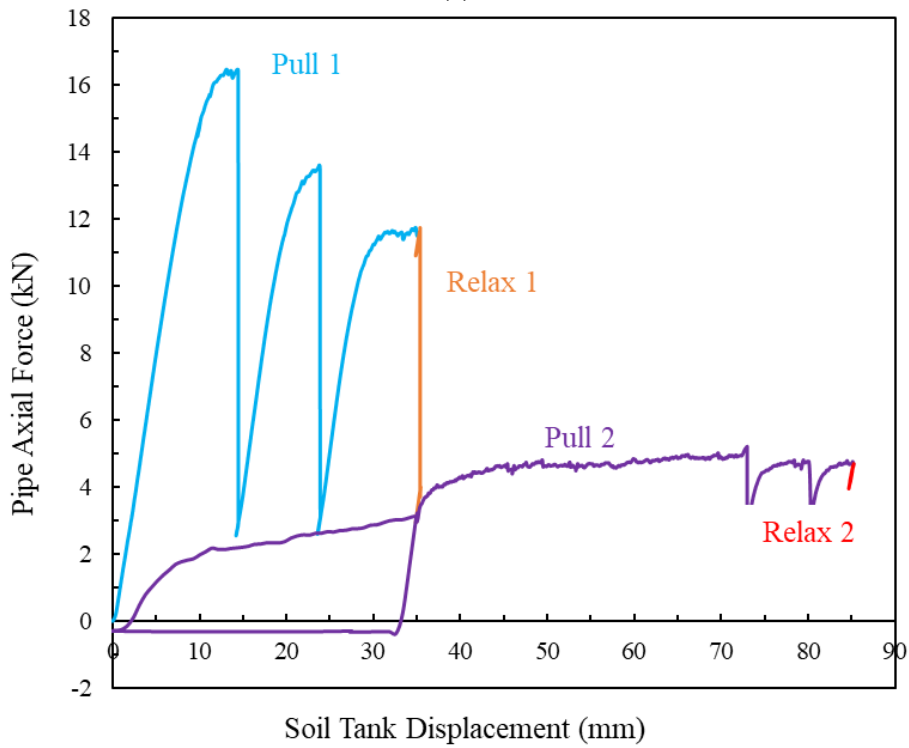


(b)

Fig A-1. Results from the first test on 60.3 mm diameter pipe deemed unsuccessful: (a) Force–displacement plot showing load-cell capacity and power outage timing, (b) Axial strain distribution along the pipe at varying soil displacements



(a)



(b)

Fig A-2. Results from an initial trial of ST-03 (60.3 mm pipe) showing saw-tooth behaviour: (a) Force vs time, (b) Force–displacement plot showing erroneous tank behaviour during Pull 2

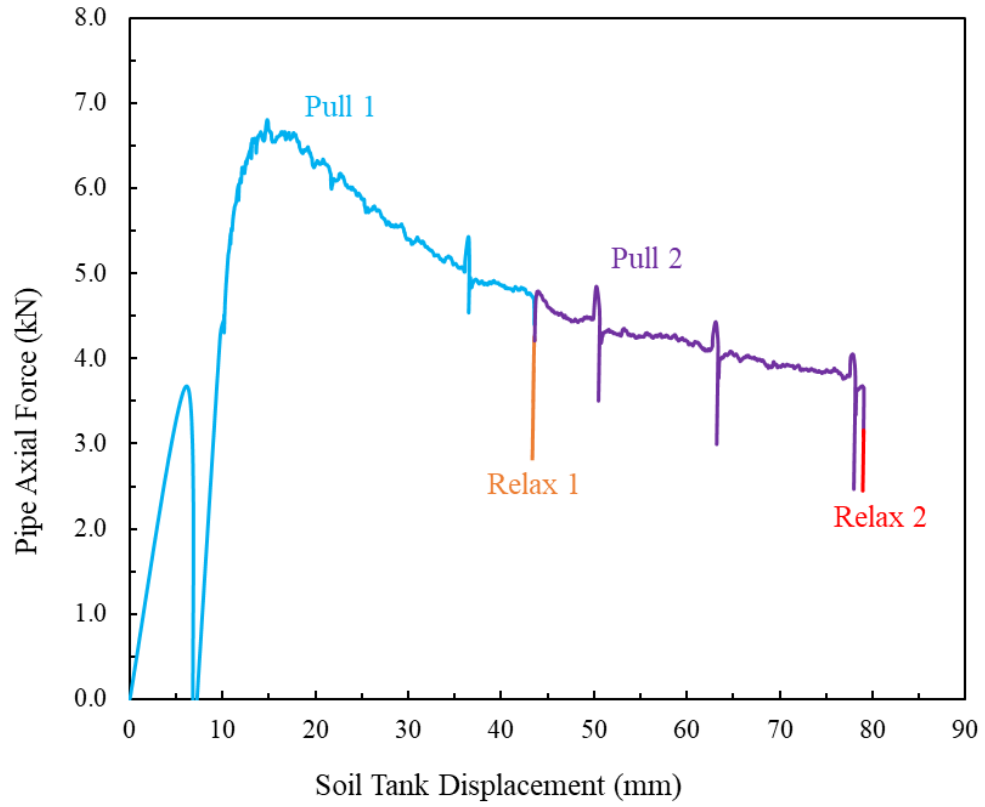


Fig A-3. Results from an unsuccessful trial of ST-19 (26.7 mm diameter) (Force–displacement plot showing erroneous tank movement during Pull 1)